BIOMECHANICS OF THE MAMMALIAN JAW

by

FUTANG ZHANG

B Med (Dent), Shandong Medical University, 1988
M Med (Dent), Shandong Medical University, 1991

A THESIS SUBMITTED IN PARTIAL FULFILLMENT OF THE REQUIREMENTS
FOR THE DEGREE OF

DOCTOR OF PHILOSOPHY

in

THE FACULTY OF GRADUATE STUDIES

(Department of Oral Health Sciences)

We accept this thesis as conforming to the required standard

THE UNIVERSITY OF BRITISH COLUMBIA

28 August 2001

In presenting this thesis in partial fulfilment of the requirements for an advanced degree at the University of British Columbia, I agree that the Library shall make it freely available for reference and study. I further agree that permission for extensive copying of this thesis for scholarly purposes may be granted by the head of my department or by his or her representatives. It is understood that copying or publication of this thesis for financial gain shall not be allowed without my written permission.

Department of Oral Health Sciences

The University of British Columbia

Vancouver, Canada

Date Sep 28, 2001

ABSTRACT

Mammalian jaw biomechanics are not fully understood. They can be studied by different approaches, including, but not limited to, jaw cross-sectional measurements, stress and strain analysis, and computer modeling. Five studies comprise this thesis:

In the first study, three cross-sections were examined with high-resolution computed tomography (CT) in the human jaw. Although the cross-sectional areas varied among the three locations, the cross-sectional masses were homogeneous, suggesting uniform shear rigidity. Despite similarities in shape among the three cross-sections, cortical bone thickness and density varied, indicating regional loading conditions may be determinants in the cross-sectional design.

The second study tested two hypotheses. The first postulated that symphyseal stress and strain are similar in pigs and humans. The second proposed that the symphyseal orientation in the pig jaw keeps the stress and strain level within a functional range. Individual muscle lever arms, cross-sectional moments of inertia, symphyseal centroids, and mean muscle tensions were considered in the pig and human jaws. The estimated stress and strain levels were markedly similar for pigs and humans with their symphyses in normal "functional" orientations. However, the estimated strain for the pig mandible was higher than the reported maximum functional strain when the symphysis was in a simulated "upright" orientation.

In the following two studies, pig and human jaw mass properties were estimated from CT scans. The mass and geometric centers were close in

both pig and human mandibles, and consistently located at the last molar region, suggesting imaging methods revealing 3D shape alone can be used to estimate mass properties. Jaw mass and moments of inertia could also be predicted by simple dimensional measurements of the jaw. Dynamic modeling of individual jaws is, therefore, possible. The sensitivity of mass properties in dynamic modeling was confirmed in a previously published dynamic human jaw model.

In the final study, the respective mass properties were estimated by CT for each half of a pig jaw split into two halves, and rejoined with a rigid link. Dorsoventral shear, medial and lateral transverse bendings were predicted in the pig jaw symphysis during a unilateral chewing stroke. The prediction supported the hypothesis that the pig symphyseal orientation is essential to keep symphyseal stresses and strains within functional levels.

TABLE OF CONTENTS

LIST OF FIGURES

LIST OF TABLES

ACKNOWLEDGEMENTS

I am extremely grateful to Dr. Alan Gordon Hannam for his scientific guidance and inspiration that have made this project such a rewarding experience. One could not ask for a better mentor and teacher, and I only hope that some of his brilliance has rubbed off onto me.

I would also like to thank Drs. Virginia Diewert and Colin Price for their invaluable instruction, constructive criticism and guidance throughout my candidacy, from the initial planning of the proposal to the final stages of thesis compilation.

I want to express my sincere thanks to Drs. Christopher Charles Peck and Geerling Evert Jan Langenbach for their scientific assistance. I appreciate the availability of Dr. Susan W. Herring as the academic consultant during my whole study period. I am also grateful to Dr. Douglas Waterfield for his valuable advice towards my graduate studies. I appreciate all the helps from the department, especially those from Ms. Vicki Beretanos Koulouris, the wonderful graduate secretary.

I have been very lucky to enlist the expertise of Ms. Joy Scott, who has provided direction and support for many of the computational aspects of my experiments.

I have been very fortunate to have family and friends who have always been a constant source of encouragement and support. Special thanks go to Nancy and Rick, whom I have relied upon very much.

Finally, I would like to thank those who have developed today's computers. This thesis would not exist without this technology.

1 INTRODUCTION

1.1 INTRODUCTION TO THE THESIS

The complexity of the biomechanical behavior of the masticatory system challenges researchers. During the power stroke of mastication, the jaw interacts with various muscle forces, gravity, reaction forces from the occlusion and the temporomandibular joints. All these forces demand a mechanically optimized system. Unfortunately, the interactions are not fully understood. Our knowledge of the jaw biomechanics is limited, and our current understanding is not based so much on cause-effect relationships, but mostly derived from associations, interpretations and assumptions.

For a load-bearing system like the jaw, stress and strain analysis is a key method to comprehend mechanical significance, and *in vivo* surface strain analysis of cortical bone reflects the functional environment (Bouvier and Hylander, 1981a, 1981b; Daegling and Hylander, 1997, 2000; Dechow and Hylander, 2000; Herring *et al.*, 1996; Herring and Teng, 2000; Hylander, 1977, 1979a, 1984, 1986; Hylander *et al.*, 1987, 1998; Hylander and Crompton, 1986; Hylander and Johnson, 1997a, b; Liu and Herring, 2000; Mikic and Carter, 1995; Ravosa *et al.*, 2000). Understandably, this methodology has limitations, and is not available in living humans.

Alternative approaches not directly involving living material include the biomechanical analysis of jaw cross-sections based on physical and engineering principles (Daegling, 1989, 1993; Daegling *et al.*, 1992; Daegling and Grine, 1991; Daegling and Hylander, 1998; Daegling and

Jungers, 2000), and stress and strain estimation derived from jaw cross-sectional and musculoskeletal information (Hylander, 1985; Vinyard and Ravosa, 1998). Mathematical modeling (both static and dynamic) founded on jaw morphometric and functional data (Curtis *et al.*, 1999; Hannam, 1994; Hannam *et al.*, 1997; Koolstra *et al.*, 1988; Koolstra and van Eijden, 1995, 1997a, b; Korioth *et al.*, 1992; Korioth and Hannam, 1994a; Langenbach and Hannam, 1999; Ng, 1994; Peck *et al.*, 2000) also offers insight into jaw biomechanical behavior, design, and stress and strain conditions.

Though numerous investigations have been conducted in the above areas, they are incomplete. For example, cross-sectional biomechanical analyses have not taken regional bone densities into account, and have been limited to molar sections only; stress and strain estimations have been based on scaling factors, and thus cannot provide comparable data to *in vivo* strain studies; the mass properties (i.e., mass, mass center, and moments of inertia) incorporated by dynamic jaw models have been crude and generic; and dynamic models have not been used to predict jaw internal forces and torques, which could lead to better understanding of the jaw loading conditions.

This thesis probed these areas in order to cast more light on them. Three dimensional (3D) computed tomography (CT) was employed to analyze the cross-sectional biomechanics in the human mandible. Focus was directed on whether the human mandibular corpus cross-sections at different locations behave homogeneously, and how regional variations in bone density and cortical thickness within each cross-section are related to regional loading conditions. Second, the jaw's cross-sectional data, plus jaw muscle and morphometric data, were used to predict the stress and strain magnitudes along the lingual surface of the mandibular

symphysis in both pigs and humans. Attention was placed on the hypotheses that the pig jaw symphysis is uniquely oriented so as to increase its ability to resist high wishboning stress and strain, and that stress and strain similarity is maintained across mammalian orders (in this case pigs and humans). Third, 3D CT was used again, this time to estimate the jaw's mass and inertial properties in pigs and humans. One issue addressed here was whether these mass properties might be estimated or predicted with less invasive methods than CT so that this highly radiation-dependent method could be replaced with other morphological tools. A second issue was assessing the significance mass properties have in dynamic modeling. Finally, the method was used to estimate mass properties in a pig jaw artificially segmented into two halves, and later joined with a rigid link in a dynamic working model of the pig masticatory system. By analyzing the forces and torques transmitted through the symphysis link, it was possible to predict the functional demands placed at the pig symphysis during a unilateral chewing stroke.

In summary, the work introduced several new experimental approaches applicable to the study of human and other mammalian jaw biomechanics, and provided some additional insight into the structural and functional interactions which take place in the mammalian masticatory system.

1.2 MANDIBULAR FORM AND FUNCTION

1.2.1 Form and function of the mammalian jaw

The mammalian jaw system is the functional unit of the body primarily responsible for mastication. The mandible is a major part of the jaw

system. It is suspended below the maxilla by muscles, ligaments and other soft tissues to provide the mobility involved in functions which include suckling, swallowing, speech, and most importantly the incision and chewing of food. This system also plays a major rule in tasting and breathing.

Unlike its reptilian precursor, the complexity of the mammalian mandible has been greatly reduced. It consists of a single bone, the dentary, rather than a series of bones (Dechow and Carlson, 1997). Large variations, however, exist in the mammalian jaw size, articular and muscle form, which may be presumed to have biomechanical consequences.

1.2.2 Research models

Numerous experimental animals have been used to study human jaw structure and function. These include rodents and carnivores (Bouvier and Hylander, 1984; Lieberman and Crompton, 2000; Otten, 1987; Weijs, 1973, 1975; Weijs and Dantuma, 1975), rabbits and ungulates (Herring, 1972, 1976, 1977; Herring and Teng, 2000; Langenbach *et al.*, 1992; Langenbach and Weijs, 1990), and anthropoid primates (Hylander, 1979a, b; Hylander *et al.*, 2000).

The resemblance of the miniature pig mandible (*Sus scrofa*) to the human jaw makes the pig a useful animal model for functional studies of the masticatory system (Ström *et al.*, 1986). The pig and human mandibular anatomies, occlusions, movements, and loading patterns are actually quite similar (Herring, 1995). The pig jaw muscles are also similar to the human jaw muscles (Herring *et al.*, 1993; Ström *et al.*, 1986). The pig mandible differs from the human mandible however, in that: A) it is relatively larger in overall size; B) it is more prognathic; C)

the two mandibular corpora and dental arches are long and parallel to each other rather than divergent; D) the functional occlusal plane is almost parallel to the lower border of the mandible; E) there are large diastemata between incisors and canines and between canines and premolars; and F) the symphysis is large and oriented differently.

1.3 MAMMALIAN JAW BIOMECHANICS

In the text "Vector Mechanics for Engineers: statics and dynamics", Beer and Johnston (1988) state "Mechanics may be defined as that science which describes and predicts the conditions of rest or motion of bodies under the action of forces". We can extend the above definition and define biomechanics as mechanics applied to biological bodies. Mechanics is divided into three parts: the mechanics of rigid bodies, the mechanics of deformable bodies, and the mechanics of fluids.

In the bioengineering literature, the mandible has been treated either as a rigid body (Koolstra and van Eijden, 1997a, b; Langenbach and Hannam, 1999; Peck *et al.*, 2000) or a deformable one (Chen *et al.*, 1998; Chen and Xu, 1994; Korioth *et al.*, 1992; Korioth, 1997; Korioth and Hannam, 1994a; Korioth and Versluis, 1997). The biomechanical behavior of bone tissue and of the mandibular bone as a whole has been thoroughly reviewed recently (see van Eijden, 2000). Here, only those points most relevant to the thesis are discussed.

Due to the relative scarcity of biomechanical data on pig and human mandibles, much of the information presented in this literature review was obtained from primate studies. This information may not be entirely applicable to pigs and humans.

1.3.1 Material properties of bone

While bone is a hard tissue composed mainly of hydroxyapatite, in which the crystals are very stiff and strong, it is also a living organ, a composite of collagen fibers and hydroxyapatite. The arrangement of the collagen fibers and hydroxyapatite determines its mechanical properties. Bone is not isotropic. It is stiffest longitudinally, less stiff tangentially and least stiff in a direction normal to the bone's surface (Dechow *et al.*, 1993; Dechow and Hylander, 2000). The strength of bone also differs under different stress regimens (van Eijden, 2000). Despite the above reservations, bone is often treated as being similar to many engineering materials, not least allowing its stresses and strains to be analyzed in much the same way as the methods used in engineering structural analysis (Fung, 1981).

1.3.1.1 Stress and strain under normal load

Stress is "the internal force exerted by either of two adjacent parts of a body upon the other across an imagined plane of separation" (Roark and Young, 1975). It is defined as force per unit cross-sectional area or intensity of the forces distributed over a given section (Beer and Johnston, 1981), i.e.

$$\sigma = \frac{P}{A} \qquad \text{Equation 1.1}$$

where σ denotes stress; P and A are the load and the cross-sectional area, respectively. The unit of stress is Newton per square meter (N/m^2) or Pascal (Pa). Practically, stress is expressed as MPa ($=10^6$ Pascal) or GPa ($=10^9$ Pascal).

When the load is normal to the cross-section, it is called normal stress.

If the normal stress is directed toward the part on which it acts, it is called compressive stress; if the normal stress is directed away from the part on which it acts, it is tensile stress. The maximum stress that the bone can sustain is called ultimate stress and is a measure of bone strength. Bone is weaker in tension than in compression. For example, the ultimate tensile stress for the human femoral cortical bone is 124 MPa while the ultimate compressive stress is 170 MPa (Fung, 1981). The ultimate compressive strength for the pig mandibular compact bone is reported to be 120 MPa (Robertson and Smith, 1978).

Strain is a measure of a body's deformation under stress. It is expressed as the ratio of the total deformation over the total length, i.e.

$$\varepsilon = \frac{\delta}{L} \qquad \text{Equation 1.2}$$

where ε denotes strain; δ and L are the amount of deformation (length change) and the total length, respectively. Strain is a dimensionless quantity. As a convention, strain is depicted as με. For example, a 1,000 με is 0.1% deformation. Stretch is a tensile strain, and shortening is a compressive strain. The functional strain level for human cortical bone is reported to be below 3,000 με and the maximum strain that the human cortical bone can sustain is reported to be 6,300 με (Hylander, 1985).

It has been suggested that certain load-bearing skeletal elements experience similar strain magnitudes during habitual dynamic loading. This concept of dynamic strain similarity, which has been proposed to be determined by the material properties of bony tissue (Rubin and Lanyon, 1984), has been observed in a large number of different vertebrates from birds to horses, disregarding their significant differences in body size and locomotor behavior (Bertram and Biewener, 1988; Biewener, 1982;

Biewener *et al.*, 1983, 1986; Lanyon and Rubin, 1984; Rubin and Lanyon, 1984; Vinyard and Ravosa, 1998).

When bone is compressed or tensed, not only will it deform in that direction, but it will also deform in a perpendicular direction. The first strain is called primary strain and the second is called secondary strain. The ratio of the secondary strain over primary strain is Poisson's ratio, and a measure of the ability of a structure to resist deformation in a direction perpendicular to that of the applied load.

$$\nu = -\frac{\varepsilon_y}{\varepsilon_x} \qquad \text{Equation 1.3}$$

where ν is Poisson's ratio; ε_y and ε_x are the secondary and primary strains, respectively. Poisson's ratio for human mandibular cortical bone has been reported to be 0.27-0.41 (Dechow *et al.*, 1993), i.e. a 1% primary strain will cause 0.27-0.41% strain in a direction perpendicular to the load.

The stress strain relationship follows Hooke's law if the deformation can be completely recovered when stress is released. This deformation is called elastic deformation. The ratio between the stress and strain is the Young's or elastic modulus.

$$E = \frac{\sigma}{\varepsilon} \qquad \text{Equation 1.4}$$

where E is the elastic modulus. Young's modulus is a measure of the ability of bone tissue to resist deformation in the direction of the applied load. Young's modulus is positively related to bone mineral density (Currey, 1984a). Because strain has no unit, its unit inherits the stress's unit Pa and is often expressed as GPa. Since bone is an anisotropic

material, the elastic modulus differs according to applied load directions. The elastic moduli for macaque mandibular buccal cortex are reported to be 9.0 GPa in the direction normal to the bone surface, 15.9 GPa in the tangential direction to the bone surface, and 21.0 GPa in the longitudinal direction. They are a little higher for the lingual cortex in macaque (Dechow and Hylander, 2000).

1.3.1.2 Shearing stress and strain

When forces are parallel to the plane of cross-section, they yield shearing stress. These forces are called shearing forces. The average shearing stress in the section can be depicted as

$$\tau = \frac{P}{A} \qquad \text{Equation 1.5}$$

where τ is the shearing stress; P is the shear load.

The amount of deformation occurring under shearing force is the shearing strain. The relationship between the shearing stress and strain in the elastic range also follows the Hooke's law, i.e.

$$G = \frac{\tau}{\gamma} \qquad \text{Equation 1.6}$$

where G is the shear modulus; γ is the shearing strain. The shear modulus is also called the rigidity modulus and is a measure of the ability of a structure to resist shear stress in a given plane. Bone is especially weak in shear. The shear modulus tends to be one third to half of the value of the elastic modulus (van Eijden, 2000). For example, the shear modulus for macaque mandibular buccal cortex is only 3.8-7.0 GPa depending on the directions (Dechow and Hylander, 2000). The shear

rigidity of bone cross-section can be raised by increasing the absolute amount of bony material (volume and/or density) in a cross-section.

1.3.1.3 Strength and stiffness

Both strength and stiffness are important properties of bone. Strength is related to stress and stiffness to strain. The stress at which bone yields is called the yield strength. This is the point that separates elastic from plastic deformation. The maximum stress that bone can sustain defines the ultimate strength. The breaking strength is the stress corresponding to bone break. Bone can be treated as brittle material and there is little difference between the ultimate strength and breaking strength (Beer and Johnston, 1981; van Eijden, 2000). The value of ultimate strength of bone tissue depends on the type of stress. Bone has lowest value for ultimate shear strength, middle value for ultimate tensile strength, and the highest value for ultimate compressive strength (van Eijden, 2000).

Stiffness is the ability of bone tissue to resist deformation within the linear range. Therefore, it is expressed as the modulus of elasticity. As mentioned earlier, bone is stiffest in its longitudinal direction, less stiff in its tangential direction and least stiff in the direction normal to its surface.

1.3.2 Biomechanical design of the mandibular corpus

A complete review on methods used in mandibular stress and strain studies can be found elsewhere (Daegling and Hylander, 2000). Here focus is placed on the methods that infer stress and strain patterns through study of the mandibular cross-sectional size, shape and bone distribution, i.e. the biomechanical design. First, two more basic concepts regarding engineering considerations in structural design are introduced.

1.3.2.1 Bending

When a beam is loaded under pure bending, it undergoes a stress gradient, i.e. tensile stress grows from zero at the centered neutral surface to maximum at the beam surface on one side and compressive stress increases from zero at the beam neutral surface to maximum on the other (Figure 1.1, p12). The neutral surface is also called the neutral axis.

The bending stress at any given point in the section (either compression or tension) can be given as

$$\sigma = \frac{Mc}{I} \qquad \text{Equation 1.7}$$

where M is the bending moment; c is the distance from the neutral surface; I is the cross-sectional moment of inertia (see Equation 1.10, p20) with respect to the axis perpendicular to the bending moment. Therefore, it is not difficult to deduce that the amount of stress can be decreased with an increased cross-sectional moment of inertia.

There are two ways to increase the cross-sectional moment of inertia. One is to add more material. An adverse effect of this approach is the increase in body weight. If material economy is the main concern, this is not a good remedy. Another method is to redistribute the material by moving the material from the less-stressed center to the outer surface, and thereby increases the external dimension of the beam. Expansion of the external dimension also increases the distance from the neutral surface to the external surface linearly, but the second moment of inertia is a function of the square distance. This will eventually increase the cross-sectional ability to resist bending. As the actual mass remains the

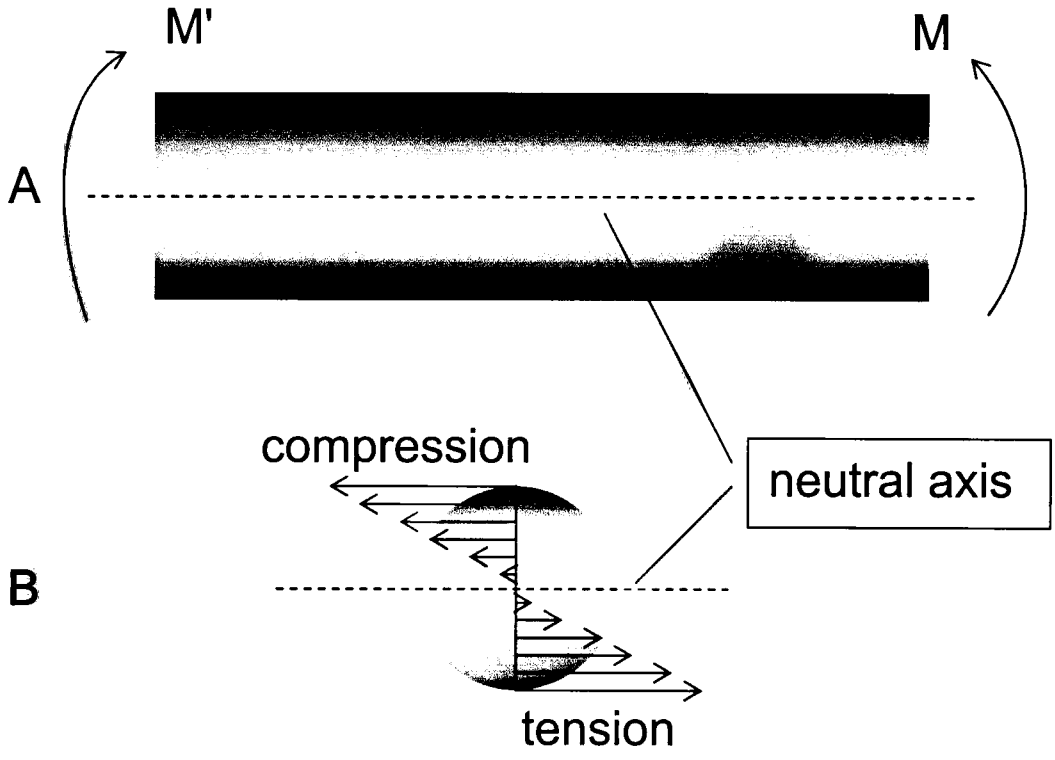

Figure 1.1 Beam bending theory. A: bending moment couple (M and M'); B: stress pattern in the cross-section. There is no stress at along neutral axis or surface. Both compressive and tensile stresses increase towards the beam surface. Based on van Eijden (2000).

same, this is an efficient, robust, and economic design. Because bending stress demonstrates a gradient with the highest stress at the surface and a gradual reduction towards the center, it demands that the material strength is also highest on the surface and lower towards the center. The ability to resist bending in one direction can be increased more efficiently if the dimension in the plane of bending is enlarged more than the dimension orthogonal to that plane (Figure 1.2, p14).

1.3.2.2 Torsion

When a torque is applied to a circular beam, the beam will twist. The fibers towards the surface twist more than those towards the center. The stress pattern in any given cross-section is shown in Figure 1.3 (p15). The torsional shear stress at any given point in the section can be described as

$$\tau = \frac{T\rho}{J} \qquad \text{Equation 1.8}$$

where τ is the torsional shearing stress; T is the applied torque; ρ is the distance from the beam center; and J is the cross-sectional polar moment of inertia (see Polar moment of inertia, p20). Therefore, to increase the ability to resist torsion, the best way is to raise the polar moment of inertia.

As in bending, there are two ways to increase the polar moment of inertia in a cross-section. One is to add more material to the section, with the adverse effect of increasing the mass of the beam. The second, and the best, method to increase polar moment of inertia is to move the material from the less-stressed center, to the outer surface (to increase the external dimension of the beam). Expansion of the external

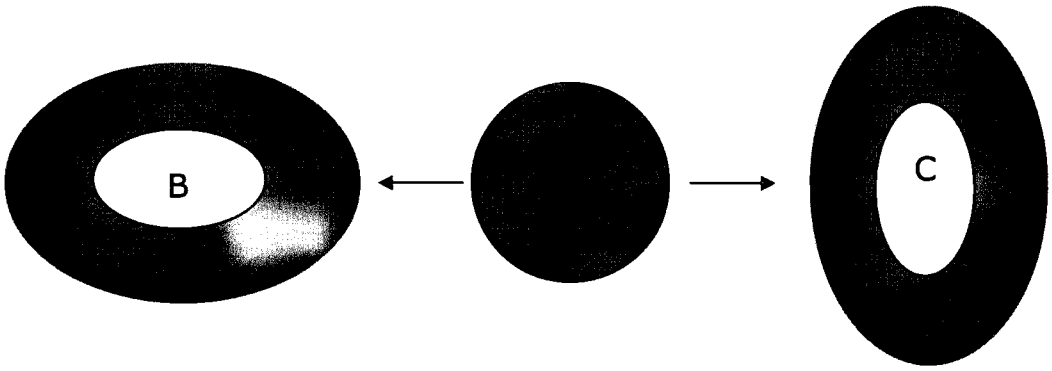

Figure 1.2 Best designs for resisting bending (by moving material from the center to the outer surface to create hollow sections). A: the original solid circular section; B: increased ability to resist transverse bending; C: increased ability to counter vertical bending.

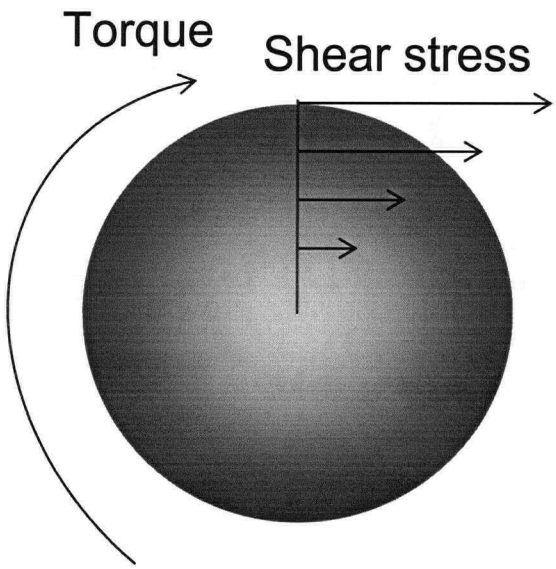

Figure 1.3 Stress pattern of a cross-section under torsion. Torsional shear stress increases from the center to the surface.

dimension also increases the distance from the center to the external surface linearly, but the polar moment of inertia is a function of the radius squared. This will eventually increase the cross-sectional ability to resist torsion. As the actual mass remains unchanged, this is an efficient, robust, and economic design. Because the torsional stress is in a gradient with the highest stress at the surface and the stress gradually reducing towards the center, it demands that the material strength is also highest on the surface, and gradually reducing towards the center. The best shape to resist torsional shear stress is a circular section, i.e. a hollow section retaining the circularity (Figure 1.4, p17).

1.3.2.3 Mandibular corpus cross-sectional form

Studies of the mandibular corpus cross-sectional form can provide insight into the biomechanical design of the mandible (Daegling, 1989). There are a number of ways to achieve a mechanically robust mandible, though how the mandible is designed may depend upon species. Primate studies (Dechow and Hylander, 2000; Hylander, 1979b) suggest that the mandible is built so as to use its bony material more economically than a solid rod of similar rigidity, i.e. it is a hollow section with the densest material distributed along the surface (cortical bone).

Daegling (1989) carried out what seems to be the first study on the "internal design" of the mandibular corpus. He used CT to examine mandibular cross-sections of Pan, Pongo, Gorilla Homo and two fossil specimens of Paranthropus at the first and second molars. The mandibular corpus cross-sections were measured as cortical and total sections. One of the significant findings in this study was that while the fossil hominids did not differ significantly from extant hominoids in the relative contribution of compact bone to total subperiosteal area, the

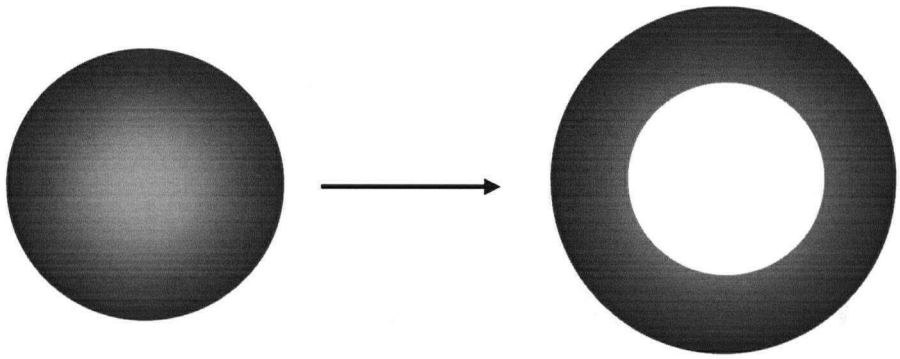

Figure 1.4 A better design for resisting torsion is to move material from the center to the outer surface to create a circular hollow section.

shape of the robust australopithecine mandible was fundamentally different from that of modern hominoids in terms of its ability to resist transverse bending and torsion (Daegling, 1989).

It has been suggested that the mandibular corpus might behave as an open and/or closed section under load (Hylander, 1979a; Smith, 1983). Previous studies (Daegling, 1989; Korioth *et al.*, 1992) support neither idea because the corpus is actually a combination of both (i.e. open for sections through the teeth and closed for sections between the teeth). Moreover, it seems that neither a solid- nor hollow-ellipse model adequately describes the mechanical behavior of the mandibular corpus cross-section, since neither model predicts cross-sectional area and moments of inertia with acceptable accuracy (Daegling, 1989).

Due to the structural complexity or irregularity of the mandibular corpus cross-section, it seems an investigation which includes regional cortical density (Daegling *et al.*, 1992; Daegling and Hylander, 1998) and cortical thickness might provide a better understanding of corpus biomechanics. Moreover, since the reported first and second molar sections are quite similar in their cross-sectional forms (Daegling, 1989), one would need to know whether this similarity applies to mandibular cross-sections at other locations, e.g. the canine and symphysis regions.

1.3.2.4 Cross-sectional measurements and their significance

1.3.2.4.1 Cross-sectional area

Since the stress is defined as internal resistance provided by a unit area (Beer and Johnston, 1981; Mott, 1996), cross-sectional area is one of the most important measurements in material mechanics for countering stress under normal or shearing load (Hearn, 1997; Mott,

1996; van Eijden, 2000). Unfortunately, this parameter does not reflect the distribution of material. It is obvious that the differential redistribution of the bony material is equally important for changes in mandibular mechanical properties as modification of the amount of compact bone utilized (Daegling and Grine, 1991). For example, adding more cortical bone at the center of the mandibular corpus does not have the same effect as adding the same bone to the periphery.

Because the mandibular corpus cross-section is not regular, the best way to calculate the area is by calculus, i.e. dividing the whole section into small, but equal-sized, square elements. The area of a cross-section can be calculated as

$$A = \int d_A \qquad \text{Equation 1.9}$$

where A is the cross-sectional area; dA is the area of each element. The unit can be expressed as cm^2 for the mandibular cross-section.

1.3.2.4.2 Second moment of inertia

Second moment of inertia or area is a measure of the distribution of bone around a particular axis. By depositing bone as far as possible from the neutral axis of the cross-section, the moment of area can be increased without an increase in the actual amount of material. In a cross-section with a large cross-sectional moment of area, stress can be kept relatively low. Hence, an increase in the cross-sectional moment of area is more optimal to sustain heavy bending loads (van Eijden, 2000). The second moment of area is axis-dependent. For any given cross-section, unlimited numbers of second moments of inertia can be calculated because the number of axes is infinite. In reality, it is usual to choose a pair of orthogonal axes (usually denoted as x, y). For a cross-

section with an ovoid shape like the mandibular corpus, it is intuitive to choose the major and minor axes. Therefore, the second moment of area with respect to the major axis (Iy, vertical axis in corpus section) is a measure of its ability to resist facio-lingual bending, and the second moment of area with respect to the minor axis (Ix, transverse) is a measure of its ability to counter sagittal bending.

Second moments of area must also be calculated by calculus for irregular section such as the mandibular corpus.

$$I_x = \int y^2 d_A$$

$$I_y = \int x^2 d_A$$

Equation 1.10

where *Ix*, *Iy* are the second moments of area with respect to the x-, and y-axis, respectively; *x*, *y* are the location of each element in the coordinate system with its origin at the centroid. The units for *Ix*, *Iy* are cm^4. Actual calculation of the second moments of inertia needs their translation from the original image matrix origin to the centroid by the parallel-axis theorem (Beer and Johnston, 1981; Beer and Johnston, 1988) because the centroid is unknown initially.

1.3.2.4.3 Polar moment of inertia

The polar moment of inertia or area, (which is actually the sum of the above two second moments of area), takes into account not only the amount of cortical bone area, but also the disposition of the cortical bone with respect to the center of mass. The further the bone tissue is deposited from the center of mass, the larger the polar moment of area. The larger the polar moment of area, the smaller is the induced shear stress and the larger the ability of the bone to resist torsional load.

Although this parameter has been used in literature to indicate the ability of a mandibular cross-section in torsion (Daegling, 1989; van Eijden, 2000), according to Gere and Timoshenko (Gere and Timoshenko, 1990), the torsion theory in formula (Equation 1.8, p13) is applicable to solid or hollow bars of circular cross-section only. Such shapes are not actually applicable for the mammalian mandible.

The danger of using Equation 1.8 (p13) to analyze mandibular torsion is obvious. In the cross-section as illustrated in Figure 1.5 (p22), the formula predicts stress at location A is less than stress at location B because A is closer to the center than B. This is in conflict with experimental results reported by Daegling and Hylander (1998).

1.3.2.4.4 Cortical index

The cortical index (a ratio between cortical and total areas) is a measure of the relative amount of cortical bone to the total bone. Daegling (1989) used the cortical area (all area enclosed by the cortical outline joined at the alveolar margins by a one mm thick cap, i.e. a hollow beam) and the total subperiosteal area (all area enclosed by the periosteal border to the alveolar margins, with a straight line connecting those margins, i.e. a solid beam). By definition, these areas do not take into account the density and possible porosity of the cortical and cancellous bone, so they do not measure true bony material. It seems that a higher value, i.e. relatively more cortical bone, might indicate a stronger cross-section. This may be misleading, however, as a solid section of compact bone has a cortical index equaling unity. This is not the ideal design for the mandibular corpus. A low cortical index may indicate a more economical use of material and therefore is a measure of robusticity (Daegling and Grine, 1991). The reported cortical indices for

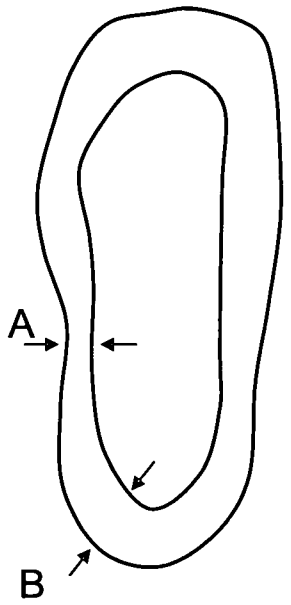

Figure 1.5 Diagram of a cross-section with variable wall thickness under torsional load. According to formula (Equation 1.8, p13), $\tau_A < \tau_B$, which conflicts with experimental data.

hominoid molar cross-sections vary between 0.29-0.54 (Daegling, 1989; Daegling and Grine, 1991). Whether this large variation indicates how efficiently different hominoids use material in their mandibular corpora varies greatly or not remains unknown.

It is possible to define another cortical index which takes such things as bone density and porosity into consideration, and to measure true bony material. The cortical area should be the bony cortex only, and the total area should include all bony material in the section. In both area measurements, areas not filled by bone (i.e. porosity) would be excluded. For example, if there is a hole in the cortex, it should not be counted as part of the cortical area. For a hollow section, a high value of this cortical index would indicate less trabeculation, and vice versa. Therefore, this index is also an indirect measure of the degree of trabeculation.

1.3.2.4.5 Bending index

The bending index (Iy/Ix, when Iy<Ix) is a shape indicator, because size is eliminated (Daegling, 1989). A low value signifies increased ability to resist bending stress about the short axis, with the loss of the ability to resist bending stress about the long axis. It is also a torsional rigidity index because if the size is constant, a bending index of unity indicates a rounded cross-section, which is the best design to sustain torsional stress (van Eijden, 2000). Therefore, there are two biomechanical consequences of high bending index values: an enhanced resistance to transverse bending rigidity and a more efficient shape for torsional rigidity (Daegling and Grine, 1991). This index, however, cannot be used to compare absolute bone rigidity. This bending index for the hominoid mandibular corpus has been reported to vary between 0.30-0.69 at the molar sections, in which the fossil hominoids demonstrate highest bending

indices (Daegling and Grine, 1991). The authors interpret this as structural response to elevated torsional moments.

1.3.2.4.6 Bone density

Another important factor, yet one which has not been taken into account in the previous studies (though mentioned by Daegling *et al.*, 1992, and Daegling and Hylander, 1998), is regional bone density. It is commonly recognized that bone mineral density is a consistent predictor of bone strength (Currey, 1984a; Hobatho *et al.*, 1997; Martin and Ishida, 1989; Stenström *et al.*, 2000), especially for cancellous bone (Rho *et al.*, 1995). The high linearity between the CT grayscale value and bone mineral density (Cheng *et al.*, 1995; Lampmann *et al.*, 1984; Zhang *et al.*, 2001a) encourages the use of CT grayscale values to represent regional bone density. When CT grayscale values are included, cross-sectional mass, second and polar moments of mass can be estimated in proportion. Cross-sectional mass seems to be a better variable indicating beam uniformity in the mandibular corpus, for the relative amount of material use by one cross-section can be easily compared to another within the same mandible.

It is understandable that CT grayscale values vary among different CT machines, and among different scans. Even a routinely calibrated CT machine does not guarantee a grayscale value consistency between different scans. Therefore, care must be taken when comparing specimens scanned in different machines and/or sessions, i.e. a reliable calibration phantom should always be included in the CT scan.

1.3.2.4.7 The centroid of a cross-section

In case of a homogeneous cross-section, the centroid or the center of

gravity or the center of mass can be calculated as

$$C_x = \frac{1}{A}\int x d_A$$

$$C_y = \frac{1}{A}\int y d_A$$

Equation 1.11

where *Cx*, *Cy* are the *x* and *y* coordinates of centroid, respectively.

In case of a heterogeneous cross-section like the mandibular corpus, the centroid can be calculated as

$$C_x = \frac{1}{M}\int x d_m$$

$$C_y = \frac{1}{M}\int y d_m$$

Equation 1.12

where *M* denotes the total cross-sectional mass; *dm* is the mass of each element.

When the second or polar moment of inertia is discussed, (if not specified), it should be with respect to the centroid instead of the origin of the image matrix, because the centroid is independent upon the cross-sectional position and orientation in the image matrix.

The centroid for all the cross-sections of a beam forms the centroidal axis. In a unified straight beam, the centroidal axis coincides with the neutral axis. In a curved beam with heterogeneous material like the mandible, however, the neutral axis does not coincide with the centroidal axis and is not determined immediately (Beer and Johnston, 1981). Since the two axes may actually be very close to each other, the centroidal axis has been used to approximate the neutral axis in primate jaw studies

(Hylander, 1985).

1.3.2.4.8 Variation in bone density and cortical thickness

If the assumption, that the stress pattern is linked to the distribution of cortical bone in a mandibular corpus cross-section, is valid, then the regional difference in bone density and cortical thickness in the mandibular cross-section should be taken into account. If we assume that regional bone rigidity is a function of the cortical thickness times the mean density of that region as demonstrated by the formula,

$$Rigidity = K \times Cortical\,Thickness \times Density \qquad \text{Equation 1.13}$$

where K is a constant, the product of the cortical thickness and mean CT grayscale value would be a cortical rigidity index (CRI). This index could be used to compare the cortical rigidities among cortices at different locations within a cross-section or cross-sections in the same mandible.

It must be stressed that this may not be a truly linear index, because the relationship between bone mineral density and bone mechanical property may not be linear (Lang *et al.*, 1997; Rho *et al.*, 1995; Stenström *et al.*, 2000).

1.3.2.5 Mandibular corpus loading and stress and strain

1.3.2.5.1 Sagittal bending of the mandible

Sagittal bending of the mandibular corpus is due to the vertical components of bite force, muscle force and condylar and symphyseal reaction forces acting in the tangential plane (the orthogonal plane to both the longitudinal and transverse planes) of the mandibular corpus

(Weijs, 1989). During unilateral biting, sagittal bending occurs on both sides of the mandibular corpora. On the working-side, sagittal bending causes tension along the lower border and compression along the alveolar side of the mandibular corpus. A reverse bending moment which tenses the alveolar processes and compresses the lower border of the mandible occurs on the balancing-side (Hylander, 1979b; Korioth *et al.*, 1992; van Eijden, 2000; Weijs, 1989). The ideal structural form for responding to this particular load is a relatively deep corpus in the molar region, which increases the cross-sectional second moment of inertia with respect to the transverse axis of the corpus (Daegling and Grine, 1991). In this respect, the prehistoric Polynesian "rocker" mandibles (Houghton, 1977, 1978) seem well-designed for such a loading condition.

Sagittal bending of the corpus also induces shearing stresses along the entire length of the mandible (Weijs, 1989). Shearing forces attain their largest values in the mandibular region between bite force and muscle force on the working-side, and in region between muscle force and joint force on the balancing-side (van Eijden, 2000). Shearing stress is inversely proportional to the cross-sectional area of the mandibular corpus, irrespective of its shape. Hence a certain amount of bony material should be present along the entire mandibular corpus.

As the shape of the mandibular corpus section is somewhat elliptical, both solid and hollow ellipse models have been proposed (Smith, 1983). And because of the extensive trabecular bone in some cross-section, a semi-solid model has also been mentioned (Hylander, 1985). Since the role of tooth is undetermined, both open and closed models have been considered (Korioth *et al.*, 1992). However, according to the formula (Equation 1.7, p11), for cross-sections to resist sagittal bending, all of the above models may be valid as long as the second moment of inertia truly

reflects the material distribution.

1.3.2.5.2 Transverse bending of the mandible

Medial transverse bending occurs during the jaw opening phase and lateral transverse bending occurs during the jaw closing phase (Hylander, 1985; Hylander and Johnson, 1994). Both lateral bending moments become largest at the symphysis. Thus the stresses caused by them are quite low at the molar region of the mandibular corpus but grow larger towards the symphysis in a linear manner (Daegling and Grine, 1991).

1.3.2.5.3 Mandibular torsion

Torsion of the mandibular corpus occurs on the working-side during the power stroke of mastication and on both sides during the power stroke of ingestion. In both cases, the twisting tends to evert the lower border of the mandible and invert the alveolar process. On the working-side, this specific load is partially reduced by the resultant masticatory bite force which tends to twist the corpus in an opposite direction (Hylander, 1979b). These twisting moments are highest in the molar regions (Daegling and Grine, 1991). To counter this kind of stress effectively, both the cross-sectional shape and bone distribution are critical. A circular hollow section with the maximum possible external dimension is the ideal design.

The bending index is a measure of the cross-sectional circularity. A value approaching unity indicates better circularity. The fact that mandibular corpus sections for modern hominoids are not as circular as the fossil specimens of Paranthropus supports the hypothesis that the Paranthropus mandible is more robust in resisting torsion (Daegling, 1989; Daegling and Grine, 1991).

Under torsional load, the mandibular corpus can be modeled as single- or multi-cell thin-walled tubular members (Cook and Young, 1985; Ugural and Fenster, 1987) depending on the intensity of the trabeculation. A single-cell thin-walled tubular member may be adequate to model cross-sections with less trabeculation. A multi-cell thin-walled tubular member might be appropriate for the mandibular corpus cross-section with extensive trabecular struts and columns.

For a thin-walled tubular member, the torsional shear follows a constant shear flow (f) throughout the shell, i.e.

$$f = \tau t \qquad \text{Equation 1.14}$$

where τ is the shearing stress for a location and t is the wall thickness at that location. Since f is constant, the largest shear stress occurs where the thickness of the tube is smallest and vice versa. As discussed earlier, use of a torsion formula (Equation 1.8, p13) causes conflicts with experimental results.

The calculation of shear stress can be performed according to the following formula:

$$\tau = \frac{T}{2tA_m} \qquad \text{Equation 1.15}$$

where T is the applied torque; Am is the area bounded by the centerline of the cross-section (dashed line in Figure 1.6, p30).

A multi-cell thin-walled tube can be analyzed by a simple extension of the one-cell analysis (Figure 1.7, p31).

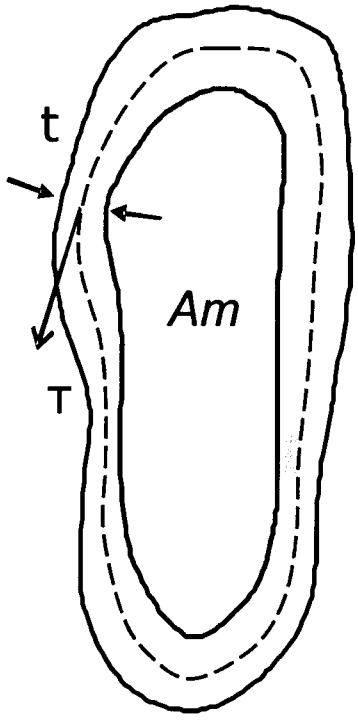

Figure 1.6 Cross-section of a thin-walled tube. The highest shear stress occurs where the thickness of the tube is smallest. The dashed line is the centerline of the cross-section and *Am* is the area bounded by the center line. T is the torsional stress and t is the wall thickness.

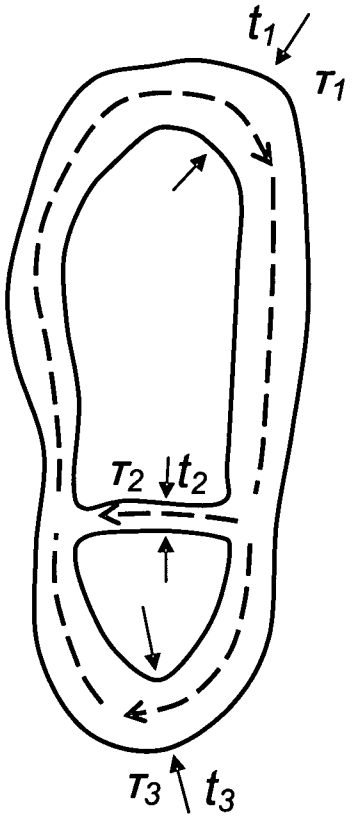

Figure 1.7 A multi-cell thin-walled tube can be modeled as an extension of a single-cell thin-walled tube. It is assumed shearing stresses are directed as shown, the shear flow yields $\tau 1t1 = \tau 2t2 + \tau 3t3$. This diagram shows a simple example of two cells, but the number of cells is not limited to two.

1.3.3 Biomechanical significance of the jaw symphysis

1.3.3.1 Symphyseal form and function

The mandibular symphysis remains unfused throughout life in most mammalian species. Fused symphyses only occur in some specific taxa including anthropoid primates and many artiodactyls. The functional advantages of fused and unfused mandibular symphyses in mammals have been reviewed recently by Lieberman and Crompton (Lieberman and Crompton, 2000). The unfused symphysis, by allowing independent inversion and eversion of the two halves of the mandible before and during the masticatory power stroke, enables the steep occluding surfaces of opposing teeth in some mammals to match during mastication (Hylander, 1979b; Kallen and Gans, 1972; Lieberman and Crompton, 2000; Oron and Crompton, 1985; Scapino, 1981). In contrast, the fused symphysis strengthens and stiffens the jaw, reducing its risk of structural failure as a result of lateral transverse bending or "wishboning", and from the dorsoventral shear stresses which occur during unilateral mastication (Hylander, 1984; Hylander *et al.*, 2000; Ravosa, 1996; Ravosa and Hylander, 1993; Ravosa and Simons, 1994). Mammals producing predominantly vertically-oriented occlusal forces tend to have unfused symphyses (which can transfer dorsally-directly forces with equal efficiency as in fused symphyses through their interdigitating rugosities), while mammals producing mainly transversely-oriented occlusal forces tend to have fused symphyses (Lieberman and Crompton, 2000).

Symphyseal fusion accompanies development of a functional occlusion. Partially-fused symphyses are common in juvenile animals, and complete fusion often takes place with the eruption of the permanent first molars (Ravosa, 1999). In the miniature pig, adult-like transverse masticatory

movements develop after weaning, and the mandible is subject to wishboning similar to that in anthropoids (Huang *et al.*, 1994).

The shape and size of the Cercopithecine symphysis appear to be allometric with body size and mandibular dental arch width, i.e. symphyseal width and length scale positively allometrically with body size, and negatively with mandibular dental arch width (Hylander, 1985). Since the width of the symphysis increases more rapidly than its length, there is also a change in symphyseal shape with increased body size (Figure 1.8, p34). These changes are believed to maintain functional equivalence in bone stresses and strains across taxa and ontogeny (Hylander, 1985; Vinyard and Ravosa, 1998). During wishboning, for example, tensile strains at the lingual border of the primate symphysis can approach 2,000 με, well-below 3,000 με, when structural failure is possible, i.e. adaptive remodeling alone cannot occur fast enough to cope with functional demands in animals which chew vigorously every day (Bouvier and Hylander, 1981a; Hannam *et al.*, 1997; Hylander, 1979b).

There is a general agreement that the form is linked to function. It has been suggested that the superior and inferior tori commonly found in anthropoid primates function to resist the effects of wishboning of the mandibular corpora (Hylander, 1984). However, due to large variation of the shape of the symphysis, using symphyseal morphology as a marker in species identification, or in systematic arguments is problematic (Daegling, 1993; Daegling and Jungers, 2000).

1.3.3.2 Symphyseal loading and stress and strain

If the purpose of the symphyseal fusion were to strengthen and stiffen the jaw, thereby reducing its risk of structural failure from the high stresses and strains during function (Hylander, 1984; Hylander *et al.*,

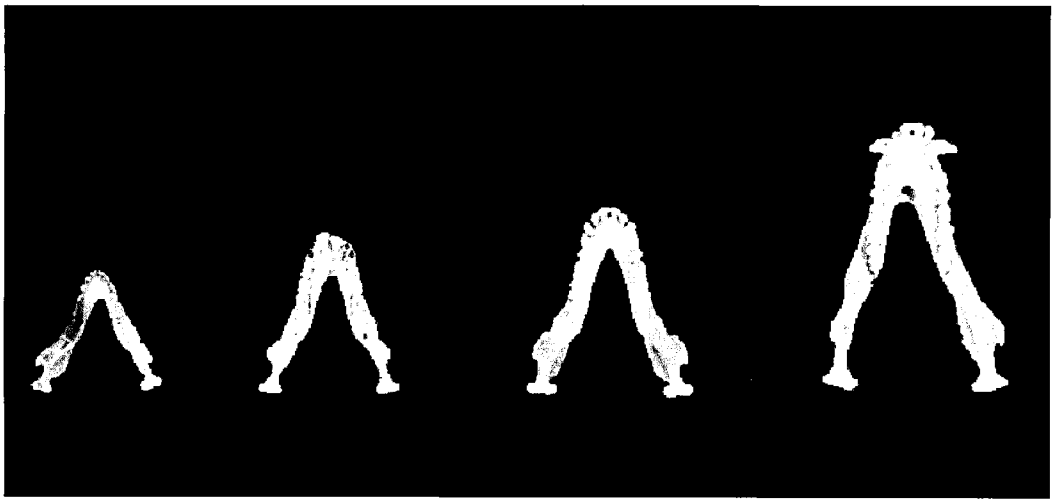

Figure 1.8 A growth series of Macaca fascicularis mandibles illustrating ontogenetic changes in symphyseal curvature. Shown from left to right are a juvenile with M1 erupting, a "subadult" with M2 erupting, an adult female, and an adult male. Inspection of this ontogenetic series indicates that the macaque mandible gets relatively longer during growth, while mandibular arch width becomes relatively narrower. This suggests a postnatal increase in symphyseal curvature—a pattern duplicating the interspecific allometric changes in curvature. From Vinyard and Ravosa (1998).

2000; Ravosa, 1996; Ravosa and Hylander, 1993; Ravosa and Simons, 1994), stress and strain analysis would be an appropriate method to reveal functional adaptation in the mammalian symphysis.

Several patterns of stress have been postulated to occur in the primate symphysis during function. These stresses have been reviewed in detail elsewhere (see Hylander, 1984). In brief, tension occurs along the lingual and/or infero-lingual side of the symphysis and compression occurs along the facial and/or supero-facial side of the symphysis during wishboning and/or twisting of the mandibular corpora. Wishboning is due to 1) the force from the deep masseter muscle on the balancing-side at the very end of the power stroke, 2) the lateral components of the bite force on the working-side, 3) probable transverse components to working-side jaw closing muscle forces (Hylander, 1984; Hylander and Johnson, 1994), and 4) the reaction force applied to the medial pole of the condylar head by the medial wall of the condylar fossa (Figure 4.4, p111). Twisting of the jaw occurs on the working-side during the power stroke of mastication and on both sides during the power stroke of ingestion due to the masticatory muscle forces (Hylander, 1979a, b).

Wishboning can create high tensile stresses and strains on the lingual surface of the symphysis. In primates, these tensile stresses are about 2.5 times larger than the compressive stresses on the labial surface (Hylander, 1985; Ravosa and Simons, 1994). They can be resisted by synostosis (Ravosa, 1996, 1999; Vinyard and Ravosa, 1998), bony enhancement (e.g. superior and inferior transverse tori), and increased horizontal orientation of the symphysis. These features are often seen in primates (Daegling, 1993; Hylander, 1984, 1985; Ravosa and Simons, 1994).

Tension occurs along the facial surface of the symphysis and

compression occurs along the symphyseal lingual surface during medial transverse bending of the mandibular corpora. Medial transverse bending of the corpora is due mainly to the bilateral contraction of the lateral pterygoid muscles (Hylander, 1985).

Torsion occurs along the transverse axis of the symphysis during powerful chewing when the working-side of the mandible is depressed and the balancing-side corpus is elevated (see Hylander, 1984).

Several patterns of shearing stress also occur in the symphysis. Dorsoventral shear is caused by the balancing-side jaw muscle force and due to the downward and upward movements, respectively, of the working-side and balancing-side mandibular corpora (Hylander, 1975, 1977, 1979a, b; Ravosa, 1996, 1999; Ravosa and Simons, 1994). Anteroposterior shear is due to the balancing-side temporalis having the tendency to pull the balancing-side dentary in a posterior direction relative to the working-side dentary during the power stroke (Beecher, 1977). Although this is observed in unfused symphyses, it is likely true in fused symphysis too (see Hylander, 1984).

Despite the complexity of the stresses occurring at the symphyseal region, the most important stresses are the tension and compression caused by wishboning, and dorsoventral shear. The cross-sectional area of bone and symphyseal shape affect the jaw's resistance to these stresses (Hylander, 1984, 1985), and an adequate cross-sectional area of bone in the plane of stress is needed to resist dorsoventral shear. In contrast, both the cross-sectional area of bone and symphyseal shape are significant in order to counter stress effectively during symphyseal wishboning (Hylander, 1984, 1985).

While *in vivo* bone strain studies provide a faithful depiction of the true

in vivo mechanical environment (Daegling and Hylander, 2000), there are some limitations. An alternative approach is to use the theories normally employed by mechanics of materials. This seems appealing. Unfortunately, many assumptions have to be made here; e.g. assuming the symphyseal cross-section is of regular shape, and made of uniform material, assuming the muscle force is constant or allometric to body weight, assuming the jaw length scales to the muscle lever arm, and assuming dental arch width represents the radius of mandibular curvature. If any of these assumptions are not true, the estimated stress and strain are questionable. Even so, postulates can be made, explained or defended (Vinyard and Ravosa, 1998). One approach might be to apply as much individual morphological and cross-sectional data as is available and compare the estimated stress and strain to the *in vivo* experimental results. Success here would complement *in vivo* experiments and offer stress and strain information where *in vivo* approaches are impossible.

1.3.4 Modeling jaw biomechanics

The data collected from direct human and animal experiments are often incomplete, though mathematical models can use incomplete data to provide hypothetical values for the missing variables (Hannam, 1994).

Models allow postulates to be demonstrated, explained, defended or altered as required. They invite informed speculation, for different scenarios can be constructed to explore new ideas, develop novel hypotheses, and gain insight into the consequences of system variables (Hannam *et al.*, 1997). Plausible models can mimic jaw function and biomechanics in the virtual environment, and allow alteration of variables. This is usually difficult or impossible to achieve *in vivo*.

1.3.4.1 Static jaw modeling

An easy way to simulate jaw, articular and occlusal function is to assume that the biological structures are rigid. In the static situation (e.g. during tooth clenching), equilibrium theory can be invoked to solve any bi- (two dimensional model) or tri-axial (three-dimensional model) forces acting within an arbitrary coordinate system, including unknown forces and torques created at locations of interest. The known inputs can be occlusal forces, and the unknown outputs can be muscle tensions and condylar forces (or vice versa), for it is axiomatic that all forces and torques in a closed, static system must be zero. Based on this theory, various models have been developed (Greaves, 1978; Koolstra *et al.*, 1988; Korioth *et al.*, 1992; Korioth and Hannam, 1994b; van Eijden *et al.*, 1988). The most advanced statics models are three dimensional finite element (FE) models in which regional physical properties are assigned to each group of elements to represent different tissues. These have been loaded by simulated muscle tensions to demonstrate deformation, stress and strain patterns in the mandible, and the differential loading patterns on the mandibular condyle (e.g. Korioth and Hannam, 1994b; Beek *et al.*, 2001). Evolution of these models involves comparing actual surface strains recorded on excised mandibles with strains predicted by the model (Korioth *et al.*, 1992).

1.3.4.2 Dynamic jaw modeling

The main limitation of static modeling is its inability to simulate jaw dynamics. Three-dimensional dynamic models of the human masticatory system have been developed by only a few groups very recently e.g. those by Koolstra and van Eijden (1995, 1997a, b), by Langenbach and Hannam (1999), and by Peck *et al.* (2000). These models work according to rigid body mechanics, although they can mimic compression and

distortions in the temporomandibular joint and muscles with "energy-storage" components such as spring-damper analogues (Peck, 1999). They incorporate a great deal of information with respect to jaw muscle morphology and properties, muscle tension and timing, dental occlusion, and jaw physical properties. The models are promising because they can use complex mathematical integration and convergence algorithms to predict jaw motion, the resulting reaction forces between parts, and derivatives of these values (Hannam *et al.*, 1997).

In contrast to static models, dynamic jaw models require specification of the jaw's mass properties including mass, mass center and moments of inertia. These can be difficult to estimate in biological tissues (Braune and Fischer, 1988) and the methods can be invasive and prone to errors (Braune and Fischer, 1988; Koolstra and van Eijden, 1995, 1997b). For example, to calculate the jaw's moments of inertia, Koolstra and van Eijden (1995, 1997b) cut an excised female cadaver jaw into cubic-centimeter blocks of tissue. In related studies, Hannam *et al.* (1997), Langenbach and Hannam (1999), Peck *et al.* (2000) assumed mass properties predicted by an FE model of the human jaw developed earlier (Korioth *et al.*, 1992). The FE model was constructed from CT images, and included elements with tissue properties specific for different jaw regions. The functional significance of these mass properties in dynamic modeling remains unclear, although it has been suggested the moments of inertia are less significant than mass center location in a simulated jaw-closing movements (Koolstra and van Eijden, 1995).

CT imaging is useful for mass-property calculation because x-ray linear attenuation discloses regional mineral densities (Cheng *et al.*, 1995; Lampmann *et al.*, 1984; Williams *et al.*, 1980), which account for much of the jaw's mass. Thus individual pixels with different intensity values,

distributed non-uniformly in the imaged mandible, can be assigned densities reflecting mineral content, making it possible to estimate the jaw's mass properties (Smith *et al.*, 1995).

To calculate mass properties from 3D CT, the CT grayscale value must first be converted into equivalent BMD. This can be fulfilled with a calibration phantom. Phantom studies have shown that the relationship between CT grayscale value and phantom equivalent BMD is almost linear ($r=0.99$ for KH_2PO_4 solutions; Cheng *et al.*, 1995; Lampmann *et al.*, 1984). Therefore the conversion from CT grayscale value to BMD is possible.

Because CT is invasive, it would be useful to explore less invasive approaches for estimating these mass properties in living humans. Candidate 3D imaging modalities include magnetic resonance imaging (MRI), 3D optical surface scanning and other 3D surface digitizing methods (Smith *et al.*, 1995). MRI seems more appropriate than others for it discloses both surface and internal structures. It does not however, image bone, nor reflect mineral density. Methods revealing jaw shape alone (like MRI) will not be valid unless it is clear that the jaw's mass and geometric centers coincide.

Jaw mass and moments of inertia also seem allometric with its dimensions. If a consistent relationship could be shown between them, it would be possible to estimate jaw mass and moments of inertia by simple, direct measurements.

1.4 FINAL COMMENT

Previous approaches in the study of jaw biomechanics, such as

analyses of cross-sectional shape and size, theoretical stress and strain, and mathematical modeling employ principles adopted from physics and/or the mechanics of materials. Although these principles are quite solid, the biological materials do not usually have the properties of engineering materials. Therefore, theoretical analyses need to be validated, where possible, by experimental results. In other words, theoretical analyses at best only complement experimental studies. Since *in vivo* experimental studies are presently limited in scope, and are likely to remain so, the approaches are interdependent. The exchange of information between experimental and theoretical studies is the way of scientific research; when based on available theoretical and experimental data, current hypotheses can be defended and novel hypotheses can be postulated and tested.

2 STATEMENT OF THE PROBLEM

Since the biomechanics of the mammalian jaw are not fully understood, experimental and theoretical studies can be used to complement each other. Elevating the value of one above the other is of dubious benefit. For example, even if *in vivo* bone strain studies are considered "gold standards", their interpretation depends upon assumptions regarding physical principles and the properties of a loaded beam. Conversely cross-sectional shape and size analyses, stress and strain estimation, and mathematical models are obviously theoretical, though they can incorporate more physical and engineering principles.

Cross-sectional shape and size analyses previously carried out on hominoid mandibles have only focused on the molar region, yet provided valuable biomechanical information linked to *in vivo* and *in vitro* stress and strain in the post-canine corpus. The biomechanical behavior of other mandibular corpus regions remains unclear. Furthermore, the bone-density contribution to corpus cross-sections is unknown, and regional variations in bone density and cortical thickness are not defined. Without such information, modeling the whole mandibular corpus is very difficult.

Although *in vivo* bone strain studies have provided insight into the symphyseal stress and strain patterns in non-human primates, it is impossible to apply this methodology in humans. Also, the literature has been devoid of *in vivo* bone strain information in the pig symphysis, despite the fact this is a preferred animal model for the study of the human masticatory system. The distinct morphological characteristics of the pig and human jaw symphyses however, encourage study of their respective stress and strain patterns.

Dynamic human jaw models require specification of mass properties, some of which have been necessarily derived from invasive measurements. Specification of mass properties would seem desirable for successful dynamic models simulating the human jaw function, especially when this might conceivably involve living subjects and subjects with missing jaw fragments. Biomedical computed tomographic imaging offers a solution here, for it discloses regional bone density at high resolution. MRI is even more promising because it is less-invasive and can unveil jaw shapes, though it is unable to disclose bone density.

Previous dynamic jaw models have been used to study jaw movements (Koolstra and van Eijden, 1995, 1997b), muscle functions (Koolstra and van Eijden, 1996, 1997a; Langenbach and Hannam, 1999; Peck, 1999; Peck *et al.*, 2000) and temporomandibular joint functions (Peck, 1999; Peck *et al.*, 2000). One of the advantages of dynamic jaw models is their ability to accept various structural and functional parameters to mimic situations difficult or impossible to study *in vivo*. They seem an ideal way to study forces and torques related to stress and strain in artificially created joints since the models are usually run in mathematically and physically proscribed environments.

In the present study, therefore, the following working hypotheses were proposed:

1. In humans, the densest cortical bone is found in sections with the least cortical area, and cross-sectional mass is uniform throughout the entire mandibular corpus and symphysis. Confirmation of this hypothesis would suggest that cross-sectional shear of the corpus is the main loading state of the human mandible.

2. Regional cortical rigidities (i.e. thickness and density) in human jaw

cross-sections differ with respect to locations, and are associated with local loading conditions. Confirmation of this hypothesis would relate bone regional rigidity to current hypotheses of jaw loading conditions, and suggest that modeling mandibular corpus cross-section requires specification of these differences.

3. The distinct shape and orientation of the pig jaw symphysis compared to that in man are adaptations to resist concentrated wishboning stresses and strains caused by strong muscle tensions, long lever arms and large symphyseal curvatures; these are important structural features to keep stresses and strains within the functional tolerance that bone tissue sustains. Confirmation of these hypotheses would contribute further evidence to existing notions of strain similarity, and improve comprehension of the structural and functional adaptations in mammals.

4. Mass properties of the mammalian jaw can be estimated with computed tomography. Bone density is uneven throughout the mandible, but mass is distributed symmetrically with respect to the geometric center, and mass and moments of inertia are positively allometric with the jaw dimensions. Confirmation of these hypotheses in pig and human mandibles would make approaches less-invasive than CT practical for future estimation, and widen the possibility for individual dynamic modeling in living subjects (including humans, pigs and other extant mammals).

5. Dynamic models of jaw biomechanics can be used to predict forces and torques passing through the mandibular symphysis during simulated normal function. These forces and torques change in time and reflect the complex loading conditions induced by changing muscle

contractions. Confirmation of these hypotheses would reinforce the suggestion that the pig mandibular symphysis is uniquely designed to accommodate the symphyseal loading, and encourage development of similar dynamic models in humans. Additionally, further modification of the model along similar lines would be feasible to predict loading patterns in other regions of the jaw, such as the molar and canine.

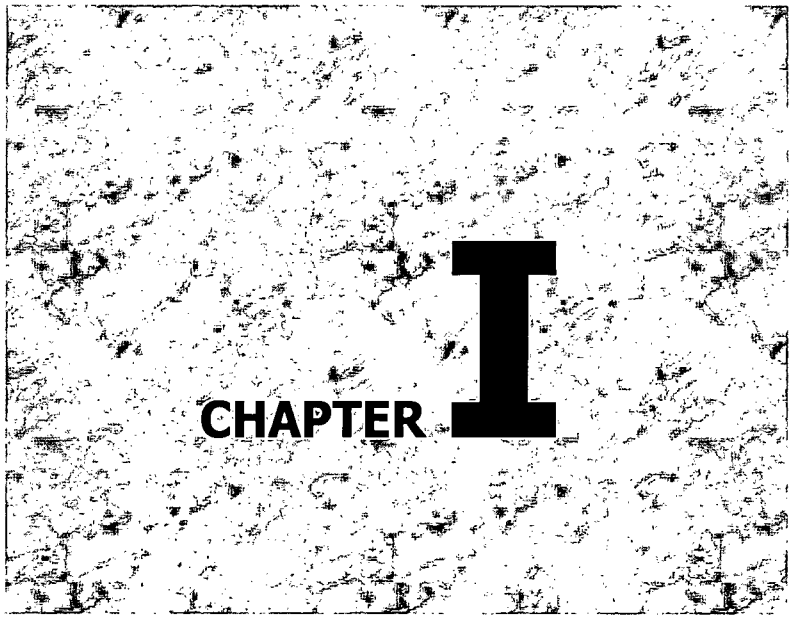
CHAPTER I

3 CROSS-SECTIONAL BIOMECHANICS OF THE HUMAN MANDIBLE

3.1 ABSTRACT

Cross-sectional analysis of the human mandibular corpus facilitates the understanding of its biomechanical behavior. Previous studies have focused on the post-canine region only, and have not included the effect regional bone density may have on cross-sectional mechanics. In this study, eight dry adult human mandibles were scanned with computed tomography (CT). Each mandible was resliced digitally to obtain cross-sections at the first molar, canine, and symphysis. Binary and grayscale total and cortical sections at each location were segmented. The cortical section was further segmented into lingual, facial and basal aspects. CT grayscale values were used as indices for regional bone density. The cross-sectional area and mass, second moments of area and mass were measured. Cortical and bending indices were also calculated. Paired t-tests (with Bonferroni's correction) were used to disclose significant differences among cross-sections at the three locations, and among the three regions of the cortical sections. Though cross-sectional areas varied among the three locations, their masses were similar, suggesting uniform shear rigidity. The distribution pattern of the cortical bone for each cross-section seems designed to withstand the specific stress pattern at that location. Since sagittal bending and torsion are the main stresses at the molar region, the cross-sections follow a hollow ovoidal shape with its long axis oriented almost vertically. In the symphyseal region, wishboning is the main source of stress, and this section had the most robust bone

on its lingual aspect. The canine region represented a transition between the molar and symphysis. In addition to sagittal bending, tooth-loading seems associated with basal bone robusticity. The bending indices indicated little shape differences among the three locations. The high grayscale cortical indices at the molar section signified less trabeculation. This study suggests, when modeling the mandibular corpus, cortical bone distribution, regional bone density, and trabeculation all need to be taken into account.

3.2 INTRODUCTION

During the power stroke of mastication, the mandible is subjected to forces produced by the jaw muscles and gravity, reaction forces at the temporomandibular joints, and reaction forces at teeth. These forces generate stresses and strains along the mandibular corpus and symphysis. The stresses can be analyzed individually by means of principles borrowed from the mechanics of materials. A number of stress-inducing conditions can occur in the mandibular corpus and symphysis during function. They include bending, torsion, and shear of the corpus and the symphysis.

Sagittal bending of the corpus is due to the vertical components of bite force, muscle force and condylar and symphyseal reaction forces acting in the tangential plane of the mandibular corpus (i.e. an orthogonal plane to both the longitudinal and transverse planes; Weijs, 1989). During unilateral biting, sagittal bending occurs on both sides of the mandible. On the working-side, sagittal bending causes tension along the lower border, and compression along the alveolar side of the mandibular corpus. A reverse bending moment which tenses the alveolar processes and compresses the lower border of the mandible

occurs on the balancing-side (Hylander, 1979b; Korioth *et al.*, 1992; van Eijden, 2000; Weijs, 1989). The ideal structure responding to this particular load is a relatively deep corpus in the molar region, which increases the cross-sectional second moment of inertia with respect to the transverse axis of the corpus (Daegling and Grine, 1991).

Sagittal bending of the corpus also induces shearing stresses along the entire length of the mandible (Weijs, 1989). Shearing forces attain the largest values in the mandibular region between bite force and muscle force on the working-side and in region between muscle force and joint force on the balancing-side (van Eijden, 2000). Shearing stress is inversely proportional to the cross-sectional area of the mandibular corpus, irrespective of its shape. Hence a minimum critical amount of bony material is required along the entire mandibular corpus.

Medial transverse bending of the corpus occurs during the jaw opening phase and lateral transverse bending of the corpus occurs during the jaw closing phase (Hylander, 1985; Hylander and Johnson, 1994). Both lateral bending moments become largest at the symphysis. Thus the stresses caused by them are quite low at molar region of the mandibular corpus but grow larger towards the symphysis in a linear manner (Daegling and Grine, 1991).

Torsion of the mandibular corpus occurs on the working-side during the power stroke of mastication, and on both sides of the jaw during the power stroke of ingestion. In both cases, the twisting tends to evert the lower border of the mandible, and inverts the alveolar process. On the working-side, this effect is partially reduced by the resultant masticatory bite force which tends to twist the corpus in

opposite direction (Hylander, 1979b). These twisting moments are highest in the molar regions (Daegling and Grine, 1991). To counter this kind of stress effectively, both the cross-sectional shape and bone distribution are critical, and a circular hollow section with a maximum possible external dimension is ideal.

Medial transverse bending of the symphysis is due mainly to the bilateral contraction of the lateral pterygoid muscles during the jaw opening phase of the chewing cycle (Hylander, 1985). Contraction of the medial pterygoid muscles may also contribute to this effect during the jaw closing phase (Hylander and Johnson, 1994). Lateral transverse bending (or wishboning) of the symphysis is mainly due to force from the deep masseter muscle on the balancing-side at the end of the power stroke, and to lateral components of bite force on the working-side, transverse components in the working-side jaw closing muscle forces (Hylander, 1984; Hylander and Johnson, 1994), and possibly the reaction force applied to the medial pole of the working-side condylar head by the medial wall of the condylar fossa (Figure 3.1, p51).

Medial transverse bending of the jaw symphysis produces tension along the facial surface and compression along the lingual surface in the symphysis (Hylander, 1984, 1985). Wishboning creates tensile stresses on the lingual surface and compressive stress on the facial surface of the symphysis. In a curved beam like the mandible, these stresses are not linear and the tensile stresses on the concave side are higher than the compressive stresses on the convex side (Figure 3.1, p51). In primates, these tensile stresses can be 2.5 times larger than compressive stresses (Hylander, 1985; Ravosa and Simons, 1994). They can be resisted by synostosis (Ravosa, 1996, 1999; Vinyard and

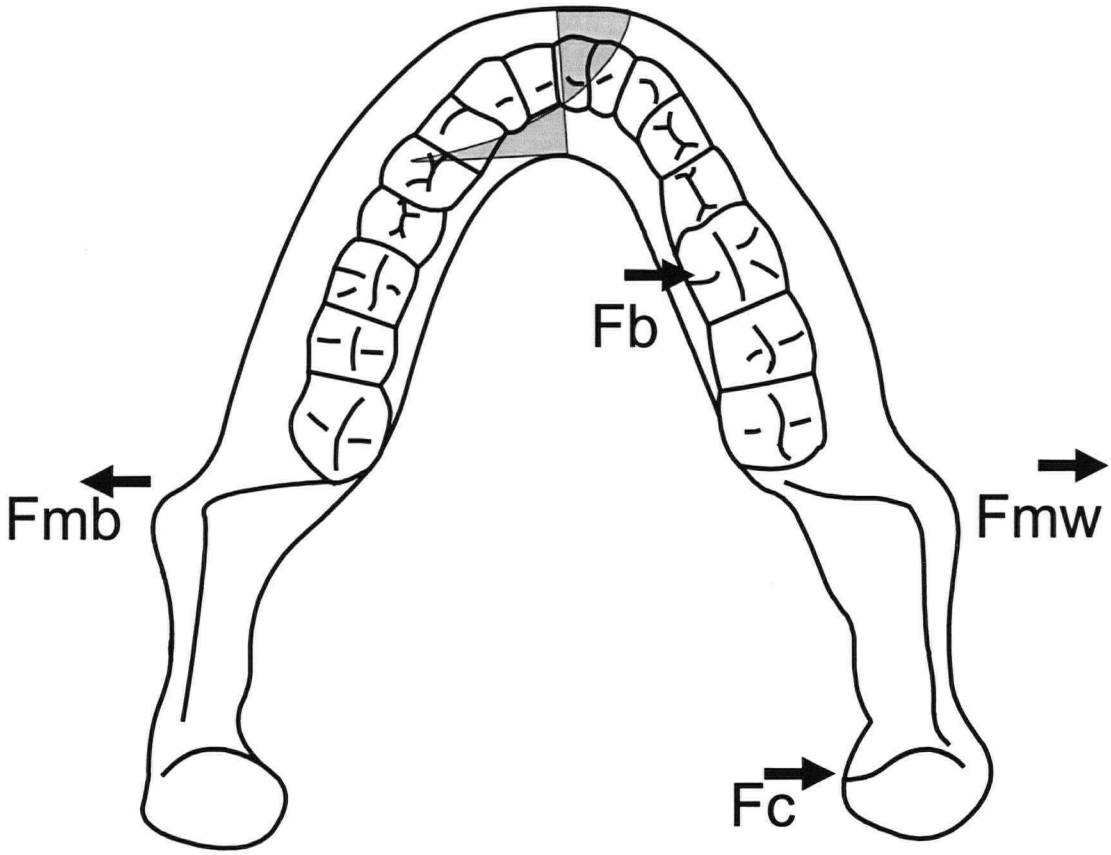

Figure 3.1 Suggested mechanism of wishboning in the human mandible. The main active forces are the balancing-side deep masseter (Fmb) and probably the transverse component to the working-side jaw closing muscle force (Fmw). Reaction forces from occlusion (Fb) and medial condylar pole (Fc) are the passive forces. Fb and Fc act in opposite direction of Fm. The force resultant tends to bend the mandible in its plane of curvature, causing tension on its lingual side and compression on its facial side. All force vectors indicate directions only. Their magnitudes are unknown. Based on Hylander and Johnson (1994).

Ravosa, 1998). Medial transverse bending of the symphysis causes reversed wishboning effect and the induced stresses are relatively low compared to the wishboning stresses (Hylander, 1985). The cross-sectional area of bone and symphyseal shape affect the jaw's resistance to these wishboning stresses (Hylander, 1984, 1985).

Symphyseal dorsoventral shear is caused by the balancing-side jaw muscle force and due to the downward and upward movements, respectively, of the working-side and balancing-side mandibular corpora (Hylander, 1975, 1977, 1979a, b; Ravosa, 1996, 1999; Ravosa and Simons, 1994). Adequate cross-sectional area of bone in the plane of stress is needed to resist dorsoventral shear.

There are a number of ways to achieve a mechanically robust mandible. The two extremes are to add cortical bone within the endosteal margins while external cross-sectional dimensions remain constant, and to increase the corpus dimension without adding additional compact bone. While the former is inefficient because material is added in regions where bending and torsional stresses are low, the latter is efficient in terms of material cost. How the mandible is designed in nature may depend upon species. Primate studies (Dechow and Hylander, 2000; Hylander, 1979b) have demonstrated that the mandible is built so as to use its bony material more economically than a solid rod of similar rigidity.

It is possible to quantify the amount of stress-bearing material in the mandibular corpus cross-sections through the nondestructive technique of computed tomography (CT) (Daegling, 1989; Daegling and Grine, 1991). This method also makes it feasible to estimate regional bone density. However, previous studies involving hominoid

mandibles (Daegling, 1989; Daegling *et al.*, 1992; Daegling and Grine, 1991; Daegling and Hylander, 1998) have been focused on the cross-sectional biomechanics of molar region only, and have not included bone density in their analyses. The importance of bone density in such studies has been emphasized previously (Daegling *et al.*, 1992; Daegling and Hylander, 1998).

In the present study, we evaluated the biomechanical significance of modern human mandibles at three sites including the first molar, the canine and the symphysis. Specifically, we tested the following hypotheses: that the densest bone occurs at cross-sections with the least cortical area; that the cross-sectional mass is uniform throughout the whole mandibular corpus; and that regional cortical rigidity (thickness and density) in a cross-section differs with respect to different regions, and is associated with local loading conditions. Confirmation of these postulates would improve our understanding of human jaw biomechanics, and contribute to the more appropriate models of the human mandibular corpus.

3.3 MATERIALS AND METHODS

3.3.1 Computed tomography

The experiments were carried out on eight osseous specimens with adult dentitions. They were selected from an existing collection of modern human mandibles, in which the gender and precise age of each specimen were unknown. Use of this archival material complied with the requirements of The University of British Columbia's Ethical Review Committee. All specimens were placed in a plastic box fixed with wooden spacers and remained in water during CT scanning. High

resolution CT slices with 512x512 pixels and voxel size of 0.43 x 0.43 x 1 mm^3 were obtained with a Toshiba Xpress SX scanner (kV=100, mA=150; Toshiba Corp., Tokyo, Japan) at The University of British Columbia. Although the criteria for positioning the mandibles in the plastic box were theoretically not critical, we arranged all mandibles to be imaged in the coronal plane to save space, i.e. they overlapped anteroposteriorly without contact.

3.3.2 Image processing

The original raw images were signed big endian 16-bit data. Because the image processing program we used (3Dviewnix, University of Pennsylvania Medical Center, Philadelphia, PA) did not accept minus 16-bit numbers, we wrote a dedicated PC program (RIC - Raw Image Converter, Craniofacial Laboratory, The University of British Columbia, available online at http://condor.dentistry.ubc.ca, or see Appendix, p222) to convert the original 16-bit images into 8-bit raw images. The 8-bit image files were then imported into 3Dviewnix running on an SGI Indigo Extreme workstation (Silicon Graphics Inc., Mountain View, CA). Each mandible was segmented and saved as a single file.

Cross-sectional slices at the left first molar (M1), the left canine (CA), and the symphysis (SY) regions were obtained by reslicing. The reslicing plane was oriented so that it was located at the center of the structure parallel to its long axis, and perpendicular to the facial surface at that region (Figure 3.2, p55). This procedure ensured a true cross-section at each location. Each slice was saved as uncompressed Microsoft Windows (Microsoft Corp., Redmond, WA) bitmap file for further processing on a desktop PC (Dual Pentium III 450 MHz).

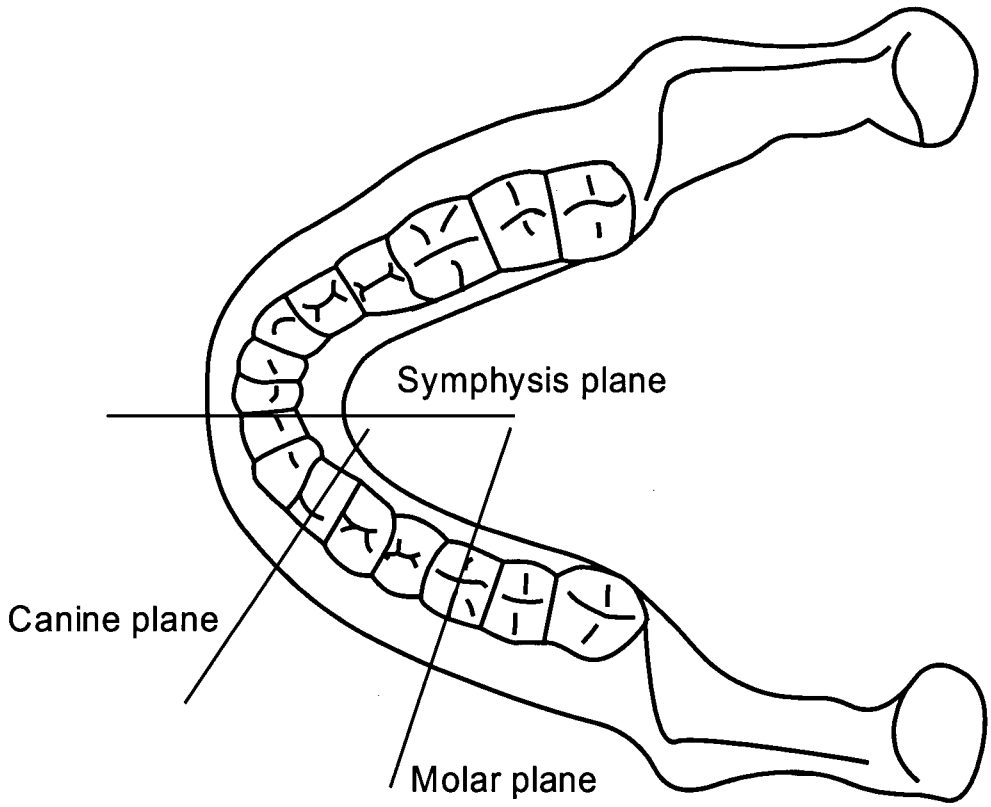

Figure 3.2 Diagram showing the three reslicing planes seen from above. See text for detail.

Commercial software (Paint Shop Pro 7, Jasc Software, Inc., Eden Prairie, MN) was used to complete further segmentation. Each section was first oriented so that its anatomical major axis was vertical in the image matrix. Four groups of segmented images were created. They included grayscale total sections, grayscale cortical sections, binary total sections and binary cortical sections. For grayscale sections, inhomogeneities in cortical bone and porosities in cancellous bone were left intact; for binary sections, the enclosed areas were filled with white pixels. The cortical sections did not include any cancellous bone or marrow spaces. This was accomplished by means of a freehand selection tool, which enabled all internal structures (including trabecular bridges) to be removed. The resultant sections thus provided either open or closed hollow models. To obtain binary cortical sections, we selected the edges of the cortex contour, deleted the cortical contents, and converted this area to pure black, then inverted the cortex. This ensured that the cortex was a unique white area. To obtain binary total sections, we took the binary cortical sections, capped the cross-sections with a single pixel line across the top margin of the alveoli (see Daegling, 1989) and performed the same tracing and inverting method described above. These final total sections were closed sections with unique white contents (Figure 3.3, p57).

To reveal regional differences within each cortex, the grayscale cortex was further segmented into lingual, facial and basal aspects. The lingual and facial aspects were split by the major axis, while the basal cortex was considered to be the lower part below a horizontal line at the upper edge of the basal cortex (Figure 3.4, p58).

3.3.3 Cross-sectional measurements

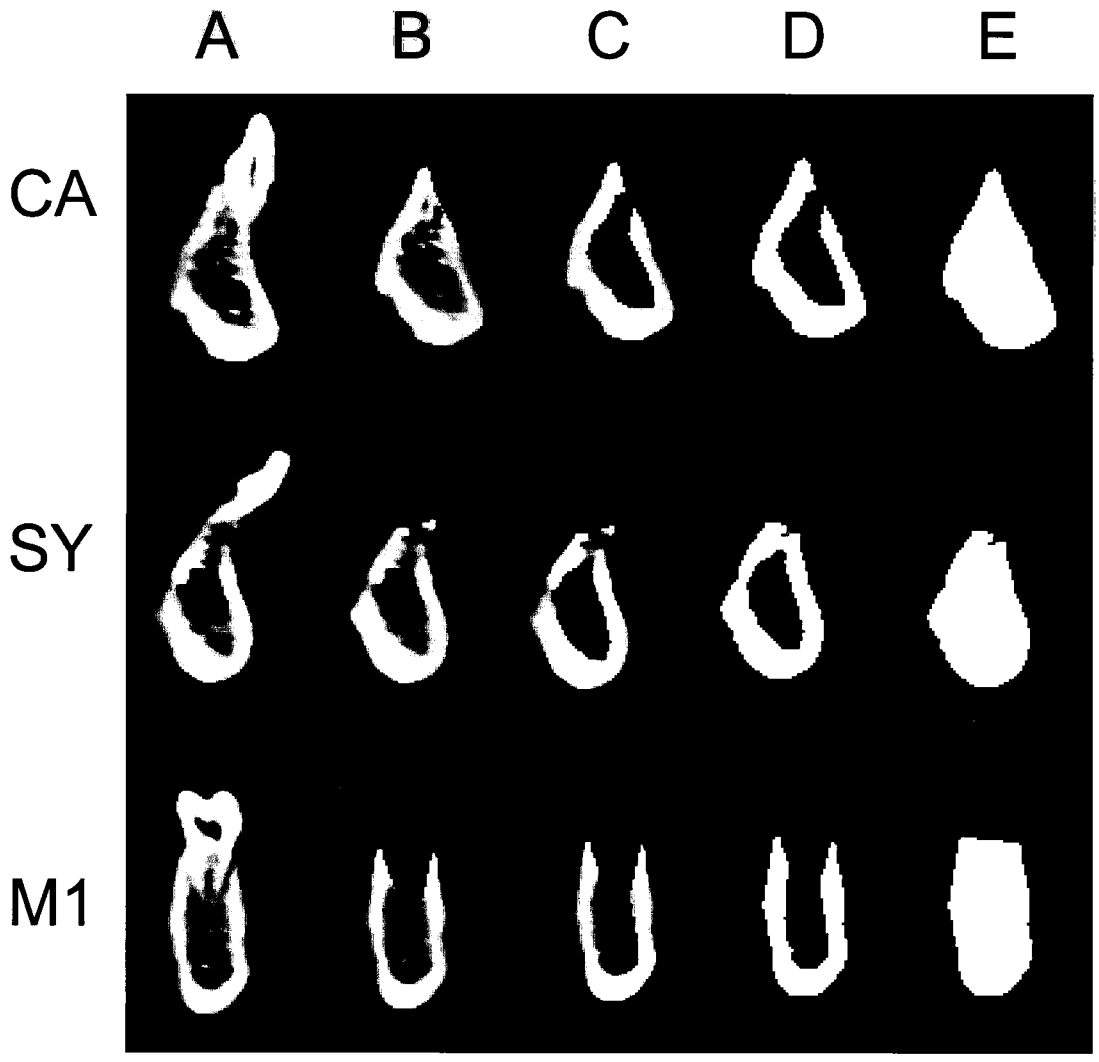

Figure 3.3 Three typical cross-sections at the canine (CA), the symphysis (SY) and the first molar (M1). Vertically, A: original sections; B: grayscale total sections; C: grayscale cortical sections; D: binary cortical sections; E: binary total sections. For all sections, left side is lingual and right is facial.

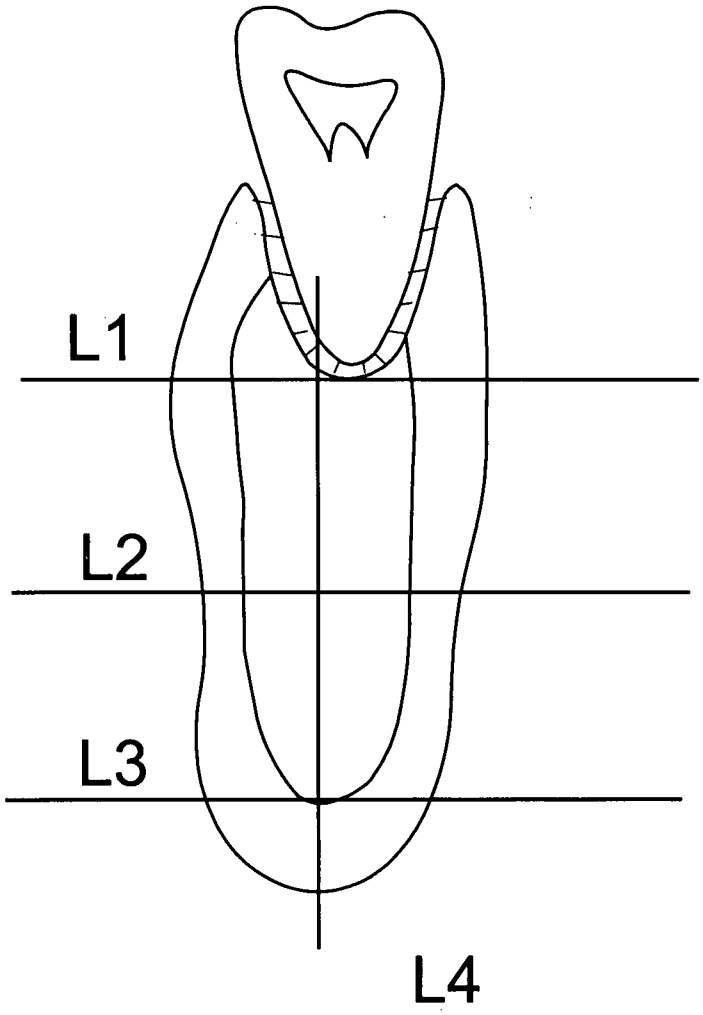

Figure 3.4 Definition of regional cortical thickness. L1, L2 and L3 represent the three levels for the facial and lingual cortical measurements, from which the mean cortical thicknesses were calculated; L4 denotes the location where the basal cortical thickness was measured. L4 is also the line that separated the facial and lingual cortices and L3, the line where the basal cortex was detached.

For each cross-section, the cross-sectional area and second moments of area (Ix, Iy) were measured, and the cortical index (a ratio between cortical area and total area, CI), and the bending index (BI, Iy/Ix) were also calculated. For each grayscale cross-section, the mean grayscale value (MGSV), cross-sectional mass, and second moments of mass (Ixm, Iym) were measured, and the mass cortical index (CIM) and the mass bending index (BIM, Iym/Ixm) were then calculated. All measurements were performed digitally at the pixel level by a custom program (Calimage - Calculate Image, Craniofacial Laboratory, The University of British Columbia; available from http://condor.dentistry.ubc.ca, or see Appendix, p226). This program batch-processed all image files, and output the results in comma-delimited text formats, which were then imported into Microsoft Excel® (Microsoft Corp., Redmond, WA). We wrote this program with Borland C++ Builder 5.0 (Imprise Corp., Scotts Valley, CA). All area and second moment calculations were made according to conventional formulae (Beer and Johnston, 1988).

To assess regional variations within each grayscale cortical section, we calculated the MGSV, and measured the mean cortical bone thickness in each of the three regions. The mean cortical bone thickness was measured on the binary cortical cross-section. We divided this distance (from below the tooth root apex towards the upper edge of the basal cortex) into two portions, and performed three measurements, each representing the horizontal thickness of the cortex at that location. A mean value was calculated to represent the mean cortical bone thickness for each side. The cortical thickness at the basal aspect was measured from the point where the major axis intersects with the basal cortex. The thickness multiplied by its

corresponding MGSV provided the cortical rigidity index (CRI), considered an indicator for cortical bone rigidity (Figure 3.4, p58).

3.3.4 Statistical Analysis

Since the image processing included subjective segmentation operations, we carried out an error study, in which we allowed two persons to perform the same segmentation processes according to the same criteria. We then calculated the number of pixels included in each image, and applied paired t-tests on the two sets of images. For operator one, the mean number of pixels was 1201 (SD 264), while for operator two, it was 1192 (SD 229). There was no statistical difference between the two samples ($P>0.05$).

Since we were interested in comparing the biomechanical properties of the cross-sections at the three regions (M1, CA and SY), and as each site was represented by a group, paired t-tests with Bonferroni's inequality corrections (B-method) were used to indicate any statistically significant difference (at the 5% level) for each measured or calculated parameter. This correction reduced the chance for false positive results. The same test was used to detect regional differences between the lingual, facial and basal aspects of the grayscale cortical section.

To test whether cortical bone distribution was isometric, one sample t-tests were used for differences between the geometric centers of binary cortical and total cross-sections versus zero.

Finally, the areas and moments of inertia predicted by ideal solid and hollow ellipse models (i.e. with the calculated vertical and horizontal dimensions representing their respective major and minor

axes, and mean cortical thickness representing the uniform wall thickness) were compared by means of paired t-tests to the measured binary total and cortical areas and moments of inertia.

All statistical analyses were carried out with SPSS 8 (SPSS Inc., Chicago, IL).

3.4 RESULTS

3.4.1 Binary cross-sections

Descriptive statistics for the areas, second moments of areas, cortical indices, bending indices, and B-method paired t-test results are presented in Table 3.1 (p62). There were no statistically significant differences between cross-sections at CA and M1, or between CA and SY for all area and moment measurements. However, the cross-sections at M1 differed from SY in total area, and in total Ix. In each case, cross-sections at M1 were greater than at SY. Differences were also found between cortical indices for cross-sections at M1 and SY. The cross-sections at M1 had the least relative cortical bone. The bending indices for both cortical and total sections were similar through the entire mandibular corpus.

3.4.2 Grayscale cross-sections

Table 3.2 (p63) provides the results of measurements, and B-method paired t-tests for the grayscale cross-sections. Unlike the binary cross-sections, more differences were disclosed. First, MGSV of M1 was the greatest, and there was no MGSV difference between CA and SY. Though the total area at M1 was the least, its total mass, and

Table 3.1 Area (cm^2), moment of area (cm^4), bending and cortical indices for the binary total and cortical cross-sections. Also shown here are the paired t test (B-method) p values. Blank spaces indicate non-significant comparisons. Abbreviations: CA, canine; M1, first molar; SY, symphysis. Ix and Iy, moments of inertia around x and y axes respectively; BI, bending index; CI, cortical index.

	CA		M1		SY		Paired t test		
	Mean	SD	Mean	SD	Mean	SD	CA vs. M1	CA vs. SY	M1 vs. SY
Total									
Area	2.83	0.37	2.98	0.48	2.63	0.40			0.03
Ix	1.44	0.55	1.52	0.56	1.16	0.44			0.03
Iy	0.36	0.11	0.37	0.13	0.31	0.09			
BI	0.26	0.08	0.25	0.06	0.28	0.09			
Cortical									
Area	1.78	0.45	1.53	0.21	1.64	0.27			
Ix	1.10	0.63	0.86	0.34	0.90	0.36			
Iy	0.30	0.10	0.30	0.11	0.27	0.08			
BI	0.31	0.10	0.36	0.09	0.31	0.09			
CI	0.63	0.11	0.52	0.03	0.63	0.06			<0.01

Table 3.2 Area (cm^2) and mass (cm^2), MGSV, second moment of area (cm^4) and second moment of mass (cm^4), bending and mass bending indices, and cortical and mass cortical indices of the grayscale total and cortical cross-sections. Also shown here are the paired t test (B-method) p values. Blank spaces indicate non-significant comparisons. Abbreviations: CA, canine; M1, first molar; SY, symphysis. Ix and Iy, moments of inertia around x and y axes respectively; BI, bending index; CI, cortical index; Ixm and Iym, mass moments of inertia around x and y axes respectively; BIM, mass bending index; CIM, mass cortical index; MGSV, mean grayscale value.

	CA		M1		SY		Paired t test		
	Mean	SD	Mean	SD	Mean	SD	CA vs. M1	CA vs. SY	M1 vs. SY
Total									
Area	3.17	0.52	2.4	0.44	3.17	0.47	<0.01		<0.01
Mass	125.2	25.8	110.7	20.9	117.6	19.3			
MGSV	39.26	3.18	46.07	1.74	37.08	2.65	<0.01		<0.01
Ix	1.77	0.84	1.23	0.53	1.66	0.59	0.03		0.03
Iy	0.57	0.14	0.45	0.15	0.5	0.14			
Ixm	71	37.1	60.39	26.4	53.86	20.2			
Iym	18.25	6.62	19.93	7.58	15.92	5.32			
BI	0.35	0.1	0.38	0.09	0.32	0.11			
BIM	0.28	0.1	0.34	0.1	0.31	0.1			
Cortical									
Area	2.43	0.51	1.9	0.24	2.29	0.32	0.03		<0.01
Mass	105.5	27.9	102.7	16.1	89.13	16.4			0.01
MGSV	43.13	3.76	53.91	3.79	38.87	3.22	<0.01		<0.01
Ix	1.62	0.83	1.12	0.4	1.46	0.5			0.04
Iy	0.53	0.13	0.42	0.13	0.46	0.13			
Ixm	65.36	38.4	58.11	24	47.79	18.4			0.03
Iym	17.07	6.25	19.43	7.28	14.59	4.9			
BI	0.36	0.1	0.39	0.09	0.34	0.11			
BIM	0.3	0.11	0.34	0.1	0.32	0.09			
CI	0.76	0.06	0.8	0.07	0.72	0.04			
CIM	0.84	0.07	0.93	0.04	0.76	0.05	0.02	0.03	<0.01

second moments of inertia approached those of the other two sections. A similar pattern was seen for cortical sections, except for cortical mass and second moment of mass with respect to the transverse axis (Ixm) at SY (which showed an opposite relationship to those at M1).

The bending, and mass bending indices were similar for the total and cortical cross-sections. While no cortical index differences were revealed among the three sections, their mass cortical indices differed between each pair.

3.4.3 Cortical thickness, density and rigidity index

Table 3.3 (p65) summarizes the means, standard deviations, and paired t test results for MGSV, cortical thickness, and the cortical rigidity index for the lingual, facial and basal regions of the grayscale cortex. For all cross-sections, MGSV was significantly higher at the basal aspect than the facial and lingual aspects. While facial and lingual MGSVs did not differ in CA and M1 sections, MGSV in the lingual aspect was higher than that at the facial aspect for SY section.

The cortical thickness of the basal aspect was greatest in the CA and M1 sections. In M1, the cortical thickness was equal for both facial and lingual aspects. However, it was thicker on the lingual aspect in both CA and SY sections.

The basal CRI was the greatest for both CA and M1 sections. It was, however, almost equal to the lingual CRI in the SY section. There were no CRI differences between the facial and lingual regions at M1, or between the lingual and basal regions at SY.

Table 3.3 MGSV, cortical thickness and cortical rigidity index of the lingual, facial and basal cortices. Also shown are paired t test p values (B-method) between lingual and facial, lingual and basal, and facial and basal cortices at the three locations. Abbreviations are in the text. Blank spaces indicate non-significant comparisons. Abbreviations: CA, canine; M1, first molar; SY, symphysis; MGSV, mean grayscale value.

	MGSV			Thickness			CRI		
	Mean	SD	P	Mean	SD	P	Mean	SD	P
CA									
Lingual	39.1	1.9		3.74	0.67		146.05	28.05	
Facial	39.6	5.6		2.3	0.35		92.08	23.43	
Basal	53.2	3.2		4.54	0.74		242.02	44.38	
Facial vs. lingual						<0.01			<0.01
Lingual vs. basal			<0.01			0.01			<0.01
Facial vs. basal			<0.01			<0.01			<0.01
M1									
Lingual	46.7	2.3		2.68	0.24		125.15	13.03	
Facial	45.2	4.8		2.6	0.42		118.2	26.48	
Basal	60.6	4.2		4.14	0.69		252.12	53.26	
Facial vs. lingual									
Lingual vs. basal			<0.01			<0.01			<0.01
Facial vs. basal			<0.01			<0.01			<0.01
SY									
Lingual	40.4	3		3.64	0.69		148.35	39.23	
Facial	33.3	2.8		2.47	0.26		81.9	9.39	
Basal	46.1	4.5		3.17	0.72		148.3	44.59	
Facial vs. lingual			<0.01			0.01			0.01
Lingual vs. basal			0.02						
Facial vs. basal			<0.01						0.02

3.4.4 Bone isometry

The differences between the cortical geometric centers, and the total geometric centers at CA, M1 and SY were 1.30±0.62 mm, 1.96±0.41 mm, and 0.65±0.59 mm, respectively. T-tests against zero showed they all differed from zero ($p<0.05$), though it seemed SY was more isometric than others.

3.4.5 Predictions by ideal models

Ratios between areas and moments of inertia predicted by elliptical models, and the respective actual measurements, are shown in Table 3.4 (p67). T-tests against unity indicated most ratios differed from unity except for cortical Iy at CA.

3.5 Discussion

3.5.1 Error of method

There was likely minimal error in our area and moments of area calculations because they were performed at the pixel level; however, the number of pixels involved in such calculation is critical, and would have been affected by subjective segmentation. We did not trace the images on paper as has been done previously (Daegling, 1989; Daegling and Grine, 1991), but the segmentation process was nevertheless arbitrary. For example, when we removed a tooth from the cross-section, we manipulated the brightness and contrast of the monitor to optimize edge definition, and to minimize errors. To keep the original grayscale values intact, however, we did not perform any image color operations which would have altered the original grayscale

Table 3.4 Ratios between area and moments of inertia predicted elliptical models and the respective actual measurements. T tests were performed against a constant of unity. Abbreviations: CA, canine; M1, first molar; SY, symphysis. Ix and Iy, moments of inertia around x and y axes respectively.

	Total			Cortical		
	Area	Ix	Iy	Area	Ix	Iy
CA						
Mean	1.18	1.18	1.40	0.62	0.79	1.00
SD	0.14	0.20	0.31	0.02	0.06	0.18
P	0.01	0.04	0.01	<0.01	<0.01	0.97
M1						
Mean	0.94	0.83	0.89	0.59	0.70	0.65
SD	0.03	0.04	0.06	0.05	0.08	0.05
P	<0.01	<0.01	<0.01	<0.01	<0.01	<0.01
SY						
Mean	1.12	1.11	1.29	0.56	0.66	0.83
SD	0.06	0.11	0.11	0.06	0.10	0.06
P	<0.01	0.02	<0.01	<0.01	<0.01	<0.01

values. We defined the edge for cortical and cancellous bone in the same way. Also, our inter-operator error for segmentation was low. To minimize automatic edge detection errors in Jasc PaintShop Pro, we selected a tolerance value of 20 for all cross-sections, i.e. it was reproducible.

The selection of the reslicing plane used to obtain our cross-sections was arbitrary, and also subject to human error.

The multiple-comparison problem (Fisher and van Belle, 1993) could have been significant if no correction had been carried out. This problem occurs when many statistical procedures are being applied to the same data. It was for this reason we performed Bonferroni's inequality corrections on our paired t-test results, to minimize the chances of incorrectly rejecting the null hypotheses.

3.5.2 Significance of cross-sectional measurements

Since stress is defined as internal resistance provided by a unit area (Mott, 1996), cross-sectional area is one of the most important measurements in the material mechanics for countering normal (direct axial) and shear stresses (Hearn, 1997; Mott, 1996; van Eijden, 2000). Our data suggest that though cross-sectional area varies among the three sections, their total masses remain surprisingly uniform throughout the corpus, i.e. in regions with smaller areas such as the molars, denser bone is required (Table 3.2, p63), matching a previous finding that mandibular apparent density is negatively correlated with the cross-sectional area (Kingsmill and Boyde, 1998). This might lead to an immediate conclusion that the mandibular corpus is uniform in its ability to resist normal and shear stresses. The reason denser bone

has better shear rigidity can be explained theoretically. It has been reported that highly mineralized bone has high Young's modulus (Currey, 1984a), and the bone's shear modulus lies between one third to half of the elastic modulus (van Eijden, 2000). The area parameter, however, does not reflect the distribution of material, and axial loads (i.e. during anteroposterior shear) are not the main sources of stress. It is obvious that the differential distribution of bony material is more important to changes in mandibular mechanical properties than modification in the amount of compact bone (Daegling and Grine, 1991). For example, adding more cortical bone in the center of the mandibular corpus does not have the same effect as adding the same bone to the periphery.

The second moment of area is a measure of the distribution of bone around a particular axis. By distributing bone as far as possible from the neutral axis of the cross-section, the moment of area can be increased without an increase in material. In a cross-section with a large cross-sectional moment of area, stress can be kept relatively low. Hence, an increase in the cross-sectional moment of area is more optimal to sustain heavy bending loads (van Eijden, 2000). For a cross-section with an ovoidal shape like the mandibular corpus, its ability to resist bending about its minor axis (i.e., facio-lingual axis) is greater than about its major axis (i.e., superoinferior axis). This is the main bending load during mastication. Our data are consistent with this assumption (Table 3.1, p62, and Table 3.2, p63).

The cortical index (ratio between cortical and total areas) is a measure of the relative amount of cortical bone to the total bone. Different kinds of cortical indices have different meanings. The cortical index reported by Daegling (1989) used the cortical area (the entire

area enclosed by the cortical outline joined at the alveolar margins by a one mm thick cap, i.e. a hollow beam) and the total subperiostium area (the area enclosed by the periosteal border to the alveolar margins, with a straight line connecting those margins, i.e. a solid beam). By definition, both areas do not take into account the density or the possible porosity of cortical and cancellous bone. It would seem that a higher value, i.e. relatively more cortical bone, might indicate a stronger cross-section. This may be misleading, because a solid section of compact bone has a cortical index equaling unity. This is, of course, not the optimal design for the mandibular corpus for it is not efficient, or robust, or economical. A low cortical index might also indicate a more economical use of material, and is a measure of robusticity (Daegling and Grine, 1991). In this case, the molar section of the human mandible seems more robust than the canine and symphysis (Table 3.1, p62). However, our binary cortical index for the molar section was a little higher than that published previously (0.50 vs. 0.40, the latter being obtained from five female and five male human mandibles; Daegling, 1989). This may have been due to the different tracing methods used in the two studies (digital vs. paper). The indices were even higher for the canine and symphysis sections.

The cortical indices (ratios between grayscale cortical and total cross-sectional areas or masses) we introduced in the present study reflected the degree of cross-sectional trabeculation. It is obvious that the values of these indices should be higher than that of the binary cortical index. Our grayscale cortical indices at the three locations were similar. However, their mass cortical indices were different, the highest value occurring at the molar section, and the lowest at the symphysis. In other words, the symphysis had more trabeculation than the other two locations (Table 3.2, p63).

The bending index is a shape indicator, because the size factor is eliminated (Daegling, 1989), and a low value signifies an increased ability to resist bending stress about the short axis, with the loss of ability to resist bending stress about the long axis. It is also a torsional rigidity index, because if the size is constant, a bending index of unity indicates a rounded cross-section, which is an ideal design to sustain torsional stress (van Eijden, 2000). Therefore, there are two biomechanical consequences of a high bending index: an enhanced resistance to transverse bending rigidity and a more efficient shape for torsional rigidity (Daegling and Grine, 1991). This index cannot be used to compare absolute bone rigidity. Our data revealed no bending index differences between any two cross-sections either binary or grayscale, total or cortical. The molar cross-section appears to be more circular, suggesting its torsional rigidity is increased. One can easily conclude, however, that shape differences among the three locations are minimal (Table 3.2, p63).

The grayscale value is an indicator of bone density. The absolute values themselves are not useful for comparison between two different CT scans unless these have been calibrated. However, the variation in the value for individual CT scans indicates bone density variation, because there is a linear relationship between grayscale value and bone physical density (Lampmann *et al.*, 1984; Zhang *et al.*, 2001a). With a calibration phantom, true density approximation is possible for each pixel, and the mass for the mandible can also be estimated (Zhang *et al.*, 2001a). It is commonly recognized that bone mineral density is a consistent predictor of bone strength for cortical bone (Currey, 1984a; Lang *et al.*, 1997; Martin and Ishida, 1989; Stenström *et al.*, 2000). Therefore, all density-weighted measurements in this study appear valid. These include the mass,

second moments of mass, mass bending index for both the cortical and total cross-sections, and the mass cortical index. The inconsistency of the results for binary and grayscale cross-sectional measurements in Table 3.1 (p62) and Table 3.2 (p63) verifies that bone regional density needs to be taken into consideration.

We used our cortical rigidity index to compare cortices at different regions. The regional differences in cortical bone densities found in the human mandibular cross-section encouraged us to explore a new parameter combining both cortical thickness and regional bone density. We supposed the cortical bone increased its rigidity in different ways, one was by thickness, where space was not an issue (e.g. at the symphysis), or where the kind of received stress demanded it. Unfortunately, the relationship between bone density and bone mechanical properties is controversial (Carter and Hayes, 1976; Currey, 1984a; Martin and Ishida, 1989), although denser bone tends to be more rigid (Carter and Hayes, 1976; Lang *et al.*, 1997; Turner, 1989; van Eijden, 2000). Nevertheless, we suggest our cortical rigidity index is at least positively related to regional cortical rigidity.

3.5.3 Cross-sectional design of the human mandible

In general, the corpus cross-section is ovoidal. Although it appears to be anatomically "hollow" in that the cortical bone is distributed only at the periphery of the section, extensive trabeculation is routinely found within the interior of the corpus, suggesting the corpus may not behave as a hollow beam during function (Daegling, 1989). Trabeculation is believed to counter or dissipate stresses in bone (Currey, 1984b; Lanyon, 1974).

Although the cross-sectional masses were quite homogeneous in

the three locations, their bone distributions varied, suggesting specific designs may be required for different loading conditions.

3.5.3.1 The molar region

There are three stress-bearing load regimens other than vertical shear in this region: sagittal bending, torsion and transverse bending. While transverse bending requires a transversely increased dimension, it causes very low stress in the molar region (Daegling and Grine, 1991). Sagittal bending calls for a corpus section with a relatively larger vertical dimension, and it is high in this area (Weijs, 1989). In this case, bending index should differ from unity. Our reported bending indices for this region were only 0.25-0.39 (Table 3.1, p62, and Table 3.2, p63).

Torsion requires circular cross-sectional form. In such a form, the polar moment of inertia is a determinant of its ability to resist torsion (Daegling, 1989; van Eijden, 2000). The polar moment of inertia takes into account not only the amount of cortical bone area, but also the disposition of the cortical bone with respect to the center of mass. In the human mandible however, truly circular forms do not exist. For a thin-walled tube of arbitrary cross-sectional shape with variable wall-thickness (like the mandibular cross-section) subject to torsion, a model based on shear flow theory may be more suitable, i.e. one in which the product of shear stress and wall-thickness at any location is constant. The largest shear stress occurs where the wall-thickness of the tube is smallest (Gere and Timoshenko, 1990). A mandibular cross-section may be modeled as either single-cell or multi-cell thin-walled tubular member depending on the density of trabeculation (see Figure 1.6, p30, and Figure 1.7, p31). Even so, the closer to circular a

section is, the better its ability to resist torsion. The bending index is also a measure of the degree of circularity, and a truly circular section has a bending index of unity. The molar cortical section tended to have the highest bending index of the three sections (Table 3.1, p62, and Table 3.2, p63) confirms this.

Both bending and torsion require hollow designs, and the binary cortical index (0.52±0.03) indicated the molar section conformed to this (Table 3.1, p62).

There was no difference in rigidity between the facial and lingual cortices in the molar section. Both density and cortical thickness were similar. However, the basal cortex was not only the densest, but also the thickest, resulting in a cortical rigidity index twice as high as those in the facial or lingual regions (Table 3.3, p65). While this may be attributed to the high tension or compression caused by sagittal bending in this region (Weijs, 1989), here we propose a tooth-loading hypothesis. Bite force is the main reaction force exerted on mandibular corpus, and the direction of this force varies during function. These dynamic forces have transverse components which bend the facial and lingual cortex in a way reminiscent of the transverse bending seen in the mandibular symphysis. Stress concentrations can occur in the basal cortex (Figure 3.5, p75), but unlike the mandibular symphysis, part of this bending stress may be dissipated by the trabecular bridges between the facial and lingual cortices (when they exist). Our impression of an association between tooth-loading and basal cortical rigidity has been reinforced by a CT-scanned edentulous mandible we have studied, in which the thickness of the basal cortex was reduced, approaching those of the facial and lingual cortices (Figure 3.6, p76). The idea also correlates with previous observations that basal bone

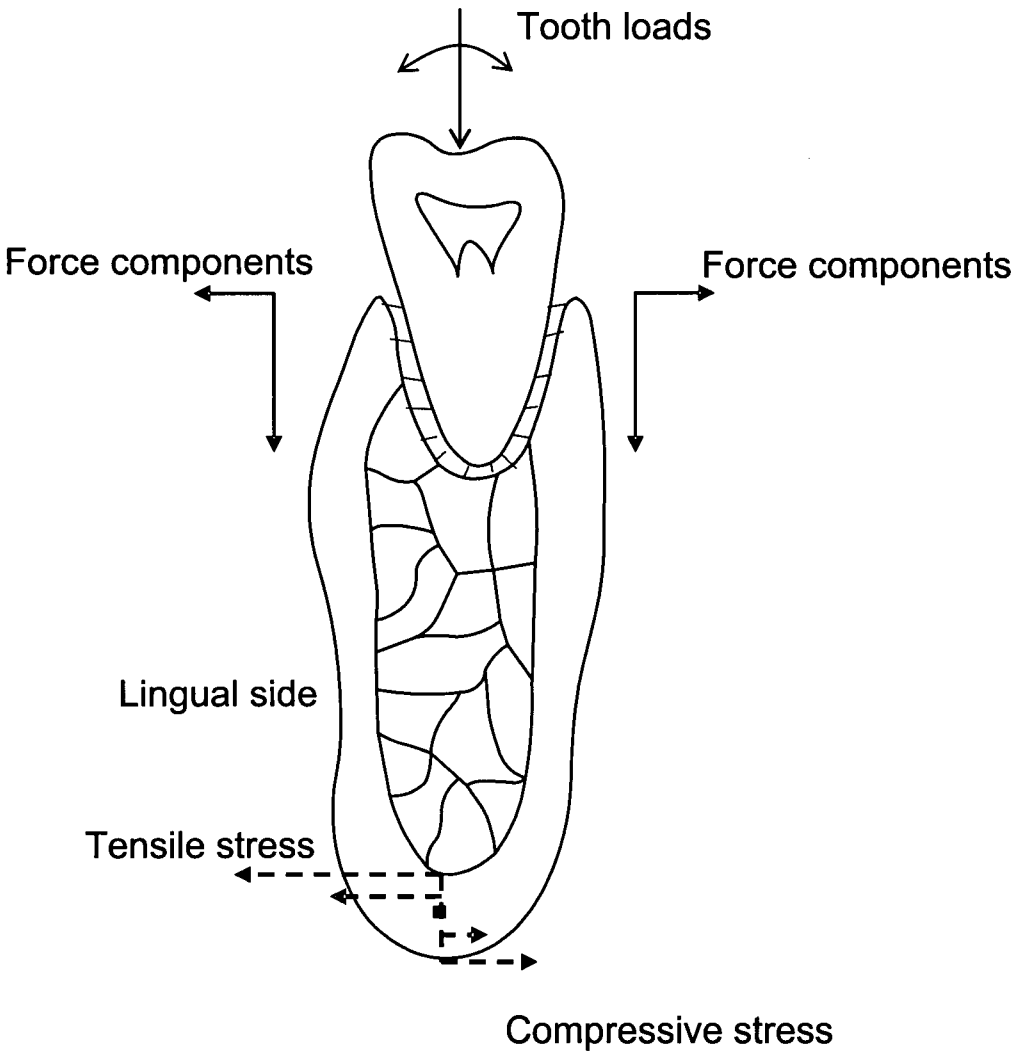

Figure 3.5 Possible stress distribution caused by tooth-loading. The transverse components of tooth forces bend the facial and lingual cortices. The bending results in compressive stress along the convex surface and tensile stress along the concave surface of the basal cortex. Vector components indicate probable directions only.

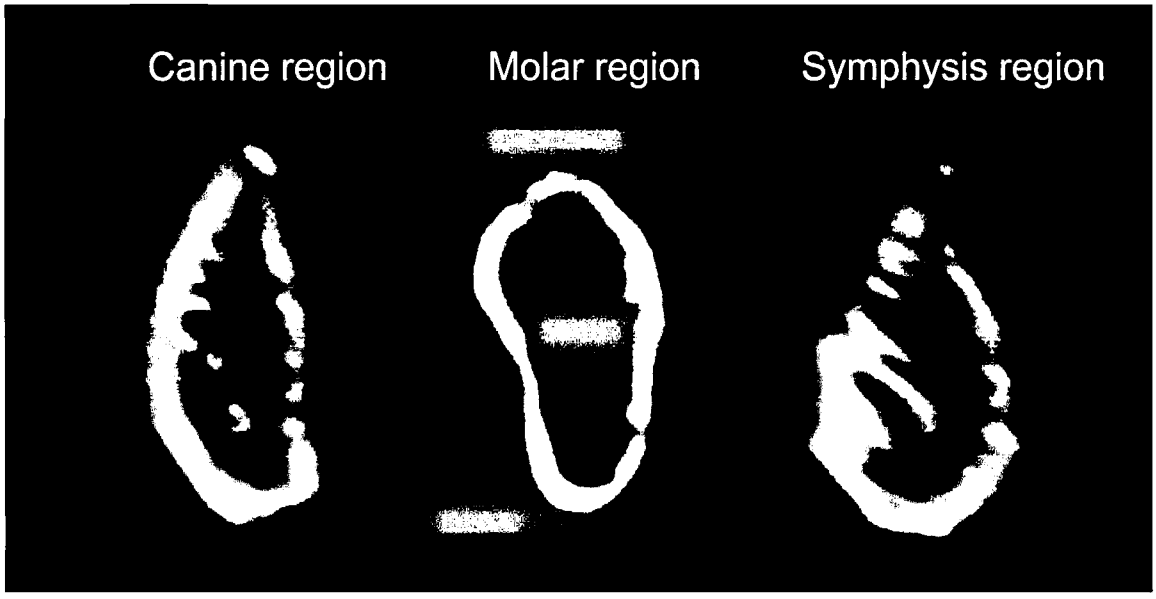

Figure 3.6 Equivalence of canine (left), first molar (middle) and symphysis (right) cross-sections of an edentulous mandible. For all three sections, left side is lingual and right is facial. See text for significance of their forms.

height correlates with alveolar bone height in human mandibles (Kingsmill and Boyde, 1998).

3.5.3.2 The symphysis

Wishboning produces higher tensile stress along the lingual cortex than the compressive stress along facial side (Hylander, 1985). This requires more rigid cortical bone on the lingual side. Our data indicated that in this region, the lingual cortex was denser and thicker than its facial counterpart (Table 3.3, p65). Twisting of the bilateral mandibular corpora generates tension along the infero-lingual aspect, and incisor biting induces vertical bending (for review, see Hylander, 1984). Although these hypotheses have mostly been based on anthropoid primates, they are probably true for humans. Both loading patterns require rigid cortical bone in the basal region. Our data support this by demonstrating the basal cortical bone was equally rigid to the lingual cortex (Table 3.3, p65). The edentulous mandible also demonstrated a reduction in cortical thickness in the basal aspect after loss of tooth loads, though not in its lingual aspect (Figure 3.6, p76).

3.5.3.3 The canine region

The loading pattern in this region has been infrequently studied although it seems to be an area of stress concentration second to the symphysis. Our study suggests this was a transitional area between the molar and symphysis; while the basal cortex was the most rigid, the rigidity of the lingual cortex superseded its facial counterpart (Table 3.3, p65). We suggest this is due to a combination of sagittal bending, torsion and transverse bending. Sagittal bending may occur during molar or incisor biting (van Eijden, 2000). Twisting of the

corpus can extend to this area and wishboning of the mandibular corpora increases here (Daegling and Grine, 1991). It is not surprising therefore that this corner structure is associated with stress concentration. Since the edentulous mandible signified a reduction in cortical thickness in its basal aspect after tooth loss, tooth-loading may also be a factor (Figure 3.6, p76).

In general, our data indicate cortical bone density increases from the alveolar ridge to the basal part, from the anterior region to the molar area, and from the facial side to the lingual aspect, though it might be too premature to draw a final conclusion because our sample was small. Nevertheless, a study on pig regional bone density indicates the same density pattern (Powell *et al.*, 1973), and a macaque study (Dechow and Hylander, 2000) also shows the lingual cortex is stronger than its facial side counterpart.

3.5.4 Modeling the mandibular corpus

Based on the above discussion, it seems cortical bone distribution and density should be taken into account when modeling the mandibular corpus. Neither simple solid, nor simple hollow elliptical models are appropriate (Table 3.4, p67). This finding is consistent with previous reports (Daegling, 1989; Daegling and Hylander, 1998). Whether trabeculation needs to be considered may depend on the regions involved. The high grayscale cortical indices for the molar region indicated this region was the least trabeculated, while the symphysis was the most (Table 3.2, p63). We postulate there is a balance between biomechanical design and functional demand in the molar region. A comparatively large internal space is needed for the multiple tooth roots and mandibular nerves and vessels here, whereas

in the symphyseal area, this demand is minimal. Thus a high mass cortical index in the molar region (94%) may imply economical space use. The strength of trabecular bone is much less than that of cortical bone (van Eijden, 2000), but these trabecular bridges, albeit with less-dense cortical bone, may provide adequate and equal efficiency, especially when regions need to respond to different loading patterns than those at the molar region.

Whether the mandibular corpus should be modeled as an open and closed section remains controversial. Although it seems open because teeth are not part of the mandibular bone, an open section only possesses a small fraction of the rigidity of a closed section in resisting torsion (Daegling *et al.*, 1992). The mandibular section may never be open because teeth seem an integral part of the section, and torsion can flow from one side of the alveolar process to the other through them (Figure 3.7, p80). For sections between the teeth, the top of the section is always linked by alveolar bone.

3.6 SUMMARY AND CONCLUSIONS

One aim in engineering design is to provide the maximum stress-bearing ability with minimum cost in material and space. The human mandible appears designed to withstand a variety of functional loads with the least possible material and space. Its stress-bearing cortical bone is distributed at the periphery, making it suitable for resisting torsion and bending. Moreover, the corpus is larger in its vertical dimension, a design which counters high sagittal bending stresses. The variation in cortical rigidity within each cross-section also reflects sound design. At the symphysis and canine, more cortical bone is found along the lingual side, a suitable strategy to resist wishboning.

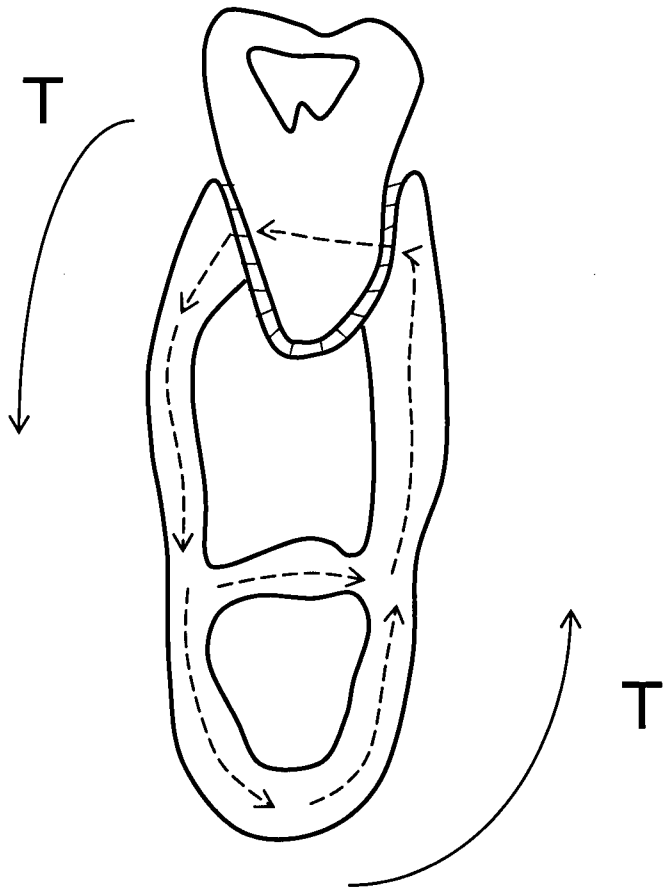

Figure 3.7 Torsion flow in a section containing a tooth. The tooth is supposed to act as a bridge transmitting torsion from one side to the other. Based on Daegling *et al.* (1992). T is the applied torque.

For cross-sections receiving high tooth loads, the basal cortex is more robust, providing high resistance to bending of the facio-lingual cortex. For the mandibular corpus as a whole, the overall ability to resist vertical shear stress appears homogeneous.

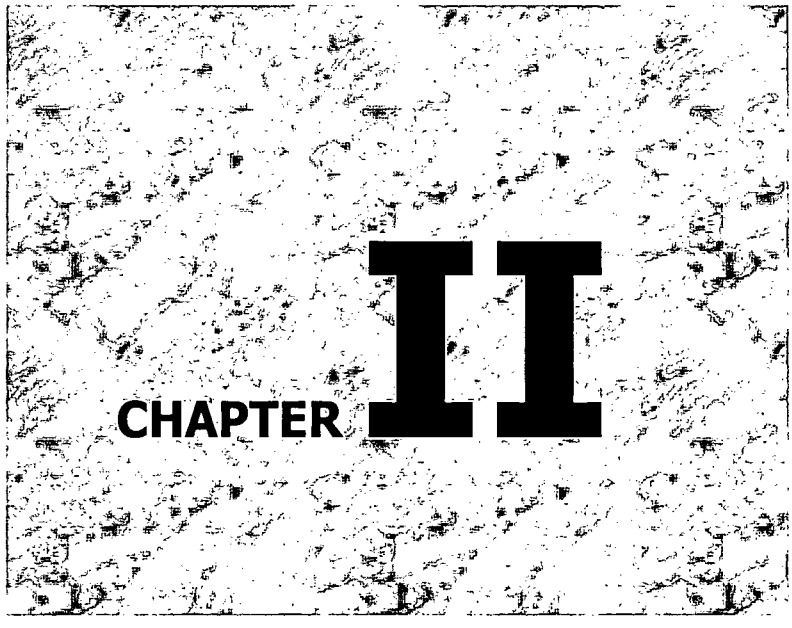
CHAPTER II

4 SYMPHYSEAL MECHANICS IN PIG AND HUMAN MANDIBLES

4.1 ABSTRACT

Monkey studies suggest that the fused mandibular symphysis prevents structural failure from lateral transverse bending, or wishboning, attributed to forces generated by the deep masseter muscle late in the chewing cycle. High symphyseal tensile stresses and strains at the symphysis are related to increased symphyseal curvature, strong jaw muscles, elongated moment arms, and decreased symphyseal width in the plane of bending. Increases in symphyseal width anteroposteriorly raise the second moment of inertia, and lessen stresses and strains. Here, we compared symphyseal mechanics in two mammals with distinctly different jaw shapes, sizes and symphyseal characteristics (pigs and humans). We wished to determine whether induced stress and strain remain similar between these mammalian orders, and in particular, the role of symphyseal orientation, if any, in this process. The experiments were carried out on 10 age-matched pig (*Sus scrofa*) mandibles (including six living animals), and eight modern dentate human jaws. CT and MR imaging were used to derive relevant bone and muscle parameters, including cross-sectional moments of inertia, centroids, moment arms, and radii of curvature. Estimated symphyseal stresses and strains for pigs (8.18 MPa for stress; 818.37 με for strain) and humans (8.21 MPa for stress; 820.92 με for strain) were markedly similar, and within the functional range previously reported for the primate symphysis (i.e. below 2000 με). Experimental upright reorientation of the pig symphysis increased

its muscle-induced strain to 2258.63 με, above the highest functional strain reported for macaques. The results suggest functional equivalence in stress and strain levels across these mammalian orders, and emphasize the importance of symphyseal orientation in the pig.

4.2 INTRODUCTION

The functional advantages of unfused and fused mandibular symphyses in mammals have been reviewed recently by Lieberman and Crompton (2000). The unfused symphysis, by allowing independent inversion and eversion of the two halves of the mandible before and during the masticatory power stroke, enables the steep occluding surfaces of opposing teeth in some mammals to match during mastication (Hylander, 1979b; Kallen and Gans, 1972; Lieberman and Crompton, 2000; Oron and Crompton, 1985; Scapino, 1981). In contrast, the fused symphysis strengthens and stiffens the jaw, reducing its risk of structural failure as a result of lateral transverse bending ("wishboning"), and from dorsoventral shear stress occurring during unilateral mastication (Hylander, 1984; Hylander *et al.*, 2000; Ravosa, 1996; Ravosa and Hylander, 1993; Ravosa and Simons, 1994). Some mammals producing predominantly vertical occlusal forces have unfused symphyses, which, despite their mobility, can transfer dorsally-directly forces through interdigitating rugosities. It has been suggested mammals with mainly transversely-oriented occlusal forces tend to have fused symphyses (Lieberman and Crompton, 2000), though selendont artiodactyls do not display fusion, nor do rodents, which have noted transverse components in their chewing strokes.

Wishboning seems mainly due to delayed activity in the balancing-

side deep masseter muscle at the end of the masticatory power stroke, and results in separation and transverse lateral bending of the two mandibular corpora (Hylander, 1975; Hylander *et al.*, 1987; Hylander *et al.*, 1998, 2000; Hylander and Johnson, 1994; Ravosa, 1999). Balancing-side muscle activation also encourages upward and downward movements of the balancing and working-side mandibular corpora respectively, producing dorsoventral shear stress (Hylander, 1975, 1977, 1979a, b; Ravosa, 1996, 1999; Ravosa and Simons, 1994). Jaw muscle activity in baboons, macaques, owl monkeys and galagos (Hylander *et al.*, 2000; Hylander and Johnson, 1994) suggests there is an association between wishboning and a need for symphyseal fusion because galagos (with an unfused symphysis) do not exhibit the deep masseter activity characteristic of wishboning. The forces involved in this form of bending are believed to include laterally-directed components of bite force on the working-side, opposing the balancing-side muscle tensions. Residual tensions in some relaxing, working-side jaw adductors may also contribute (Hylander *et al.*, 2000; Hylander and Johnson, 1994). In humans, laterally-directed force from the balancing-side masseter likely exceeds that of any medial contribution from the medial pterygoid of the same side. Differences in timing between these muscles during the late intercuspal phase of the chewing cycle argue for the deep masseter as a primary contributor to wishboning (Hannam and Wood, 1981).

Symphyseal fusion accompanies development of a functional occlusion. Partially-fused symphyses are common in juvenile animals, and complete fusion often takes place with the eruption of the permanent first molars (Ravosa, 1999). In the miniature pig, adult-like transverse masticatory movements develop after weaning, and the mandible is subject to wishboning similar to that in anthropoids

(Huang *et al.*, 1994).

Wishboning can create high tensile stresses and strains on the lingual surface of the symphysis. In primates, these tensile stresses are two to three times larger than compressive stresses on the labial surface (Hylander, 1985; Ravosa and Simons, 1994). They can be resisted by synostosis (Ravosa, 1996, 1999; Vinyard and Ravosa, 1998), bony enhancement (e.g. transverse tori), and increased horizontal orientation of the symphysis, features often seen in primates (Daegling, 1993; Hylander, 1984, 1985; Ravosa and Simons, 1994).

The cross-sectional area of bone, and symphyseal shape determine the jaw's resistance to wishboning (Hylander, 1984, 1985), and an adequate cross-sectional area in the plane of stress is needed to resist dorsoventral shear. Cross-sectional shape and regional bone density can both be revealed by high-resolution computed tomography (CT). This is a useful technique for analysing hominid mandibles (Daegling, 1989), not least because it provides true cross-sections at any location, and allows the segmentation of teeth from cortical and cancellous bone.

The shape and size of the Cercopithecine symphysis appear to be allometric with body size and the width of the mandibular dental arch, i.e. symphyseal width anteroposteriorly, and its length superoinferiorly, scale positively allometric with body size, and negatively with mandibular arch width (Hylander, 1985). Since the width of the symphysis increases more rapidly than its length, there is also a change in symphyseal shape with increasing body size. These changes are believed to maintain functional equivalence in bone stresses and strains across taxa and ontogeny (Hylander, 1985; Vinyard and

Ravosa, 1998). During wishboning, for example, tensile strains at the lingual border of the primate symphysis remain under 2,000 με, well-below 3,000 με when structural failure is possible. This kind of safety factor seems desirable, since it has been proposed adaptive remodelling may be insufficient to cope with functional demands in vigorously chewing animals (Bouvier and Hylander, 1981a; Hylander, 1979b).

Physically, the mandible is assumed to behave like a curved beam, in which the maximum tensile bending stress (σ_{max}) induced at its symphyseal surface is proportional to the bending force (F) and the moment arm (L). The bending force is related to the cross-sectional size of the balancing deep masseter muscle, and its moment arm to the distance between this muscle and the symphysis. The bending stress induced in a hollow beam is proportional to the distance between the outer surface of the beam and its centroidal axis. The radius of the (unstressed) neutral axis depends on the material, the shape of its cross-section, the curvature, and whether the beam is uniform. When a beam shaped like the mandible is bent laterally, its neutral axis deviates towards the concave side of the centroidal axis (Figure 4.4, p111). Here, the distance from the axis to the surface of the section is denoted as c. Any induced stress is inversely proportional to the second moment of inertia (I) of the section with respect to an axis perpendicular to the plane of curvature. A stress concentration factor (K) can be derived, which differs for concave and convex surfaces, and is usually found experimentally (Mott, 1996). It depends on the ratio between the radius of curvature (R) and the distance from the surface to the centroidal axis (R/c). For R/c values between 1.2 and 10.0, K ranges between 3.0 and 1.0 for a concave surface. K values for the convex surface of hollow elliptical section are

2.3 to 5.2 times smaller than those for the corresponding concave surface (Hylander, 1985; Mott, 1996; Roark and Young, 1975). The maximum stress along the concave or convex surface can be expressed as

$$\sigma_{max} = \frac{K \times F \times L \times c}{I} \qquad \text{Equation 4.1}$$

The maximum strain (ε) on the lingual surface of the symphysis can be calculated as

$$\varepsilon = \frac{\sigma_{max}}{E} \qquad \text{Equation 4.2}$$

where E is the modulus of elasticity (Young's modulus).

Recently, Vinyard and Ravosa (Vinyard and Ravosa, 1998) used some of these physical principles to estimate relative stress magnitudes in primate symphyses. Applying a formula introduced by Hylander (1985), they scaled a nominal bite force of 238 N (see Hylander, 1979a) by body mass to estimate muscle bending-forces in different species, the assumption here being bite force, muscle cross-sectional size and body mass scale proportionally. The bending moment-arm in this case was estimated by mandibular length (considered proportional to the muscle lever arm). The non-dimensional correction factor K was calculated by R/c, where the curvature R was estimated by the mandibular arch width, and the distance from the centroidal axis to the lingual surface of the symphysis (c) by the width of the symphysis. Because $\sigma \propto \frac{(F)(M)(K)}{(a^2)(b)}$, where a and b represent the symphyseal width and length respectively,

the relative magnitudes of the stresses on the lingual surfaces of the symphyses were calculated, then compared among species and species of different ages. Vinyard and Ravosa's (1998) results support the idea that changes in symphyseal form during ontogeny, and across species, maintain functional equivalence in stress levels at the papionin symphysis.

This useful study did not estimate induced strain however, and was limited by its use of bite force and body mass to estimate lateral bending forces. Bite forces are the result of synergistic activity in a number of different, bilaterally-coactivated, jaw-closing muscles, some of which have small lateral components, while others have marked medially-directed ones. Moreover, the lateral orientation of the muscle primarily implicated in wishboning (the deep masseter) varies with craniofacial form, depending on the spatial arrangement between the mandibular ramus and zygomatic arch. The magnitude (i.e. the maximum possible tension) of this lateral component (the vector responsible for transverse bending) thus depends upon the deep masseter's orientation, and is proportional to the deep masseter's cross-sectional area and degree of activation (length changes in this muscle being insignificant during the late intercuspal phase of the chewing cycle). Finally, the moment arm of any lateral force component is best measured from the muscle's line of action (e.g. the midline distance from its insertion site to the symphyseal center. These individual variables are multiplied during the estimation of any transverse bending moment.

The pig mandible differs markedly in shape and size from its human counterpart (Figure 4.1, p90). Since it is long and narrow, it has the propensity for high stress concentrations at its symphysis, i.e. pig

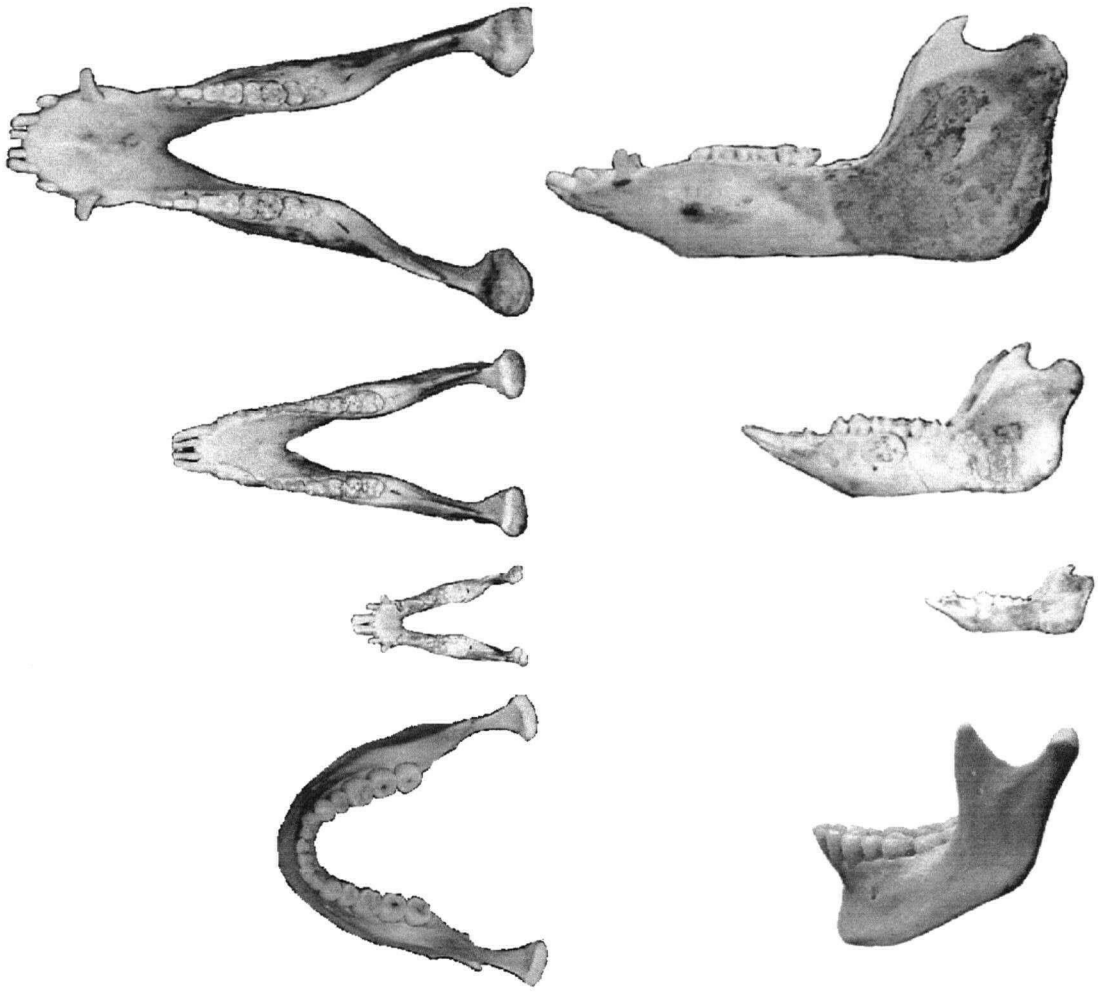

Figure 4.1 A growth series of *Sus scrofa* mandibles (rows one to three) illustrating ontogenetic changes in symphysis, and for comparison, an adult modern human mandible (bottom row). From top to bottom, the pig jaws are aged 250 days, 131 days and 29 days. The mandibles are shown from above (left) and laterally (right). With increasing age, the symphyseal width increases more rapidly than mandibular length and arch width, and the symphysis orients more horizontally. In contrast, the human mandible is shorter, and has a less-curved symphysis which is almost perpendicular to the occlusal plane.

mandibles are likely to have higher K values than human mandibles. Like that in cercopithecines (Hylander, 1985; Vinyard and Ravosa, 1998), the pig's symphyseal width appears to be positively allometric with mandibular length, and its width seems to increase more rapidly than its height during growth (unpublished observations, see Figure 4.1, p90). Other clear differences between pig and human mandibles of biomechanical significance include the relative positions and orientations of the mandibular ramus and zygomatic arch (affecting the line of action of the deep masseter muscle), closing jaw muscle cross-sectional sizes (affecting bending forces) and the inclination of the mandibular symphysis (affecting its resistance to wishboning).

These craniofacial differences encouraged us to test the proposition that the form of the pig symphysis, like its primate counterpart, reduces the likelihood of structural failure due to wishboning, quite aside from other functional advantages the form might have. We expected the physical principles presently explaining variations in form within primate species might well explain some of the differences between orders, at least in pigs and humans. A second, more general, reason for comparing symphyseal biomechanics in these two morphologically-distinct jaws is current use of the pig as a model for studying function and dysfunction in the human jaw and its articulation (Herring, 1995; Ström *et al.*, 1986). Understanding biomechanical similarities or differences in structure and function between pig and human jaws would be beneficial in other experimental settings.

In this study, we used CT imaging to analyze the mandibular cross-sections, and extended the analytical approach used previously by Vinyard and Ravosa (1998) to include the jaw's cross-sectional moments of inertia, centroidal axes, cross-sectional sizes of the deep

masseter muscles, the lateral component of their direction vectors, and the moment arms from their lines of action. We combined this information with the stress-concentration factor K, jaw curvature, muscle tensions and lever arms, to estimate the symphyseal stress and strain caused by wishboning. Two specific hypotheses were tested; first, that the shape and orientation of the pig symphysis are optimized to resist the effects of wishboning; second, that similar levels of stress and strain in the pig and human symphysis are induced by wishboning, despite their differences in form, and remain within a safe functional range, thus minimizing the risk of structural failure.

4.3 MATERIALS AND METHODS

4.3.1 Computed tomography

Images of the pig mandibles were taken from four dry osseous specimens, and six living animals (*Sus scrofa*, aged around eight months) all with mixed dentitions i.e. with only the first permanent molars erupted. The dry jaw specimens included two males and two females, and the living pigs comprised three males and three females. This material was obtained from the University of Washington, and the experimental procedures were approved by the Animal Care Committee of that University. The dry specimens were placed in a plastic box fixed with wooden spacers, and remained in water during CT scanning. High resolution CT slices with 512x512 pixels and voxel sizes 0.49 x 0.49 x 1 mm (kV=120, mA=150) were obtained with a Toshiba Xpress SX scanner (Toshiba Corp., Tokyo, Japan) at the University of British Columbia. All mandibles were imaged axially, i.e. coronal planes of section perpendicular to the occlusal plane, proceeding anteroposteriorly along the corpora. The scans on living

animals were carried out at the University of Washington with a General Electric High Advantage Tomographic Unit (Milwaukee, WI). These scans were also axial to the animal's head, and provided slices at one mm interval (field of view 240 × 240 mm, 512x512 pixels, pixel sizes of 0.47 x 0.47 mm, kV=120, mA=180).

The human jaw specimens included eight dry, adult, dentate mandibles of unknown age and gender. These scans were performed at the University of British Columbia in the same manner as that described for the dry pig jaws.

4.3.2 Image conversion and preparation

The image data were in a signed, big-endian 16-bit format. We used a custom program (RIC - Raw Image Converter, Craniofacial Laboratory, The University of British Columbia; available from http://condor.dentistry.ubc.ca) to convert these into 8-bit images, then performed manual segmentation of the hard-tissue profiles with 3DViewnix (University of Pennsylvania Medical Center, Philadelphia, PA) on an SGI Indigo Extreme computer (Silicon Graphics Inc., Mountain View, CA).

Midline reslicing revealed true symphyseal cross-sections. The reformatted slices were saved as uncompressed bitmap files for further processing on a desktop computer (Dual Pentium III 450 MHz). Commercial software (Paint Shop Pro 7, Jasc Software, Inc., Eden Prairie, MN) was used to segment teeth, cortical and cancellous bone. The cross-sections were re-oriented so each long axis was vertical relative to the image matrix. Each dental outline was traced, and the teeth (crowns and roots) were removed, leaving only bone (i.e. "total" cross-sections). Finally, we traced the outline of cancellous bone, and

deleted it to obtain cortical cross-sections. These were retained as grayscale images, preserving their regional bone density. The human symphyseal sections were treated the same way (Figure 4.2, p95).

4.3.3 Cross-sectional measurements

Quantitative calculations for each section included its cross-sectional area (Area), mean grayscale value (MGSV), cross-sectional mass (Mass), second moments of inertia of its area (Ix, Iy) and of its mass (Ixm, Iym). Bending indices were calculated from the ratios of Iy/Ix (BI) and Iym/Ixm (BIM). These calculations were made for the total and the cortical sections. Cortical indices were also calculated from the ratios of cortical area to total area (CI) and cortical mass to total mass (CIM). The area and mass calculations were related to the ability of a section to resist shear. MGSV provided an index of relative mean bone density for the cross-section. The second moments of inertia quantified the ability of a section to counter bending with respect to one of its two orthogonal axes. The bending index provided a measure of shape with respect to its resistance to bending and torsion, and the cortical index was a measure of the efficiency of the cross-sectional design (defined as the ability to resist the most stress with the least material). All cross-sectional measurements were made using a dedicated program (Calimage - Calculate Image, Craniofacial Laboratory, The University of British Columbia; available from http://condor.dentistry.ubc.ca). It also calculated the maximum horizontal and vertical cross-sectional dimensions, i.e. the bounding box, and the mass center (centroid) of each section relative to its bounding box (expressed as the distance from the centroid to the most posterior lingual surface of the symphysis).

Figure 4.2 Typical cross-sections for pig and human mandibular symphyses. Sections in the first row are pig symphyseal sections, showing the original section, total section without teeth, cortical section, total section in its normal orientation, and cortical section in its normal orientation, respectively. Sections in the second row are the corresponding human sections. In both cases, the facial surfaces are to the left. Seen here are the two symphyses oriented quite differently and more cortical bone distributed on their lingual sides. W indicates symphyseal width measurement, and H indicates symphyseal height measurement.

4.3.4 Stress and strain calculations

Estimates of the maximum stress along the lingual surface of the mandibular symphysis were derived from a formula (Equation 4.1, p88). The correction factor K (derived from R/c) was obtained from a conversion table for hollow elliptical sections (Roark and Young, 1975). The negative allometry of the mandibular arch width decreased the R/c (i.e. increased K) for the concave surface of the symphysis (Hylander, 1985). Previously, dental arch width, i.e. the distance between the left and right mandibular third molars, has been used to estimate the diameter of curvature (Hylander, 1985), but we were unable to employ this approach because our pigs were adolescents. Therefore, we used a median axis method described by Straney (1990), and Daegling (1993) (see Figure 4.3, p97). Lines were drawn to approximate each long axis of the left and right corpora. A third line was constructed through the centroid of the symphysis, perpendicular to the midsagittal plane. The three lines intersected forming an open trapezoid, a circle was constructed internally tangential to its sides, and the radius of this circle was taken to be the radius of symphyseal curvature. The centroid was used to approximate the c value. We also used this approach when measuring the human mandibles.

The deep masseter (known as zygomaticomandibularis, ZM, in pigs, Herring *et al.*, 1993) was assumed the primary bending force. Accordingly, Magnetic Resonance (MR) images from four of the living pigs were obtained as part of another study at the University of Washington with a Sigma MR scanner (General Electric Medical System, Milwaukee, WI) using Spin-Echo sequences (TR/TE 11.1/2 ms, matrix 256×192, FOV 24×24 cm, slice intervals 1.5 mm). Sections were obtained from the masseter muscles, below the zygomatic arch, parallel to the occlusal plane, and through the roots of the maxillary molars. In each case, the cross-sectional area of one whole

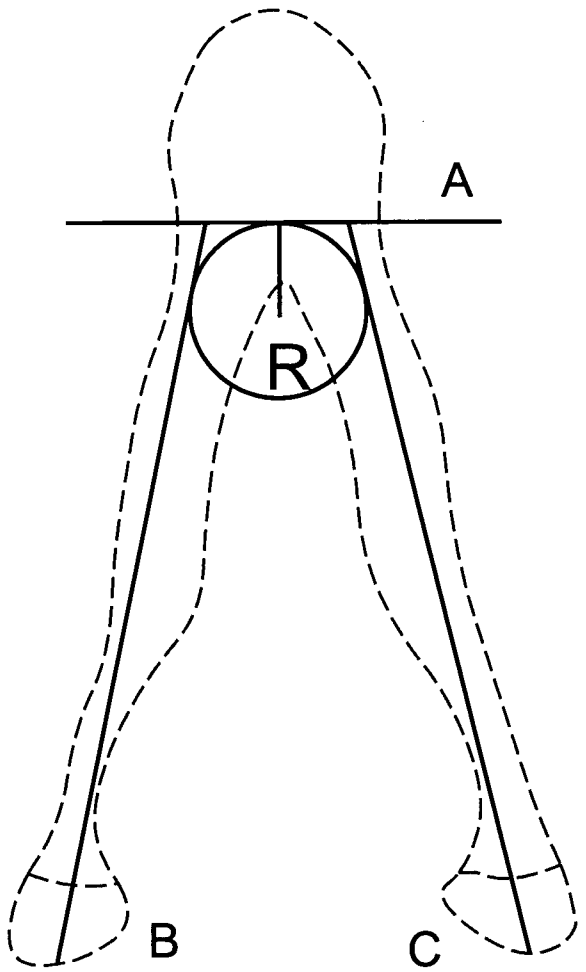

Figure 4.3 Diagram of the median axis method used to construct the circle containing the radius of curvature of the flexure. A circle is constructed so that it is tangential to the three sides of the open trapezoid. A represents a line passing through the centroid of the symphyseal section, which is also the tangential point. B and C indicate the long axes of the left and right mandibular corpora. R indicates the radius of curvature.

muscle was measured, and then halved to represent the deep masseter (clearly distinguishing the ZM muscle from superficial masseter is difficult with MRI). This mean area for the four animals was 5.91 cm^2 (range 4.72-6.59 cm^2), representing the deep masseter's cross-sectional size in all subsequent calculations for the pig. Also, coronal MR slices 1.5 mm thick were made midway through the sigmoid notch (i.e. between the coronoid and condylar processes) to disclose masseter muscle angulations in three living animals. The upper border was traced from the medial surface of the zygomatic arch to the muscle's insertion in the masseteric fossa below the sigmoid notch, and the lower border from the bottom of the arch to the insertion of the muscle on the mandible's external oblique ridge (this border was marked by a visible intramuscular aponeurosis). The angles formed by these two muscle borders relative to the occlusal plane were bisected to produce a resultant line of action for the deep masseter. Its average angle for the three animals was 46 degrees relative to the occlusal plane (range 43-51 degrees) and this value was used in all subsequent calculations for the pig.

No direct measurements were made of the human deep masseter's cross-sectional size or orientation, since average data were already available. We assumed the muscle had a mean cross-sectional area of 2.04 cm^2 (Langenbach and Hannam, 1999) and a mean frontal plane angulation of 57 degrees (Korioth *et al.*, 1992).

Since maximum tension in a mammalian skeletal muscle is proportional to its cross-sectional size (Hannam and Wood, 1989; Langenbach and Hannam, 1999; Peck *et al.*, 2000; Sasaki *et al.*, 1989; Zajac, 1989), we multiplied the masseters' cross-sectional areas in both instances by 40 N/cm^2 to estimate their maximum possible

tensions (Hannam, 1997; Langenbach and Hannam, 1999; Peck *et al.*, 2000; van Eijden and Raadsheer, 1992), and converted these to lateral force vectors by means of the muscles' mean coronal angulations.

The respective moment arms were measured from CT-derived (voxel-based) surface reconstructions of the entire jaws. In each case, a line was drawn between the centers of the rami (defined by the midpoints between the sigmoid notch and lower border, and the anterior and posterior borders respectively). The moment arm was defined as the midline distance from this line to the symphyseal centroid, parallel to the occlusal plane.

Different methods can be used to express the mandible's plane of curvature, e.g. the occlusal plane, and the lower border of the mandible. In the pig mandible, there is little difference between these as the lower border is almost parallel to the occlusal plane, but in the human jaw, there can be an 18 degree difference between them (Sadowsky, 1995). Here we chose the occlusal plane, since wishboning occurs at the end of the power stroke, i.e. near maximum intercuspation (Hylander *et al.*, 1987; Hylander and Johnson, 1994).

Definition of symphyseal length (or height) and width with respect to wishboning is related to the plane of curvature. Hylander (Hylander, 1985) defined symphyseal length as the maximum distance from the midline crest of the mandibular incisor alveolus to the most inferior portion of the mandibular symphysis. Symphyseal width was taken as the maximum dimension of the symphysis in the sagittal plane, perpendicular to symphyseal length. This definition suits the human symphysis because its long axis is almost perpendicular to the

functional occlusal plane (our definition of the plane of curvature for wishboning). However, it is inappropriate for the pig symphysis, which is markedly inclined anteroposteriorly. We considered a more appropriate definition of symphyseal width here was the maximum dimension of the symphysis with respect to the occlusal plane, and that of its height as the maximum dimension in a plane perpendicular to this. Here we use the word "height" to replace "length". When we measured these dimensions programmatically, we used the horizontal and vertical dimensions of the bounding box in the image matrix to represent the width and height, respectively; the section was oriented so that the angle between the long axis of the section and the horizontal dimension of the image matrix conformed to the angle between the long axis of the symphysis and the functional occlusal plane (Figure 4.2, p95). This angle was measured from the reconstructed whole-jaw image. We used similar criteria to define human jaw widths and heights.

The second moment of inertia with respect to the axis perpendicular to the plane of curvature, takes into account the relative amounts and distribution of cortical bone, bone mass distribution, and the shape and size of the cross-sections. The cortical cross-sectional moment of inertia was calculated with respect to the centroid and the vertical axis, i.e. Iy, and used in Equation 4.1 (p88). The parameter c (the distance from the lingual surface to the centroidal axis) was calculated programmatically. The centroid calculation took into account the shape and size of the cortical section and the distribution of bone mass. Generally, the compact bone is reported to have a Young's elastic modulus between 10 to 20 GPa (van Eijden, 2000). This is very similar to that in humans (11.3 to 19.4 GPa; Dechow *et al.*, 1993) and macaque (9.0 to 21.0 GPa; Dechow and Hylander, 2000). We assumed

the same for the pig mandible. Since cortical bone is weaker in tension, we used the lower value (10 GPa) to estimate strain. The stress and strain calculations were made for the cortical bone cross-sections on the assumption the symphysis was a hollow, elliptical section.

To assess the significance of symphyseal orientation in the pig, we also calculated its maximum tensile stress and strain when the symphysis was simulated as having an upright orientation. Because the centroid changed, the R/c ratio, K value and force moment arm were adjusted accordingly.

These criteria were also applied to the human mandible, although here each long axis was almost perpendicular to the functional occlusal plane, and no simulations were made with an altered symphyseal orientation.

4.3.5 Statistical analysis

Two-sample t-tests were used to test the differences between pig and human jaw symphyseal measurements. One way ANOVA was used to determine if there were differences in estimated stresses and strains among the pig mandible with its symphysis in a normal orientation, the pig mandible with its symphysis in the simulated upright orientation, and the human mandible. Further comparisons between groups were performed with Tukey's honestly significant difference test. The significance level was set to 0.05. All statistical analyses were carried out with SPSS for Windows 8.0 (SPSS Inc., Chicago, Illinois).

4.4 RESULTS

4.4.1 Cross-sectional measurements

For comparative analysis, the cross-sectional shapes of the pig and human symphyses were oriented so their principal axes were aligned the same way. Most cross-sectional measurements for the pig sections were significantly greater than those for humans (Table 4.1, p103). These parameters included the areas, and second moments of areas for total and cortical bone cross-sections. While the relative amounts of cortical bone in the respective samples (i.e. the cortical indices) were quite similar, the bending indices in humans were significantly greater than those in pigs.

4.4.2 Symphyseal stress and strain

The estimated stresses and strains were similar in the pig and human mandibles (Table 4.2, p104). The strains were all within the range previously reported for primates, i.e. below 2000 με. When force on the pig symphysis was simulated in its upright orientation however, the estimated stresses and strains were about three times greater, i.e. the strain exceeded the highest value of 2000 με reported for the macaque (Hylander, 1985). The cross-sectional moments of inertia for the normal pig and human symphyses in Table 4.2 (p104) differed from those in Table 4.1 (p103) because the latter were calculated for sections with their principal long axes oriented upright in the image matrices.

The radii of curvature for the pig and human mandible were unexpectedly similar (19.40±2.63 mm and 20.13±2.36 mm

Table 4.1 Area (cm^2), mass (cm^2), mean grayscale value (MGSV), second moments of area (Ix, Iy in cm^4), second moments of mass (Ixm, Iym in cm^4), area and mass bending indices (BI, BIM), area and mass cortical indices (CI, CIM), and t-test results for pig and human jaw symphyses. The symbol (-) indicates no comparison available.

	Pig		Human		t test
	Mean	SD	Mean	SD	P value
Cortical					
Area	6.59	1.70	2.29	0.32	<0.01
Mass	387.78	146.78	89.13	16.44	-
MGSV	57.30	10.09	38.87	3.22	-
Ix	17.12	7.31	1.46	0.50	-
Iy	2.20	1.06	0.46	0.13	<0.01
Ixm	760.40	394.36	47.79	18.35	-
Iym	109.60	59.99	14.59	4.90	-
BI	0.13	0.03	0.34	0.11	<0.01
BIM	0.14	0.03	0.32	0.09	<0.01
Total					
Area	8.68	1.70	3.17	0.47	<0.01
Mass	480.54	165.50	117.61	19.25	-
MGSV	54.31	11.69	37.08	2.65	-
Ix	21.03	7.97	1.66	0.59	<0.01
Iy	2.57	1.21	0.50	0.14	<0.01
Ixm	918.55	421.80	53.86	20.16	-
Iym	127.94	68.44	15.92	5.32	-
BI	0.12	0.03	0.32	0.11	<0.01
BIM	0.14	0.03	0.31	0.10	<0.01
CI	0.74	0.07	0.72	0.04	0.37
CIM	0.80	0.08	0.76	0.05	0.22

Table 4.2 Estimated stresses and strains for pig mandibles with their symphyses in their normal, and simulated upright orientations, and for human mandibles. The table includes means, standard deviations, minimum and maximum values. Abbreviations and units: R, the radius of curvature in mm; c, distance from the centroidal axis to the most posterior lingual surface of the symphysis section in mm; K, a correction factor for curved beam stress calculation; DM, mean deep masseter force in N; L, lever arm in mm; I, second moment of inertia with respect to the vertical axis in cm^4; σ, calculated stress in MPa; ε, calculated strain, in $\mu\varepsilon$. The symbol (-) indicates the variable has constant value. The symbol (*) indicates differences between groups ($P<0.01$).

	R	c	K	DMF	L	I	σ	ε
Pig normal								
Mean	19.40	20.77	3.03	164.22	118.08	16.41	8.18	818.37
SD	2.63	2.18	-	-	10.86	6.87	1.96	195.84
Min	14.00	17.80	-	-	99.86	8.60	4.78	477.86
Max	22.00	24.30	-	-	129.32	30.19	11.19	1118.82
Pig upright								
Mean	19.40	11.93	2.03	164.22	109.20	2.20	22.59	2258.68
SD	2.63	1.60	0.41	-	10.62	1.06	9.04	903.73
Min	14.00	9.67	1.54	-	90.80	0.89	14.29	1428.82
Max	22.00	14.59	3.00	-	121.49	4.38	41.89	4188.61
Human								
Mean	20.13	8.22	1.54	44.44	71.47	0.51	8.21	820.92
SD	2.36	0.69	-	-	4.34	0.13	1.27	127.28
Min	16.00	7.34	-	-	66.29	0.32	6.94	693.72
Max	23.00	9.30	-	-	77.60	0.71	10.41	1041.46

Tukey's test*			
	Pig normal vs. pig upright	**Human vs. pig upright**	**Pig normal vs. human**
σ	<0.01	<0.01	>0.05
ε	<0.01	<0.01	>0.05

respectively), but K values for the pig mandibles were about double those found in the human sample.

4.5 Discussion

4.5.1 Symphyseal cross-sections

Although our pigs were juveniles, their mandibles were larger than the human specimens. The absolute size of the pig symphysis seems important for resisting shearing stresses. Like monkeys, three shearing forces may occur here during function. Dorsoventral shear is created by vertical components of muscle force on the balancing-side during unilateral molar biting, and by non-midline incisal forces (Beecher, 1977; Hylander, 1984), though the latter may be more important in primates than in pigs. The strong adductor muscles in the latter animals are a likely source of dorsoventral shear stress. Anteroposterior shear is due to the balancing-side temporalis having the tendency to pull the balancing-side dentary in a posterior direction relative to the working-side dentary during the power stroke (Beecher, 1977). Additionally, shearing forces can be torsional (i.e. twisting about the transverse axis of the symphysis when the balancing-side corpus is elevated and working-side is depressed (see Hylander, 1984). While the former two simply require sufficient bone in the symphyseal cross-section to be resisted satisfactorily, torsional shear is best resisted by a circular cross-sectional shape (Daegling, 1989; Daegling *et al.*, 1992; Daegling and Grine, 1991; Daegling and Hylander, 1998). Though the pig symphyseal section is far from circular (indicated by a mean bending index around 0.13, see Table 4.1, p103), its resistance to torsional shear may also be helped by its internal trabeculation

(Daegling, 1989; Hylander, 1979b) which could dissipate shear flow. Shearing stresses in the human symphysis might be expected to be smaller than those in the pig due to the relative size of each jaw and its muscles.

While the pig might be predicted to have a robust symphysis given its size and feeding habits (pigs root forcefully with their long snouts), this alone does not explain the preferential distribution of cortical bone in the infero-lingual part of the symphyseal cross-section. In the upright section, there appears to be more cortical bone anteroinferiorly, but when the section is viewed in its normal anatomical orientation, the bone is thickest posteroinferiorly, as it is in the normal upright human jaw (Table 4.2, p104). As the pig likely incurs significant stress concentrations along the lingual aspect of its symphysis, our findings favor the general hypothesis proposed for primates that more bone is needed here to counter bending (Hylander, 1984).

For a cross-section to resist bending, shape is important. The ideal design is a hollow structure with its long axis in the plane of bending (Hylander, 1979b). The bending index for the pig symphysis is around 13% (Table 4.1, p103), corresponding to its long and thin shape. This form is clearly not designed to resist bending in the plane of the short axis, but the pig symphysis is very resistant to bending in the plane of its long axis. The strong jaw muscles, long muscle lever arm, high K value, and the absence in the pig of transverse bony tori or simian shelf, appear to require both the asymmetric distribution of cortical bone, and horizontal orientation of the section's long axis. We have mentioned that as pigs grow, their symphyses seem to orient more horizontally relative to the occlusal plane (see Figure 4.1, p90) since symphyseal width increases faster than its height. Therefore, during

growth, any increase in symphyseal anteroposterior width, and especially in symphyseal orientation, would seem important to help resist increasing wishboning stresses. Additionally, this orientation presumably benefits rooting behavior.

4.5.2 Stresses and strains

Although the pig deep masseter was 3.70 times larger in cross-sectional size than its human counterpart, its lever arm was 1.65 times longer, and it had a K value twice that of the human jaw, expecting to create high wishboning stresses, the high second moment of inertia in the more horizontally oriented pig symphysis compensated for them, and kept the stresses and strains within the same general ranges as those in the human jaw (Table 4.2, p104).

The predicted stresses and strains add support to the proposition that if the pig symphysis were oriented more vertically, it would be more vulnerable to failure as a consequence of wishboning (Table 4.2, p104). While the estimated strains in the normal pig symphysis (477.86 to 1118.82 με) fell within an expected functional range (e.g. below 2000 με), the strains estimated with the simulated upright symphysis could reach 4189.61 με (mean value 2258.68 με). These are well above the highest functional strain measured in the macaque symphysis (Hylander, 1985), and approach the 3000 με value considered vulnerable for bone. Our estimations may in fact be lower than those actually occurring in the pig. In addition to its contribution to wishboning, the superficial masseter everts the lower border of the mandible and inverts the alveolar process, causing tension along the lower border of the symphysis and compression on its alveolar side. The bilateral occlusion of pigs may make the symphyseal strain even

worse, as eversion would be occurring on both sides. Since the pig symphysis is obliquely oriented, its posteroinferior aspect will thus undergo tension, while its superoanterior aspect will undergo compression. This tension would superimpose upon any due to wishboning, resulting in more tensile stress (and therefore strain) than we have estimated here. Furthermore, there are shear stresses at the symphysis, and the bone's shear rigidity modulus is only one third of its elastic modulus (Dechow *et al.*, 1993; Dechow and Hylander, 2000; van Eijden, 2000). Presumably, the symphysis might be expected to function with an added safety factor, allowing the pig to accommodate its wide variety of diets (harder foods are associated with higher activity levels of the jaw-closing muscles, Herring, 1977; Herring and Scapino, 1973; Huang *et al.*, 1993).

Our results suggest relationships between dynamic stress and induced strain in the fused mammalian symphysis may be maintained across orders, since they appear similar for pig and human (818.37 με vs. 820.92 με) even though the shapes, sizes, jaw muscles and functions in the two mammalian examples differ widely. The results complement the hypothesis that the material properties of their constituent bone tissue seem to be similar in animals over a wide range of body weight (Rubin and Lanyon, 1984).

Our use of mean data to estimate muscle force, but individual measurements for skeletal tissue could explain some of the variance in estimated stresses and strains. Although we selected pigs of similar ages, their mandibular sizes nevertheless varied (the difference between the minimum and maximum lever arms was as high as 30 mm; cf. 10 mm for the human sample; see Table 4.2, p104). The cross-sectional moments of inertia also varied (the maximum-to-

minimum ratio was 3.51 for the normal pig symphyses, and 4.92 for the upright symphyses; cf. 2.22 for the human jaws; see Table 4.2, p104). The variance may also have lessened if individualized muscle data had been used in the pig sample. Even so, one should not expect this variance to exceed those from *in vivo* measurements, since the latter reflect all our anatomical variables plus additional experimental and physiological factors.

We speculate that pigs have not developed upright symphyses, nor strengthened them with superior and/or inferior tori (like cercopithecines) due to their feeding requirements. Pigs root, and do not usually rely on incisal biting. In the macaque, the superior torus and the inferior simian shelf represent a balance between the need for symphyseal strength and vertical incisal function in a long-jawed animal. In the shorter human jaw, the upright, cortically-reinforced symphysis seems adequate to meet functional demands. In the pig, the cortically-reinforced, horizontally-oriented symphysis effectively resists high wishboning stresses in a long, powerful jaw shaped for rooting.

4.5.3 Final Comment on Wishboning

Wishboning has been attributed to force from the balancing deep masseter muscle at the end of the power stroke, lateral components of bite force on the working-side, and transverse components of working-side jaw-closing muscle forces (Hylander, 1984, 1985; Hylander *et al.*, 1987; Hylander and Johnson, 1994). Medial pterygoid muscle forces reduce these wishboning stresses ("reverse" wishboning). In pigs, during the late masticatory power stroke, when the balancing-side deep masseter reaches its peak, and the working-side superficial

masseter and the working-side medial pterygoid remain active late in the stroke, the laterally-directed component of working-side (and perhaps the balancing-side in pigs) bite force would appear to be an important force contributing to wishboning. If so, one would expect wishboning to be reduced if the teeth were flat. We suggest the potential contribution of the working-side articulation seems to have been largely neglected here. If working-side teeth can react to the lateral pull of the balancing-side muscles, so can the superior and medial parts of the working-side condylar fossa, especially as the working condyle is firmly embedded at the end of the power stroke by residual elevator muscle activity. Wishboning is enhanced when any lateral components of resistive force are directed opposite the balancing-side muscles whether these forces occur at the teeth or the working-side articulation (see Figure 4.4, p111).

4.6 CONCLUSIONS

Symphyseal wishboning occurs in the mandibles of pigs and humans. The pig symphysis has larger areas of total cross-section, cortical cross-section and second moment than its human counterpart (though the relative amounts of cortical bone in both cases are similar), and it has a lower bending index. Despite these differences, and obvious dissimilarities in jaw form and muscle morphology between pigs and humans, transverse bending forces from the respective balancing-side deep masseter create similar amounts of symphyseal stress and strain (less than 2,000 με). This is accounted for by the more horizontally-oriented symphysis in the pig. The absolute size of the pig symphysis seems important for reducing shearing stresses,

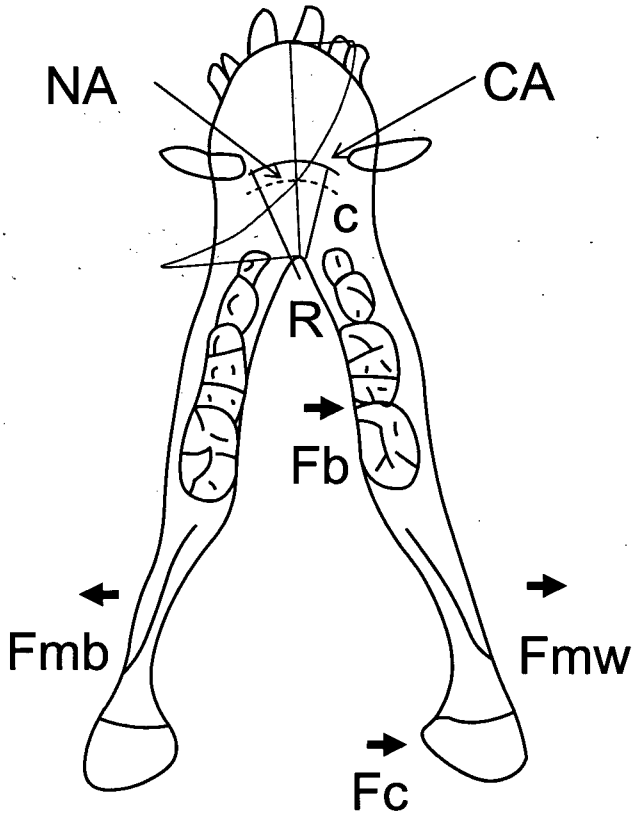

Figure 4.4 Suggested mechanism of wishboning and patterns of stress in the pig mandible. The main active forces are the balancing-side deep masseter (Fmb) and most likely the transverse component to the working-side jaw closing muscle force (Fmw, see text). Reaction forces from occlusion (Fb) and medial condylar pole (Fc) are the passive forces. Fb and Fc act in an opposite direction to Fmb when the major tooth loads are on the working-side. The force resultant tends to bend the mandible in its plane of curvature causing tension on its lingual side and compression on its facial side. All force vectors indicate directions only. Their magnitudes are unknown. R is the radius of curvature and c is the distance from the centroidal axis to the symphyseal lingual surface. The shaded area represents the stress distribution pattern across the symphysis: tensile and compressive stresses are indicated to the left and right of the midline, respectively. Due to the curvature of the symphysis, tensile stresses on the lingual side increase nonlinearly at a faster rate compared with compressive stresses on the facial side. Stress magnitudes are unknown. CA and NA represent the centroidal and neutral axes, respectively. In this curved beam, they do not coincide as in a uniform straight beam. Based on Hylander and Johnson (1994).

while the preferential distribution of cortical bone posteroinferiorly, combined with symphyseal orientation, apparently compensates for the pig's large masseters and long mandible, which otherwise would demand some form of symphyseal buttressing (e.g. in the form of lingual tori) to reduce the possibility of structural failure during function. The relationship between induced stress and strain seems to be maintained across mammalian orders (in this case, pigs and humans) as might be expected given the biomechanical principles involved, and is consistent with the hypothesis that functional equivalence, i.e. similarity in dynamic stress and strain in the fused symphysis, is common to many mammals.


CHAPTER III

5 MASS PROPERTIES OF THE PIG MANDIBLE

5.1 ABSTRACT

Specification of mass properties is an essential step when modeling jaw dynamics, but obtaining them can be difficult. Here, we used three-dimensional computed tomography (CT) to estimate jaw mass, mean bone density, anatomical locations of the mass and geometric centers, and moments of inertia in the pig jaw. High-resolution CT scans were performed at one mm slice intervals on specimens submerged in water. The mean estimated jaw mass was 12% greater than the mean wet weight, and 33% more than the mean dry weight. Putative bone marrow accounted for an extra 13% of mass. There was a positive correlation between estimated mean bone density and age. The mass center was consistently in the midline, near the last molar. The mean distance between the mass center and geometric center was small, especially when bone marrow was taken into account (0.58±0.21 mm), suggesting mass distribution in the pig jaw is almost symmetrical with respect to its geometric center. The largest moment of inertia occurred around each mandible's superoinferior axis, and the smallest around its anteroposterior axis. Bone marrow contributed an extra 9% to the moments of inertia in all three axes. Linear relationships were found between the actual mass and a mass descriptor (product of the bounding volume and mean bone density), and between the moments of inertia and moment of inertia descriptors (product of the mass descriptor and two orthogonal dimensions forming the bounding box). The study suggests imaging modalities revealing 3-dimensional jaw shape may be adequate for estimating the bone mass properties in pigs.

5.2 INTRODUCTION

Dynamic models of musculoskeletal biomechanics are a useful way to study structural and functional interactions in the mammalian masticatory system (Hannam *et al.*, 1997; Koolstra and van Eijden, 1995, 1997a, b; Otten, 1987). When driven with functions simulating motor drive to various jaw muscles, their active and passive muscle tensions produce realistic jaw motions, and generate articular and dental reaction forces. Since their properties can be changed easily, models provide a flexible environment for analyzing variations in craniofacial morphology, muscular and articular disorders, prosthetic additions, and simulated surgical alterations to the masticatory system. Also, they can be used to explain known associations, or predict new ones.

Virtual models, however, require specification of the jaw's mass properties (e.g. its mass, mass center, and moments of inertia), and these can be difficult to estimate in biological tissues (Braune and Fischer, 1988). In a study of the human head, Smith *et al.* (1995) used three different biomedical imaging modalities to compute the center of gravity and moments of inertia, and assumed the head was uniformly dense. Koolstra and van Eijden (1995, 1997b) used cubic-centimeter blocks of tissue excised from a female cadaver jaw to calculate its moments of inertia, and assumed the mass distribution of the preparation was homogeneous throughout the mandible. In related studies, Hannam *et al.* (1997), and Langenbach and Hannam (Langenbach and Hannam, 1999) assigned mass properties predicted by a Finite-element model of the human jaw developed earlier by Korioth *et al.* (1992). The FE model was constructed from computed tomographic (CT) images, and included element with tissue-properties specific for different jaw regions.

CT imaging is useful for mass-property calculation because x-ray linear attenuation discloses regional mineral densities (Lampmann *et al.*, 1984; Williams *et al.*, 1980), which account for much of the jaw's mass. Thus individual pixels with different intensity values, distributed non-uniformly in the imaged mandible, can be assigned densities reflecting mineral content, making it possible to estimate the jaw's mass properties (Smith *et al.*, 1995).

While CT has limited application in humans due to its radiation cost, it is feasible in non-human mammals like pigs, which are often employed as experimental animal models for studying human jaw function (Herring, 1995; Herring *et al.*, 1996; Teng and Herring, 1998). In the present report, we used this approach to estimate the pig jaw's mass, mass center, and moments of inertia, since none of these properties have been reported previously, and we needed them to develop a dynamic model of the pig masticatory system. In particular, we were interested in how mass properties changed with age and jaw size. Variations in regional bone density would be expected to affect the location of the mass center with respect to the pig jaw's geometric center, which is determined by shape, but is unaffected by differences in regional density. A large difference between these two centers would confirm that regional densities would have to be taken into account each time pig jaw mass properties were estimated. A small difference, however, could simplify pre-modeling procedures, because it is easier to estimate the jaw's geometric center than its mass center, and methods other than CT imaging are available for doing this. With the same goal of simplification in mind, we hypothesized that the jaw's mass and inertial properties could be satisfactorily estimated by using simple physical descriptors such as mean jaw density, and three orthogonal distances defining its size. If so, it would be unnecessary to CT scan every pig jaw used for dynamic

simulation.

5.3 MATERIALS AND METHODS

5.3.1 Material preparation

The experiments were carried out on 10 osteological specimens selected from an existing collection of miniature pig mandibles (*Sus scrofa*). We used dry specimens because we were primarily interested in the contribution of mineralized tissue to growing jaws of different shapes and sizes. In particular, we wished to define the relative magnitudes of inertial moments around their mass centers, since they may be unique to the pig jaw, given its morphology. Since we aimed for optimum edge-resolution with CT scanning, we considered the added presence of any investing soft tissues (periosteum and attached gingiva) would degrade rather than enhance image quality. By defining the internal marrow spaces however, we were able to estimate the added effect of a putative marrow component.

The sample comprised four male and five female jaws from Charles River, plus one female Purdue Minipig mandible. We selected specimens aged 29-250 days to include different jaw sizes and stages of tooth development (see Table 5.1, p126). Use of this archival material complied with the requirements of The University of British Columbia's Committee on Animal Care.

The jaws were weighed dry, and then re-weighed after hydration for 48 hours. Prior to imaging, they were separated with wooden spacers, and placed in a single, water-filled, plastic container. The specimens remained underwater during imaging to optimize resolution of the bone

interface (Daegling, 1989) and to minimize the volume-averaging error. A calibration phantom was included to permit calculation of an equation expressing bone mineral density (BMD) as a function of pixel value (Lampmann *et al.*, 1984). It consisted of four tubes of KH_2PO_4 solution at different concentrations (0.05 g/cm^3, 0.15 g/cm^3, 0.25 g/cm^3 and 0.50 g/cm^3).

5.3.2 CT scanning

Computed tomography was performed with a Toshiba Xpress SX scanner (Toshiba Corporation, Tokyo, Japan) operating at 120 kV and 150 mA. Four sequences yielded 350 near-axial slices at consecutive one mm intervals. Each slice had a 250×250 mm field of view made up of 512×512 pixels, each measuring 0.49×0.49 mm. The images were imported digitally from the scanner to a UNIX-based workstation (SGI Indigo Extreme, Silicon Graphics Inc., Mountain View, CA). Single 8-bit files were created and filtered so that any structure equal in density to or less dense than water was excluded to provide image backgrounds of uniform density and to simulate the wet bone without bone marrow.

5.3.3 Image processing

A commercial image-processing program (3DVIEWNIX, University of Pennsylvania Medical Center, Philadelphia, PA) was used for image segmentation, jaw-surface reconstruction, landmark identification and measurement. We also wrote a dedicated program (Calimage - Calculate Image, Craniofacial Laboratory, The University of British Columbia; available from http://condor.dentistry.ubc.ca) and used a desktop microcomputer (Pentium 200 MHz MMX) to perform specific image matrix operations. These two programs were run interchangeably.

5.3.4 Mass properties calculation

The three-dimensional (3D) image was consisted of voxels located relative to the scanner's coordinate system. We assumed the volume (v) of each voxel was:

$$v = w \times h \times d \qquad \text{Equation 5.1}$$

where *w*, *h*, and *d* were the width, height, and depth (slice thickness) of a voxel, respectively.

Since it has been shown that CT grayscale values (GSV) vary linearly with BMD (Lampmann *et al.*, 1984), we used the following equation to calculate BMD for each voxel:

$$BMD = a + b \times GSV \qquad \text{Equation 5.2}$$

where *a* and *b* are two constants representing the intercept and slope of the linear equation, respectively.

The mass of each voxel was then determined by:

$$dm = BMD \times v \qquad \text{Equation 5.3}$$

where *dm* is each voxel's mass. Because the voxel size for each CT image set is constant, the relative magnitude of each voxel's mass will be represented by BMD and in turn by the CT grayscale value.

With calculus, the total mass (*M*) can be easily calculated as:

$$M = \int dm \qquad \text{Equation 5.4}$$

and the three coordinates of the mass center (Cx, Cy, Cz) as:

$$C_x = \frac{1}{M} \times \int x \times dm$$

$$C_y = \frac{1}{M} \times \int y \times dm \qquad \text{Equation 5.5}$$

$$C_z = \frac{1}{M} \times \int z \times dm$$

where x, y, z are the three coordinates of each voxel relative to the image matrix origin (usually the front-left-top point in a right-hand coordinate system).

Assuming dm in Equation 5.3 (p119) to be constant, we obtain the three coordinates of the geometric center. The distance between the two centers (CD) can be calculated as:

$$CD = | MC - GC | \qquad \text{Equation 5.6}$$

where MC and GC are the mass and geometric centers as 3D vectors.

The total volume (V) of the jaw is just a product of each voxel's volume and the total number of voxels. Therefore, the mean bone density (MBD) can be calculated as:

$$MBD = M / V \qquad \text{Equation 5.7}$$

This is the estimated mean bone density of the entire jaw.

Calculations of the jaw moments of inertia from the image matrix depended upon the jaw's original orientation in the scanner, and consequently in the image matrix. These are calculated as:

$$I_{xx} = \int (y^2 + z^2) \times dm$$

$$I_{yy} = \int (x^2 + z^2) \times dm$$

$$I_{zz} = \int (x^2 + y^2) \times dm$$

Equation 5.8

$$I_{xy} = \int x \times y \times dm$$

$$I_{yz} = \int y \times z \times dm$$

$$I_{zx} = \int z \times x \times dm$$

where *Ixx, Iyy, Izz* are the three moments of inertia with respect to the three axes in the image matrix coordinate system, respectively; *Ixy, Iyz, Izx* are the products of inertia with respect to the image matrix system.

As a convention, however, it is best to express the jaw's moments of inertia relative to some anatomical reference. Therefore, moments of inertia transformation was necessary. The transformation of moments of inertia needed two steps. First was a translation from the image matrix coordinate system to the mass center by parallel-axis theorem:

$$\bar{I}_{xx} = I_{xx} - M \times r^2$$

$$\bar{I}_{yy} = I_{yy} - M \times r^2$$

$$\bar{I}_{zz} = I_{zz} - M \times r^2$$

Equation 5.9

$$\bar{I}_{xy} = I_{xy} - C_x \times C_y \times M$$

$$\bar{I}_{yz} = I_{yz} - C_y \times C_z \times M$$

$$\bar{I}_{zx} = I_{zx} - C_z \times C_x \times M$$

where r is the magnitude of the center of mass expressed as a 3D vector relative to the original image matrix origin. This step translates the moments of inertia from the image matrix to the mass center.

The second step was a rotation according to the anatomically defined coordinate system. Three unit vectors representing the orientation of the new coordinate system must be obtained from direct morphometric measurements. The rotation was completed by:

$$I_{OL} = \bar{I}_{xx} \times \lambda_x^2 + \bar{I}_{yy} \times \lambda_y^2 + \bar{I}_{zz} \times \lambda_z^2 - 2 \times \bar{I}_{xy} \times \lambda_x \times \lambda_y - 2 \times \bar{I}_{yz} \times \lambda_y \times \lambda_z - 2 \times \bar{I}_{zx} \times \lambda_z \times \lambda_x$$

Equation 5.10

where λ_x, λ_y, and λ_z are the three components of each unit vector representing the three new axes, and I_{OL} is the moment of inertia with respect to the new axis.

Calculation of mass properties was performed programmatically by Calimage. Moments of inertia were expressed in the anatomical coordinate system as illustrated in Figure 5.1 (p123). The program also inserted an artificial "marker" voxel of known intensity at the mass center. When the image was reconstructed as a 3D object, the marker could be visualized and measured with respect to each jaw's anatomy.

To estimate the potential contribution of bone marrow space to the jaw's mass properties, we segmented the non-mineralized, marrow component in each CT section, assigned these pixels a density value of one g/cm^3, and recalculated the mass properties. The density assigned to the marrow component was based on a calibrated tissue density of 1.003±0.034 g/cm^3, which we measured from calibrated CT scans of the marrow space in the mandible of a living pig. Thus, we assumed the mean density of all non-mineral fluid and cellular components in the marrow space was very close to one g/cm^3.

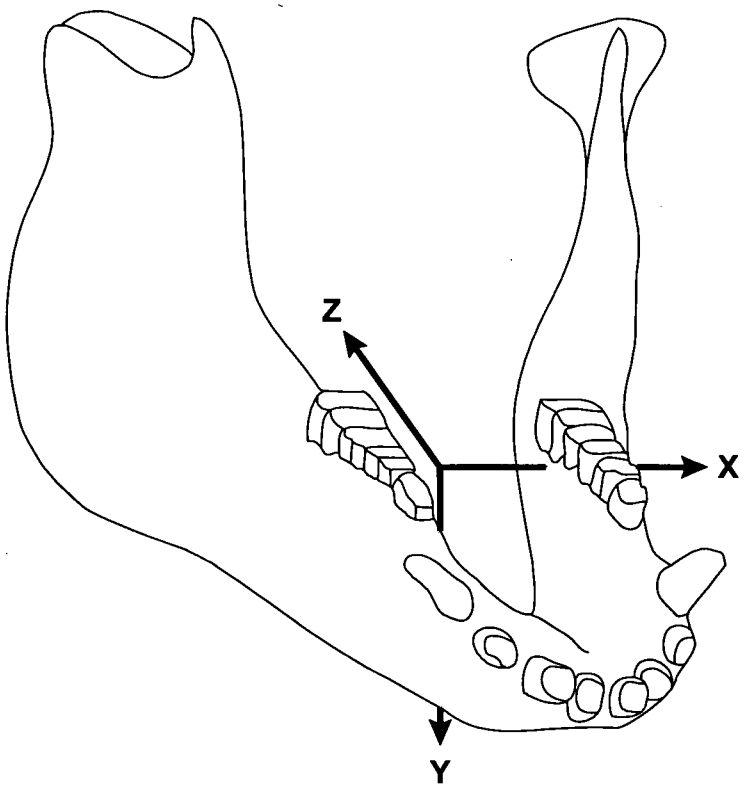

Figure 5.1 Diagram of the coordinate system used to express moments of inertia of the jaw. The origin was located at the mass center. The X-axis was directed transversely, the Y-axis superoinferiorly in the midsagittal plane, and the Z-axis anteroposteriorly in the midsagittal plane, with the X-Z plane parallel to the occlusal plane.

The following variables were used to determine how effectively "global", rather than CT-derived descriptors could be used to predict the jaw's mass and inertial properties:

- Jaw width (WD), defined as the horizontal distance between the two lateral condylar poles
- Jaw height (HD), defined as the vertical distance from the tip of the coronoid process to the lower border of the ramus
- Jaw length (LD), defined as the horizontal distance between the tip of the central incisor and the posterior border of the ramus
- Jaw Volume (VD), defined as the product of WD, HD and LD
- Jaw Mass (MD), defined as the product of VD and MBD
- Three moments of inertia (Ixx D, Iyy D, and Izz D), each defined by the product of MD and two orthogonal descriptors describing moments of inertia with respect to the third axis

The descriptors for jaw width, height and length represented linear measurements determined by the respective bounding box of the bone volume, i.e. they defined the anatomical limits of the specimens in each dimension. Descriptors normally used for cephalometric measurements in humans (e.g. jaw length) were inappropriate in the pig since they do not include the limits of tissue contribution to mass property estimation.

Regression curves describing the relationships between the descriptors and the specific mass properties derived from the CT data were then fitted to the data.

5.4 RESULTS

As expected, the phantom-derived data revealed a linear relationship between pixel values and mineral density (correlation coefficient 0.999).

The equation describing the relationship was

$$BMD = 0.997 + 0.013 \times PixelValue .$$

As this function was obtained after all pixel values less than those for water were set to zero, the procedure was in effect self-validating (with a pixel value of zero, the BMD was 0.997, very close to the density of water).

Estimated masses with and without bone marrow, the measured weights, and mean bone densities with and without bone marrow, are shown in Table 5.1 (p126). Overall, the estimated jaw mass was 12% greater than the wet weight (mean EM/WW=1.12±0.05; coefficient of variation 4.64%), and 49% greater than the dry weight (mean EM/DW=1.49±0.13; coefficient of variation 8.72%). The inclusion of bone marrow added 13% to the mass estimated without marrow (mean EMM/EM=1.13±0.06). The estimated mass with marrow was 68% greater than the measured dry weight of the jaw (mean EMM/DW=1.68±0.23). When bone marrow was included in the calculations, the mean bone density decreased by 6%, for the bone marrow was less dense than mineralized bone. The mean bone density (which included dentin and enamel) was greater in the older animals, but there was no clear relationship between mean bone density and gender.

The mass center was always located near the last-erupted tooth (DP4 or first molar in this sample, Figure 5.2, p127). Relative to the dentition, mass center positions in young mandibles were further forward than in older animals (Figure 5.3, p128). When mass center was calculated relative to the normalized, mid-sagittal distance between the intercondylar point and infradentale, there was no systematic pattern in the sample as a whole (Figure 5.3, p128). Inclusion of simulated bone marrow in the calculations altered mass center locations by a mean distance of 1.03±0.29 mm, and geometric center locations by 1.74±0.49 mm, but in no systematic direction (Figure 5.3, p128). Differences

Table 5.1 Descriptive statistics of the dry and wet weights (DW, WW), estimated masses without and with bone marrow (EM, EMM), calculated mean bone densities without and with bone marrow (MBD, MBDM), and the ratios between these variables. The table also contains each animal's gender and age. All mass measurements are in g, and all density measurements are in g/cm^3.

Jaw #	Sex	Age	DW	WW	EM	EMM	EMM/EM	MBD	MBDM	MBDM/MBD	EM/DW	EMM/DW	EM/WW	EMM/WW
1	F	29	5.28	7.04	8.55	10.63	1.24	1.41	1.31	0.93	1.62	2.01	1.21	1.51
2	M	35	11.16	18.60	19.59	23.84	1.22	1.38	1.29	0.93	1.76	2.14	1.05	1.28
3	F	77	45.71	62.60	68.09	77.63	1.14	1.56	1.46	0.94	1.49	1.70	1.09	1.24
4	F	86	46.65	64.90	73.57	82.91	1.13	1.55	1.46	0.94	1.58	1.78	1.13	1.28
5	M	115	79.16	98.95	113.01	123.22	1.09	1.70	1.61	0.95	1.43	1.56	1.14	1.25
6	F	131	67.42	85.81	94.20	104.53	1.11	1.64	1.54	0.94	1.40	1.55	1.10	1.22
7	M	175	114.83	147.64	154.95	169.78	1.10	1.73	1.63	0.94	1.35	1.48	1.05	1.15
8	F	186	155.46	190.23	215.16	230.01	1.07	1.77	1.69	0.95	1.38	1.48	1.13	1.21
9	F	230	116.15	146.19	168.64	184.09	1.09	1.73	1.63	0.94	1.45	1.58	1.15	1.26
10	M	250	180.91	217.09	255.83	280.02	1.09	1.74	1.63	0.94	1.41	1.55	1.18	1.29
Mean		131.40	82.27	103.91	117.16	128.67	1.13	1.62	1.53	0.94	1.49	1.68	1.12	1.27
SD		77.27	58.80	70.08	81.02	87.03	0.06	0.14	0.14	0.01	0.13	0.23	0.05	0.09
Adj.*					104.61	114.88		1.45	1.36		1.33	1.50	1.00	1.13

* Adjusted value: since the phantom overestimated all masses by 12%, the adjusted values are those divided by 1.12.

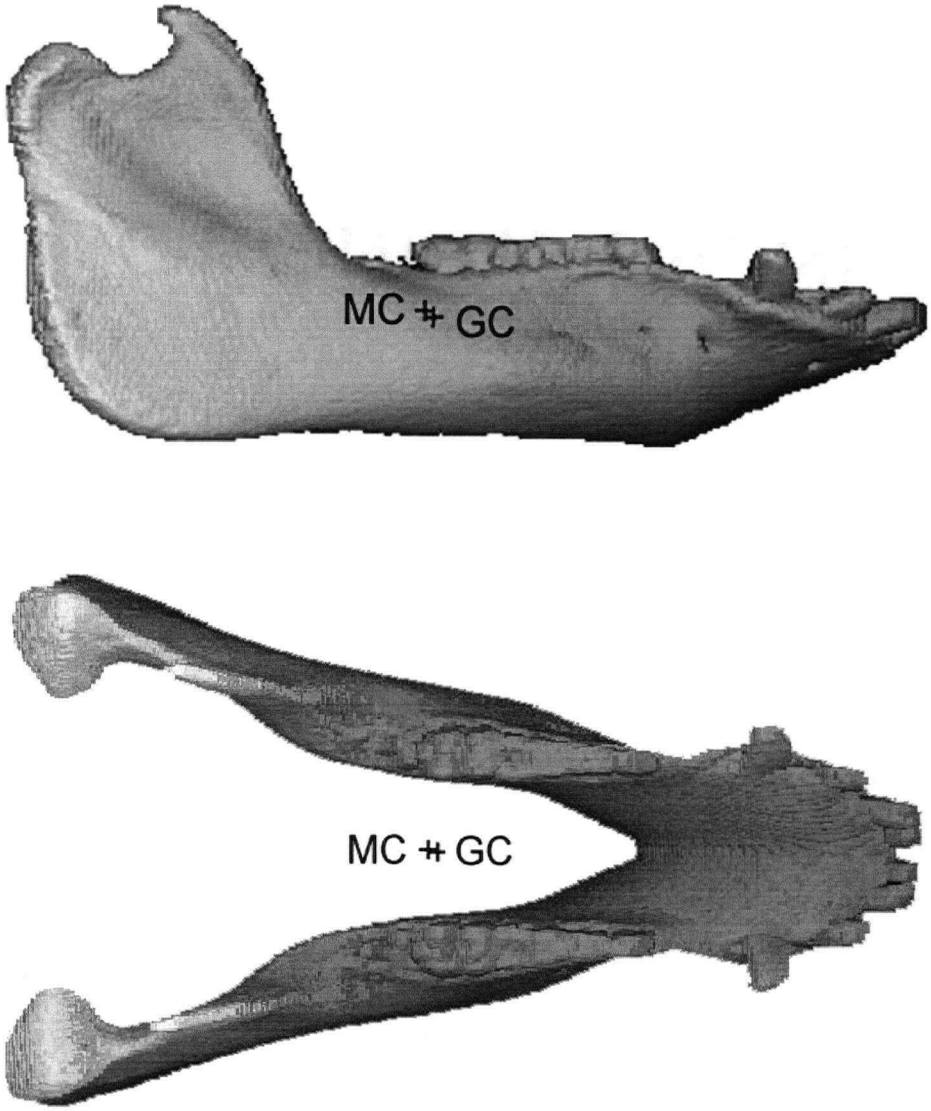

Figure 5.2 Lateral (above) and horizontal (below) views of a voxel-based, reconstructed dry mandible with calculated mass center (MC) and geometric center (GC) locations.

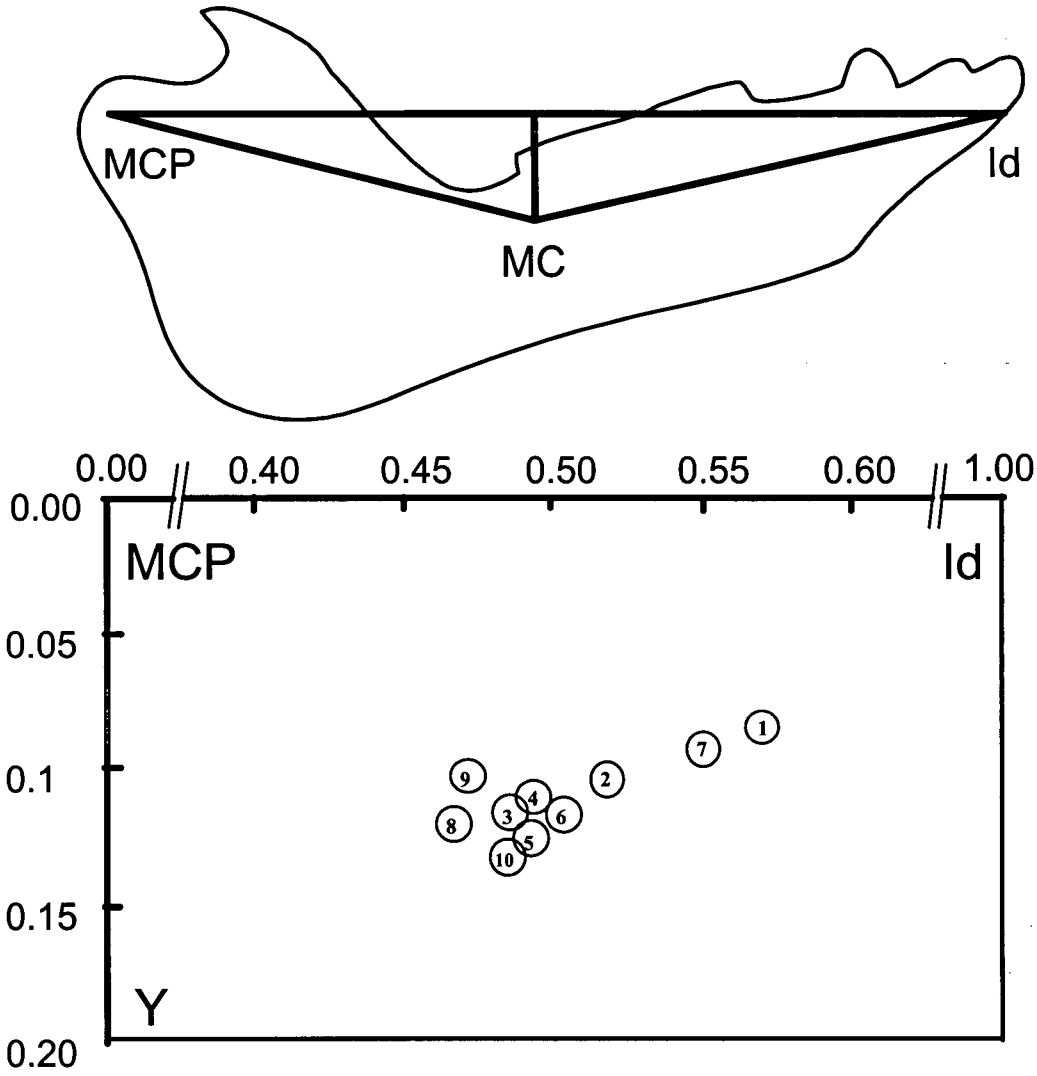

Figure 5.3 Distribution of mass center (MC) locations relative to the mid-condylar point infradentale (MCP-Id) line for 10 pig mandibles. The MCP-Id line length is normalized to unity. The central region of the MCP-Id axis has been expanded for clarity (indicated by broken MCP-Id axis). Numbers for each plot indicate specimens from Table 5.1 (p126).

between the mass center and geometric center locations were small, especially when the bone marrow space was included. Table 5.2 (p130) shows the mean linear distances between mass center and geometric center were 1.15±0.30 mm without bone marrow, and only 0.58±0.30 mm with marrow.

The moment of inertia was smallest around the jaw's anteroposterior z-axis, and largest around the vertical y-axis. Inclusion of bone marrow increased the moments of inertia around each axis by about 9% (Table 5.3, p131).

Regression analysis revealed virtually linear relationships between estimated masses, measured weights and the general mass descriptor (R^2=0.9945, 0.9930, 0.9851, and 0.9909 for EMM, EM, WW and DW, respectively, Figure 5.4, p132). There were also linear relationships between the three moments of inertia and their respective moments of inertia descriptors (R^2=0.9978, 0.9964 and 0.9854 for Ixx D, Iyy D, and Izz D respectively, Figure 5.5, p133). Linear regression equations are also presented in Figure 5.4 (p132) and Figure 5.5 (p133).

5.5 Discussion

X-rays are attenuated according to the density of the structure, and the degree of beam attenuation in a CT image is expressed in Hounsfield units or CT numbers (Lampmann *et al.*, 1984). Although the distribution of this attenuation maintains an almost linear relationship with structural density (making it possible to measure tissue density indirectly from the CT image; Lampmann *et al.*, 1984), the accuracy of measurement is affected by intrinsic artifacts. One of these is the result of volume averaging. If the slice thickness is too thick, or the pixel size too large to

Table 5.2 Differences between calculated mass center and geometric center without and with bone marrow (CD, CDM in mm), and the anteroposterior anatomical locations of the mass center. Abbreviation: DP4, deciduous fourth premolar; M1, permanent first molar.

Jaw #	CD	CDM	Anteroposterior mass center location
1	1.08	0.77	Mesial cusp DP4
2	0.72	0.28	Middle cusp of DP4
3	1.47	0.95	Distal cusp of DP4
4	1.02	0.37	Distal cusp of DP4
5	1.07	0.38	Mesial cusp of M1
6	1.44	0.75	Mesial cusp of M1
7	0.71	0.55	Mesial cusp of M1
8	1.10	0.53	Distal cusp of M1
9	1.48	0.63	Mesial cusp of M1
10	1.44	0.54	Distal cusp of M1
Mean	1.15	0.58	
SD	0.30	0.21	

Table 5.3 Moments of inertia without and with bone marrow (Ixx, Iyy, Izz, IxxM, IyyM, IzzM) and the ratios between the two groups. Units for all moments of inertia are g·cm².

Jaw #	Ixx	IxxM	IxxM/Ixx	Iyy	IyyM	IyyM/Iyy	Izz	IzzM	IzzM/Izz
1	23.97	27.28	1.14	33.52	38.89	1.16	12.64	15.11	1.20
2	102.65	117.75	1.15	123.00	142.36	1.16	64.32	75.28	1.17
3	662.31	752.19	1.14	906.98	1030.46	1.14	446.51	499.49	1.12
4	892.14	962.35	1.08	1154.79	1253.82	1.09	520.87	565.14	1.08
5	1519.55	1617.49	1.06	2069.83	2203.69	1.06	843.30	890.54	1.06
6	1218.20	1315.04	1.08	1414.10	1527.74	1.08	638.71	688.31	1.08
7	2817.68	3004.58	1.07	3513.63	3747.36	1.07	1449.34	1526.26	1.05
8	4644.09	4846.24	1.04	5185.03	5431.21	1.05	2465.34	2559.35	1.04
9	3190.93	3404.54	1.07	3594.85	3835.34	1.07	1855.17	1969.05	1.06
10	7230.04	7667.65	1.06	8626.23	9169.59	1.06	3346.58	3541.30	1.06
Mean			1.09			1.09			1.09
SD			0.04			0.04			0.05

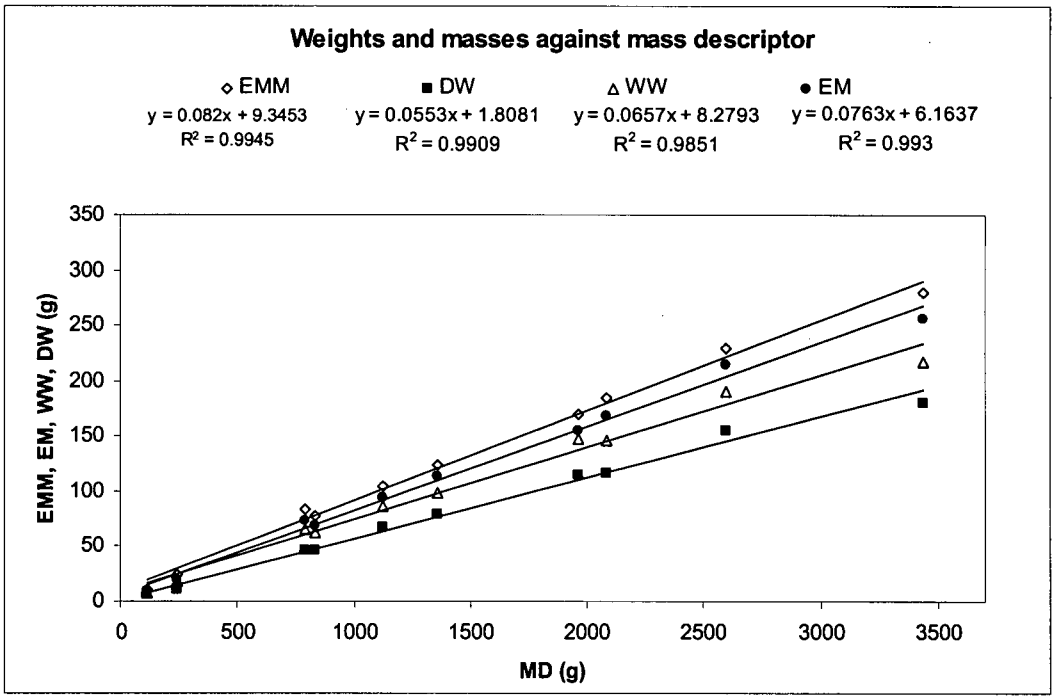

Figure 5.4 Estimated mass with bone marrow (EMM), estimated mass (EM), wet weight (WW) and dry weights (DW) plotted against the mass descriptor (MD). Figures also include the regression equations and coefficients of determination (R^2).

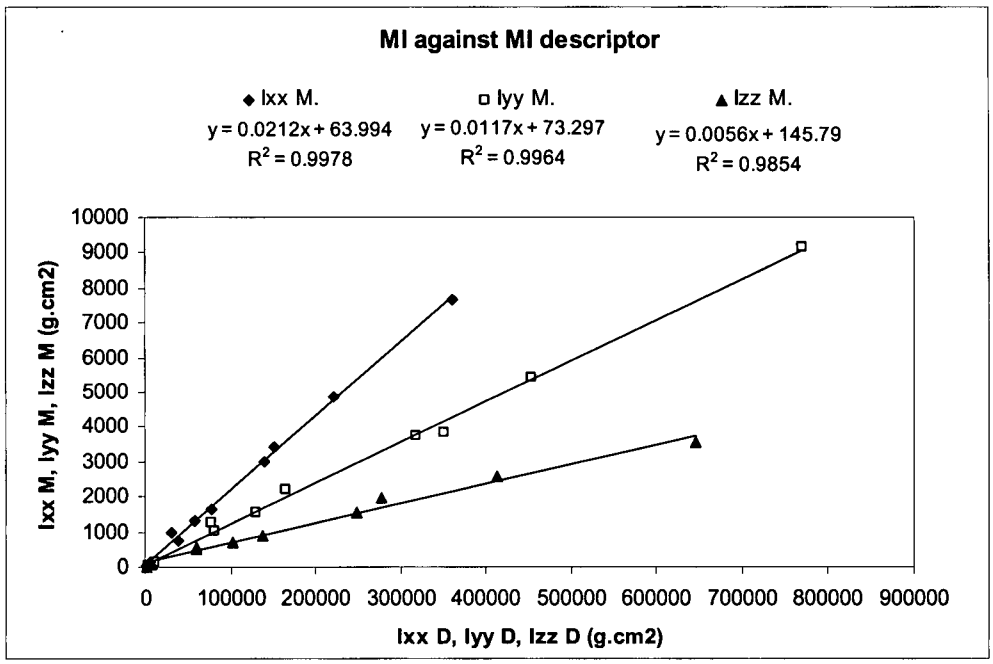

Figure 5.5 Moments of inertia with marrow (IxxM, IyyM, IzzM) plotted against moment of inertia descriptors (Ixx D, Iyy D, Izz D). Figures also include the regression equations and coefficients of determination (R^2).

include the smallest region scanned, the area will be averaged with adjacent ones, and the CT number will not reflect the actual density of the region. This happens frequently in bone due to its porous structure. In living subjects, these small spaces are filled with soft-tissue containing cells and fluid, while in dry bone they are filled with air. The error increases when the bone is volume-averaged with air. Selecting smaller voxel sizes can minimize the artifact, but this requires higher imaging resolution than the resolution used in our study.

A second source of error is due to beam hardening. Since the scanned structure absorbs more low-energy photons than high-energy ones, the attenuation coefficient becomes non-linear (i.e. decreases) as the thickness of the structure increases (Crawley, 1990). While the thickness of the object cannot be adjusted, mathematical corrections are usually made in the scanner's image reconstruction process (Crawley, 1990). Dual-energy CT scanning aims to minimize the beam hardening effect by scanning the structure at two different kV levels, which involves additional radiation. Dual-energy x-ray absorptiometry (DEXA) is widely used clinically to measure BMD (Grier *et al.*, 1996; Jergas *et al.*, 1995; Koo *et al.*, 1995; Mazess *et al.*, 1990). The main limitation of this technique is the inability to separate cortical from cancellous bone. Furthermore, DEXA converts a three-dimensional structure into a two-dimensional image, and measures "areal" density rather than true volumetric density (Grier *et al.*, 1996). Thus, DEXA's precision depends on consistent subject positioning.

We believe single-energy CT scanning was an appropriate method in the present context because it has better precision than DEXA (Crawley, 1990; Lindh *et al.*, 1996) and the measurements are three-dimensional. Since it produces very thin slices with small pixel sizes, it is suitable for

measuring regional bone densities. Additionally, the correlation between CT numbers and BMD-equivalent phantoms is known to be quite high, with correlation coefficient over 0.99 (0.999 in the present case) for both hydroxyapatite and potassium dihydrogen phosphate solutions (Lampmann *et al.*, 1984).

There are other potential sources of error in the present study. First, we could have chosen an incorrect threshold at which to filter out the image background and bone marrow space. Ideally, everything less dense than water should be set to a zero pixel value, making the intercept of the calibrating equation exactly the density of water. Normally, this is impractical because pixel values are not consecutive numbers. For example, in this data set, when we set the pixel value threshold to 56, we obtained an intercept of 0.997. We could have used a threshold of 57, in which case the intercept would have been 1.017. Second, our choice of threshold did not guarantee removal of pixel "noise" from the very low-value single pixels around the border of each mandible, some of which could have affected the calculated moments of inertia if they were located far from the center of mass. We minimized this error by careful manual segmentation of each image before any calculations were made. A third source of error may have occurred due to the medium we selected to fill the dry bone. We used water because it more closely approximates the Hounsfield unit value for soft tissue, and provides a clear interface between bone and any background medium (Daegling, 1989; Snyder and Schneider, 1991). If we had used air for example, the bony outer margins and cancellous bone would have been volume-averaged with air, resulting in lower Hounsfield unit values. This would have significantly under-estimated bone density and mass. The fourth source of error was the volume of the assumed bone marrow space and the density we assigned it. The dry mandible had lost its bone marrow, and its space was filled

with water. If some of the marrow spaces had been smaller than the voxel size (0.24 mm^3), they would have been volume-averaged with bone. Finally, our landmark measurements on the reconstructed images may not have been accurate. Theoretically, the minimum error is determined by voxel size, because software interpolations during the 3D reconstruction process are artificial. If an anatomical landmark actually falls on a surface between two voxels, only one can be selected. Table 5.4 (p137) shows the variance in four typical landmarks that were re-measured 10 times in one specimen. The landmarks include the right condylar lateral pole, infradentale, mass center, and right molar point (defined as the tip of the mid-facial cusp of DP4). The variance, though small, differs according to axis, and might have affected our measurements of landmarks for mandibles with different orientations. Similar errors have been discussed previously (Richtsmeier *et al.*, 1995).

Notwithstanding the above reservations, the ratios between estimated mass and the actual wet and dry weights were quite consistent for the sample as a whole (1.12±0.05 and 1.49±0.13 respectively) even when simulated bone marrow was included (1.27±0.09 and 1.68±0.23 respectively), confirming the estimated values were always greater than the actual jaw weights. These relationships remained constant, even though the sample comprised different ages and genders. The two youngest mandibles contributed most to the variance, most likely due to their internal morphology (which included a much larger proportion of marrow space). Data from the eight more-mature animals suggests the variance in estimated mass with respect to measured weights (with and without bone marrow inclusion) is indeed quite low.

Overestimation of dry-bone mass for CT scanning with uniform phantom calibrators has been reported previously. For example, Cheng *et*

Table 5.4 Error distribution in landmark definition for 10 repeated measurements in pig jaw #10. Data include mean landmark coordinates (x, y, z), their standard deviations and standard errors for right condylar lateral pole (RCLP), infradentale (Id), mass center (MC) and right molar point (RMP). Units are in mm.

	Mean	SD	SE
RCLP x	-11.36	0.32	0.10
RCLP y	4.00	0.35	0.11
RCLP z	14.97	0.41	0.13
Id x	-15.43	0.14	0.04
Id y	29.39	0.27	0.09
Id z	-94.26	0.25	0.08
MC x	-7.89	0.09	0.03
MC y	18.49	0.21	0.07
MC z	8.64	0.56	0.18
RMP x	48.19	0.09	0.03
RMP y	-29.37	0.38	0.12
RMP z	-84.67	0.68	0.22

al. (1995), who used KH_2PO_4 as bone-standard solution, reported a 15% overestimation of ash-apparent density for cow bone. In the present case, a consistent 12% overestimation in pig mandibular bone mass is therefore not surprising. Most likely, it is attributable to the uniform density of the solution used for calibration (compared with the inhomogeneous structure of bone), and to the volume averaging of bone and water that occurs when pixel sizes exceed the bone components within them. It is difficult to estimate which of these two factors had the most profound effect in this instance. Theoretically, smaller pixel sizes than those used here might have lessened the overestimation.

It seems appropriate to compare masses estimated from the CT scans with the wet weights of the same jaws. In the former instance, though the imaged bone was immersed in water during imaging, all pixels containing water alone were excluded in the initial analysis (i.e. corrections for marrow space were made later); in the latter case, we drained all free water from the marrow spaces and canals immediately prior to weighing. We could not, however, ensure that all the very small spaces among the porous bone were free of water. Similarly, when we applied the filter, we could not exclude the water from those spaces smaller than the voxel size, i.e. the water was volume-averaged with bone, and would have resulted in higher pixel values than pure water. Thus we expected the estimated masses to be closest to the wet weights, and we conclude that the 12% overestimation we found represents an error attributable to the physical homogeneity of the calibrating solution and the imaging process. A 12% reduction in the mass estimated by CT scanning apparently provides a good estimate of the pig jaw's wet weight without marrow, especially in mature animals.

Comparison of the estimated mass including (theoretical) marrow with

the wet weight of the same jaws indicated an overestimation of 27%. Since the 12% reduction referred to above would still apply to the mineralized component when living animals are imaged, a useful working figure to estimate wet weight plus marrow might be to reduce the estimated mass by 13%. It should be noted however that true marrow density was not verified directly in our study, and may not actually conform to the value we assigned it (though we believe it was close).

Though DEXA expresses bone area density in g/cm^2 (a planar measurement), we expressed density in g/cm^3. Our results show that mean bone density increases with age from 1.38 g/cm^3 to 1.74 g/cm^3. As the oldest pig in our sample was actually quite young (250 days), our maximum density of 1.74 g/cm^3 might be expected to be less than that reported by Martin and Ishida (Martin and Ishida, 1989) for adult bovine femur (2.01 g/cm^3 wet, and 1.80 g/cm^3 dry, respectively). The lack of any relationship between mean bone density and gender may simply be that our sample was too small to reveal one if it was present.

While it would have been ideal to compare our estimations of the jaw's moments of inertia with direct measurements, this is not an easy task. It is difficult, for example, to balance pig mandibles across knife-edges in order to apply known tri-axial torques, and to record induced jaw motion accurately with accelerometers. Approaches like this have their own significant errors. One is then faced with the task of comparing and interpreting data from two different sources, both of which have presumed, but unknown and unprovable errors. In the present case, we were reassured by our ability to predict the jaw's mass successfully in specimens of such different shapes and sizes, since this calculation would have been influenced by errors in assigned density, and its distribution. If it can be assumed that our voxel-based predictions of mass were indeed

acceptable, our method for subsequent calculation of the jaw's moments of inertia is arguably the most accurate we know, for it depends solely on the ability of CT-scanning to express the dimensions of the jaw by means of voxels measuring sub-cubic mm. Once voxel masses are known, specification of their relative distances from a common origin is the only remaining requirement, and we consider this method an accurate way of doing this.

Because the pig mandible is U-shaped and long anteroposteriorly, its larger moments of inertia would be expected to occur with respect to its transverse x-axis and its superoinferior y-axis, and its smallest moment of inertia with respect to the anteroposterior z-axis, as confirmed in the present study. The fact that the moment around the y-axis was always the largest may be specific to the pig jaw. Different combinations of moments probably exist in different mammals, and our observation highlights the care needed when extrapolating properties like these to humans. The different moments of inertia seen in young and old mandibles in our study can be attributed directly to variations in jaw mass and size. These differences appear sizeable enough to require attention when jaw biomechanics are modeled at different stages of growth.

The extent to which inertial properties (and errors in their specification) affect jaw motion in simulation studies of the pig remains unclear, although it is obvious values must be assigned in order to predict the motion of any body in space. In a working environment that includes high active and passive muscle tensions (as well as other constraining forces such as articular and tooth loads) the significance of values used to describe moments of inertia has to be balanced against the jaw's acceleration during normal function. Since this is not particularly high, it

is possible that the jaw's dynamics are limited more by external constraints than by its inherent inertia, but this can only be established in subsequent dynamic modeling studies of the pig masticatory system.

Because dental enamel is denser than bone, we supposed the location of mass center would be related to the number, size and location of the teeth, and in fact found it was consistently located near the last-erupted tooth. Although the younger mandibles seemed to have their mass centers further forward, there was no systematic pattern. This, again, may be attributed to our small sample size.

Since the pig mandible comprises tissues of different density, we expected its mass center would differ considerably from its geometric center (which is shape-dependent), but they were quite close, even in jaws of different sizes; the linear distance between them actually decreased to an average of 0.58 mm when we included simulated marrow in our calculations. A change in the mass center would be expected with the addition of hypothetical bone marrow, but it is less obvious why geometric center would also alter, since it is defined solely by jaw shape. In our study, jaw shape was defined by both its internal and external bony boundaries. The internal boundary obviously altered when the jaw was "filled" with marrow, causing a shift in the geometric center as well as mass center. The small difference between mass center and geometric center may be specific to the pig (i.e. uniquely determined by the way tissues of different density are distributed) but would be representative of a common mammalian trend. This question can only be answered by further experiment. Our results, however, offer the option of estimating the mass center by measuring the geometric center alone, at least in the pig. Being shape-derived, geometric center may be easier to obtain by less-invasive means than CT scanning, and if future experiments show

that mass center and geometric center are also close in the human jaw, magnetic resonance (MR) imaging might be a practical way to estimate mass center when modeling living humans.

Finally, our study suggests a mass descriptor (the product of mean bone density and three simple linear measurements of jaw size and shape) can be used to predict the jaw's mass. Since we have provided estimates of average jaw density in the present study, we can make a reasonable estimate of mass in a specific pig by using these values, and three linear measurements obtained either by direct mensuration, or from various jaw images. Taken together, this method for predicting jaw mass, and the equations linking the descriptors for moments of inertia with calculated moments of inertia, offer a simple way of estimating the mass properties needed for modeling living pigs (at least in young adults of different sizes) without the need for CT scanning. A separate study of the age-density relationship would however be useful in pigs, especially in very young and very old animals.

It should be feasible to carry out a similar study to ours on human mandibles, not only to determine their mass properties, but also to verify whether these too can be predicted, with acceptable accuracy, by MR imaging or by direct measurements of the jaw. If so, it might be possible to model mass properties, and consequently jaw dynamics, in living subjects.


CHAPTER IV

6 MASS PROPERTIES OF THE HUMAN MANDIBLE AND THEIR FUNCTIONAL SIGNIFICANCE

6.1 ABSTRACT

Realistic computer simulation of masticatory system dynamics requires specification of the jaw's mass properties. Recently, we estimated these in the pig, and suggested imaging modalities with uniform representation of bone density may be adequate to perform this task (Zhang *et al.*, 2001a, see Chapter III, p114). Here, we wished to determine if this is true for the human jaw, since it differs morphologically from that in the pig. We also wished to determine the sensitivity of an existing dynamic jaw model to these mass properties during postural rest and jaw opening. High-resolution CT scans were performed on 13 osseous specimens. Calibration phantoms were used to convert CT numbers to mineral density. The mean estimated jaw mass was 13% greater than the mean wet weight for the adult dentate mandibles, and 15% greater for the whole sample. Putative bone marrow accounted for an extra 9% of mass. The mean bone densities for adult dentate mandibles were very consistent (1.72±0.02 g/cm^3). The mass and geometric centers were close (mean linear difference 0.57±0.32 mm). The largest moment of inertia (MI) occurred around each jaw's superoinferior axis, and the smallest around its transverse axis. Bone marrow added an extra 7-9% to MIs around the three axes. Linear relationships were found between the actual mass and a mass descriptor (bounding volume x mean bone density), and between MIs and three MI descriptors (mass descriptor x

two orthogonal dimensions of the bounding box). Dynamic modeling with median inertial values suggests while mass and mass center are critical aspects in modeling jaw dynamics, the moments of inertia are low, and less influential.

6.2 INTRODUCTION

Dynamic models are a useful way to observe musculoskeletal structure and function in the human masticatory system (Hannam *et al.*, 1997; Koolstra and van Eijden, 1995, 1997a, b; Langenbach and Hannam, 1999; Otten, 1987). Since they permit rapid changes in craniofacial form, muscle properties and muscle drive, these models provide a construct for explaining force interactions among the muscles, joints and teeth. Also, they are a potentially beneficial way to study the biomechanics of clinically-relevant conditions including developmental abnormalities, musculoskeletal disorders, surgical interventions and replacement prostheses.

The extent to which dynamic jaw models are sensitive to mass properties assigned to them is not fully understood. These properties can be difficult to estimate in living subjects (Braune and Fischer, 1988), and even in excised human tissue (Koolstra and van Eijden, 1995). Changes in the center of gravity alter jaw and condylar velocities during jaw-closing, though variations in the moments of inertia are reported to have little effect (Koolstra and van Eijden, 1995). A relevant factor here is muscle damping, which has been shown to affect jaw motion in living subjects and kinetic jaw models (Peck *et al.*, 2000). Muscle damping is likely to be particularly effective during jaw opening, when both active and passive muscle tensions are generated.

Recently, we used computed tomography (CT) to estimate mass properties of the pig jaw (Zhang *et al.*, 2001a, see Chapter III, p114). With suitable correction factors, the method provides a good approximation of the jaw's wet weight, including simulated bone marrow. The pig jaw's mass center and geometric center almost coincide, and there are linear relationships between the jaw's actual mass and a general mass "descriptor" (defined by jaw volume and mean bone density), and also between its moments of inertia and moments of inertia "descriptors" (defined by the mass "descriptor" and the overall dimensions of the jaw). The findings suggest the density distribution of the pig mandible is relatively homogeneous around its geometric center.

Here, we estimated the mass properties of the human jaw the same way. We considered if the mass and geometric centers also coincided in humans, and if simple dimensional descriptors could be used to estimate mass properties (as in the pig), then simple non-invasive methods might be used to estimate jaw mass properties in living subjects. We then studied the effect of modifying these mass properties, and those reported by Koolstra and van Eijden (1995), in an existing muscle-damped model of jaw-opening (Peck *et al.*, 2000). We were particularly interested in the sensitivity of the model to alterations in the mass, mass center, and moments of inertia when the jaw was at postural rest, and during active opening to maximum gape.

6.3 MATERIALS AND METHODS

6.3.1 Mass property estimation

Mass properties were estimated in 13 archived human mandibles of unknown gender. The sample included eight jaws with adult dentitions,

two with mixed dentitions, two with deciduous dentitions, and one edentulous jaw. Use of this material complied with the requirements of The University of British Columbia's Ethical Review Committee.

Details of the CT scanning, image processing and calculation of the properties have been reported elsewhere (Zhang *et al.*, 2001a, see Chapter III, p114). In brief, the jaws were weighed dry, and re-weighed after hydration for 48 hours. They were submerged in water during imaging to optimize resolution of the bone interface (Daegling, 1989), and to minimize volume-averaging errors. Calibration phantoms containing KH_2PO_4 solutions at concentrations of 0.05, 0.15, 0.25 and 0.50 g/cm^3 were used to express bone mineral density (BMD) as a function of pixel value (Lampmann *et al.*, 1984). Coronal scans at one mm intervals (field of view 220 × 220 mm, pixel sizes 0.43 × 0.43 mm) were obtained with a Toshiba Xpress SX scanner (Toshiba Corporation, Tokyo, Japan) operating at 100 kV and 150 mA. The images were converted to single 8-bit files and filtered so that structures equal in density to, or less dense than, water were excluded; thus the image background was pure black and disclosed wet bone without bone marrow (Zhang *et al.*, 2001a, see Chapter III, p114). We used a commercial program (3DVIEWNIX 1.2, University of Pennsylvania Medical Center, Philadelphia, PA) for segmentation, jaw surface reconstruction, landmark identification and measurement. Another program (Calimage - Calculate Image, Craniofacial Laboratory, The University of British Columbia; see http://condor.dentistry.ubc.ca or the Appendix, p226) performed image matrix operations and mass property calculations (Zhang *et al.*, 2001a, see Chapter III, p114). Moments of inertia were referenced to an anatomical coordinate system with its x-axis directed transversely from left to right (viewed frontally), its y-axis directed superoinferiorly, and its z-axis anteroposteriorly. The x-z plane was parallel to the dental occlusal

plane, and the y-z plane was mid-sagittal (Figure 6.1, p149). To estimate the contribution of bone marrow, we segmented the non-mineralized component in each CT section, assigned the selected pixels a density of one g/cm^3 (Zhang *et al.*, 2001a, see Chapter III, p114), and recalculated the mass properties.

6.3.2 Prediction of mass and moments of inertia

Here, we used the similar general descriptors as those in our pig study. They included jaw width (distance between the two lateral condylar poles, WD), jaw height (vertical distance from the tip of the coronoid process to the lower border of the mandible, HD), jaw length (distance between front edge of the central incisor and the posteroinferior point of the condyle on one side, LD), all representing the bounding box dimensions, jaw volume (VD=WD×HD×LD), jaw mass (product of VD and mean bone density, MD), and jaw moments of inertia (product of MD and two orthogonal dimensions of the bounding box, IxD, IyD and IzD). We also included an additional cephalometric "total" jaw length descriptor (TLD) viz. the distance between condylion and gnathion. Regression curves were then fitted to plots describing relationships between these descriptors and the mass properties derived from the CT images.

6.3.3 Jaw model

The three-dimensional, dynamic model of the jaw has been described in detail elsewhere (Langenbach and Hannam, 1999; Peck *et al.*, 2000). It included relevant musculoskeletal geometry (Baron and Debussy, 1979) and muscle properties (Otten, 1987; van Eijden *et al.*, 1995, 1996, 1997; van Eijden and Raadsheer, 1992). Jaw motion was shaped by the active and passive tensions of 16 craniomandibular actuators (representing

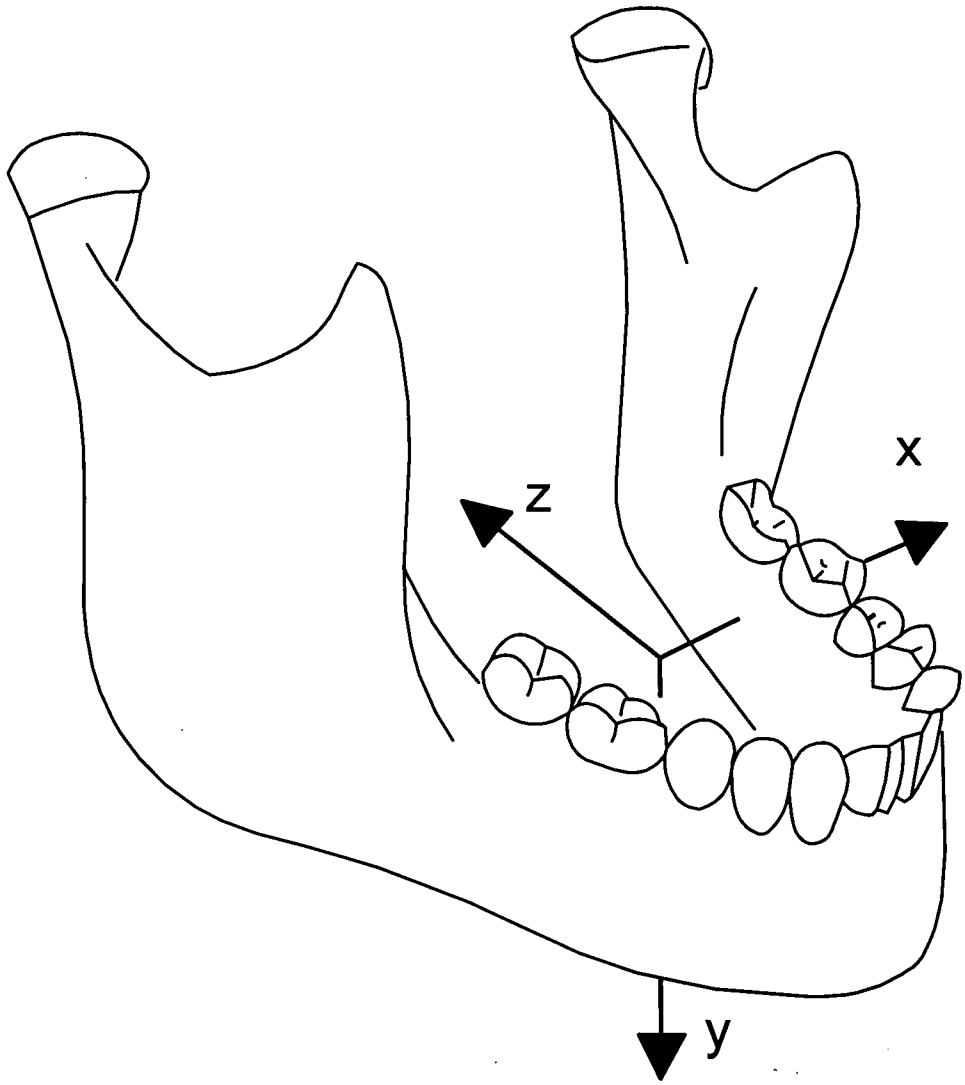

Figure 6.1 Coordinate system used to express moments of inertia. The transverse axis is represented by x, the superoinferior, by y, and the anteroposterior, by z. The axes z, y lie in the mid-sagittal plane, and x, z are parallel to the occlusal plane.

major muscle groups), by reaction forces in the two temporomandibular joints, and by gravity. The muscle subgroups were simulated with Hill-type, flexible, single-line actuators with fiber and tendon components (Zajac, 1989). Each actuator was lightly damped (10 Nsm^{-1}) to prevent high-frequency, internal oscillation. The actuators' passive tensions permitted an inter-incisal jaw gape of 50 mm when a 5 N external opening force was applied to the jaw for 0.5-1.0 sec (for details, see Peck *et al.*, 2000). This gape was also attained when jaw-opening was driven by actuators simulating digastric and lateral pterygoid muscle co-activation bilaterally (maximum active tensions 11.6 N and 16.8 N, respectively). The jaw's articulation with the cranium was modeled with paired, canted, ellipsoidal condyles rotating and sliding against frictionless curvilinear surfaces. The mandible was considered a rigid body within a vertical gravitational field of 9.8 m/s^2 (i.e. the head was assumed to be held in an upright posture).

The model was designed with commercial software (ADAMS; MDI, Ann Arbor, MI) using mixed, non-linear, differential and algebraic equations to compute its dynamics (van den Bogert and Nigg, 1999) i.e. numerical integration of component accelerations enabled calculation of their velocities and positions. An iterative, two-phase predictor-corrector technique involving user-defined tolerances produced solutions which were rejected when they did not converge.

Two versions of the model were tested, one which used the median mass property data for adult dentate jaws obtained in the present study, and another in which the mass properties reported by Koolstra and van Eijden (1995; mass, 440 g; Ix, 2900 $g.cm^2$; Iy, 8600 $g.cm^2$; Iz, 6100 $g.cm^2$) were inserted. In both models, motion of the midline incisor point (a region of unrestrained jaw motion) was measured when resting

posture and maximum jaw opening were simulated. In addition, the respective centers of mass were moved systematically one cm anteriorly, posteriorly, superiorly and inferiorly, and the moments of inertia of both models were arbitrarily halved.

6.4 RESULTS

6.4.1 Calibration

As shown in Figure 6.2 (p152), the calibration data revealed a linear relationship between pixel values and mineral density (correlation coefficient 0.995) i.e.

$$BMD = 0.012 \times \text{Pixel Value} + 1.005$$

6.4.2 Estimated masses and mean bone density

Table 6.1 (p153) illustrates the estimated masses with and without putative bone marrow, the measured weights, and the mean bone densities with and without bone marrow. Overall, the estimated jaw mass was 15% greater than the wet weight (mean EM/WW=1.15±0.04; coefficient of variation, CV 4.39%), and 38% greater than the dry weight (mean EM/DW=1.38±0.17; CV 12.32%). The inclusion of putative bone marrow added 9% more mass (mean EMM/EM=1.09±0.05). The estimated mass with marrow was 51% greater than the measured dry weight of the jaw (mean EMM/DW=1.51±0.26). When the less-dense bone marrow was included in the calculations, the mean bone density decreased by 4% (MBDM/MBD=0.96±0.01). The mean bone density (which included tooth dentin and enamel) was less in the younger and edentulous mandibles, but very similar in the adult dentate mandibles

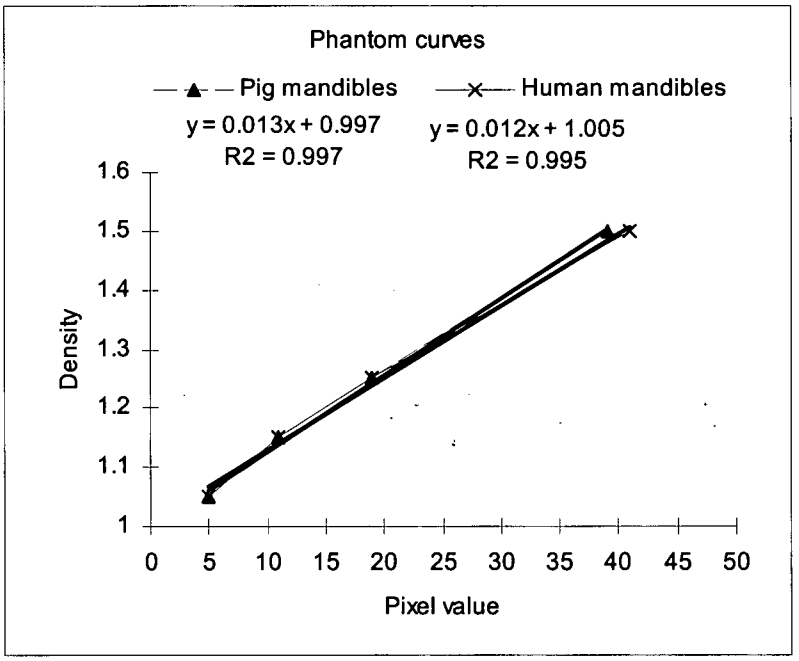

Figure 6.2 Calibration curve for the phantom used in the present study. For comparison, data are also shown for the previous study in the pig (Zhang *et al.*, 2001a, see Chapter III, p114).

Table 6.1 Measured jaw weights (dry weights, DW; wet weight, WW), estimated masses (estimated mass, EM; estimated mass with marrow, EMM), and calculated mean bone densities (MBD) and MBD with marrow (MBDM), and the ratios between these variables. All weights and masses measurements are in g, and all density measurements are in g/cm3.

	Adults		Adults + Children		Entire sample	
	Mean	SD	Mean	SD	Mean	SD
DW	80.18	14.46	62.61	28.75	59.76	29.39
WW	90.85	16.08	72.03	30.98	69.36	31.18
EM	102.32	18.33	81.69	34.30	78.93	34.31
EMM	108.90	19.02	87.34	35.77	84.97	35.30
EMM/EM	1.07	0.02	1.08	0.03	1.09	0.05
MBD	1.72	0.02	1.67	0.09	1.65	0.12
MBDM	1.65	0.03	1.60	0.09	1.58	0.12
MBDM/MBD	0.96	0.01	0.96	0.01	0.96	0.01
EM/DW	1.28	0.02	1.35	0.12	1.38	0.17
EMM/DW	1.36	0.04	1.45	0.16	1.51	0.26
EM/WW	1.13	0.02	1.14	0.03	1.15	0.04
EMM/WW	1.20	0.04	1.23	0.05	1.25	0.09

(1.72±0.02 g/cm^3, CV 1.16%).

6.4.3 Mass and geometric centers

The mass centers, and the differences between the mass and geometric centers, are shown in Table 6.1 (p153). In the adult dentate mandibles, the mass centers lay between the second and third molars when third molars were present; otherwise, they were near the last erupted tooth. They always lay within the upper one third of the distance from the dental occlusal surface to the inferior mandibular border. The mean linear difference between the mass and geometric centers was small (0.57±0.32 mm), the inclusion of simulated marrow having little effect (0.65±0.27 mm, $p>0.05$).

6.4.4 Moments of inertia

The smallest moment of inertia occurred around the jaw's transverse, and the greatest around its superoinferior (vertical) axis. Added "bone marrow" increased the moment of inertia by 8% around the tranverse axis, and by 9% around the vertical and longitudinal axes (Table 6.3, p156).

6.4.5 Mass and moments of inertia predictions

In the dentate mandibles, there were virtually linear relationships among estimated masses, measured weights and the general mass descriptor (R^2=0.9646, 0.9689, 0.9771 and 0.9710 for EMM, EM, WW and DW, respectively, Figure 6.3, p157). There were also linear relationships among the three moments of inertia and their respective moments of inertia descriptors (R^2=0.9664, 0.9259 and 0.9475 for IxD, IyD, and IzD

Table 6.2 Differences between geometric and mass centers without marrow (CD, mm), and with marrow (CDM, mm). Also included are the horizontal and vertical mass center locations relative to the teeth (HMCL), and in the vertical dimension (VMCL, expressed as percentage of the distance from the dental occlusal plane to the inferior border of the mandible). A: adult; M: mixed dentition; D: deciduous dentition; E: edentulous; M1, M2, and M3, permanent first, second and third molars; Dm2, deciduous second molar. Paired t-test p >0.05 for CD and CDM.

#	Age	CD	CDM	HMCL	VMCL
10	A	0.55	0.79	Mesiobuccal cusp of M3	0.30
4	A	0.30	0.44	Distal of M2	0.33
3	A	0.48	0.48	Distal of M2	0.33
11	A	0.15	0.72	Distobuccal Cusp M2	0.33
9	A	0.31	0.35	Mesiobuccal cusp of M3	0.30
5	A	0.47	0.61	Distobuccal cusp of M2	0.40
2	A	0.41	0.46	Distobuccal cusp of M2	0.37
1	A	0.75	0.60	Distobuccal cusp of M2	0.36
8	M	0.99	0.99	Distobuccal Cusp of M1	0.33
7	M	1.34	1.31	Distal of DM2	0.30
6	D	0.46	0.59	Distal of DM2	0.35
12	D	0.44	0.35	Distobuccal cusp of DM2	0.41
13	E	0.82	0.79	Anterior border of ramus	0.13
Mean		0.57	0.65		0.33
SD		0.32	0.27		0.07

Table 6.3 Moments of inertia without marrow (Ix, Iy, Iz), moments of inertia with marrow (IxM, IyM, IzM) and the ratios between them (IxR, IyR, IzR). All moment of inertia measurements are in g.cm².

	Adults		Adults + Children		Entire sample	
	Mean	SD	Mean	SD	Mean	SD
Ix	776.65	235.61	570.98	358.83	555.62	347.99
IxM	825.69	238.71	608.16	375.2	595.88	361.95
IxR	1.07	0.03	1.07	0.03	1.08	0.05
Iy	1482.03	421.59	1108.41	650.77	1071.76	636.92
IyM	1581.74	439.62	1186.15	686.38	1155.53	666.37
IyR	1.07	0.03	1.08	0.03	1.09	0.05
Iz	1250.08	356.12	922.92	562.92	893.67	549.18
IzM	1337.97	364.77	990.48	592.61	966.46	573.95
IzR	1.07	0.03	1.08	0.03	1.09	0.05

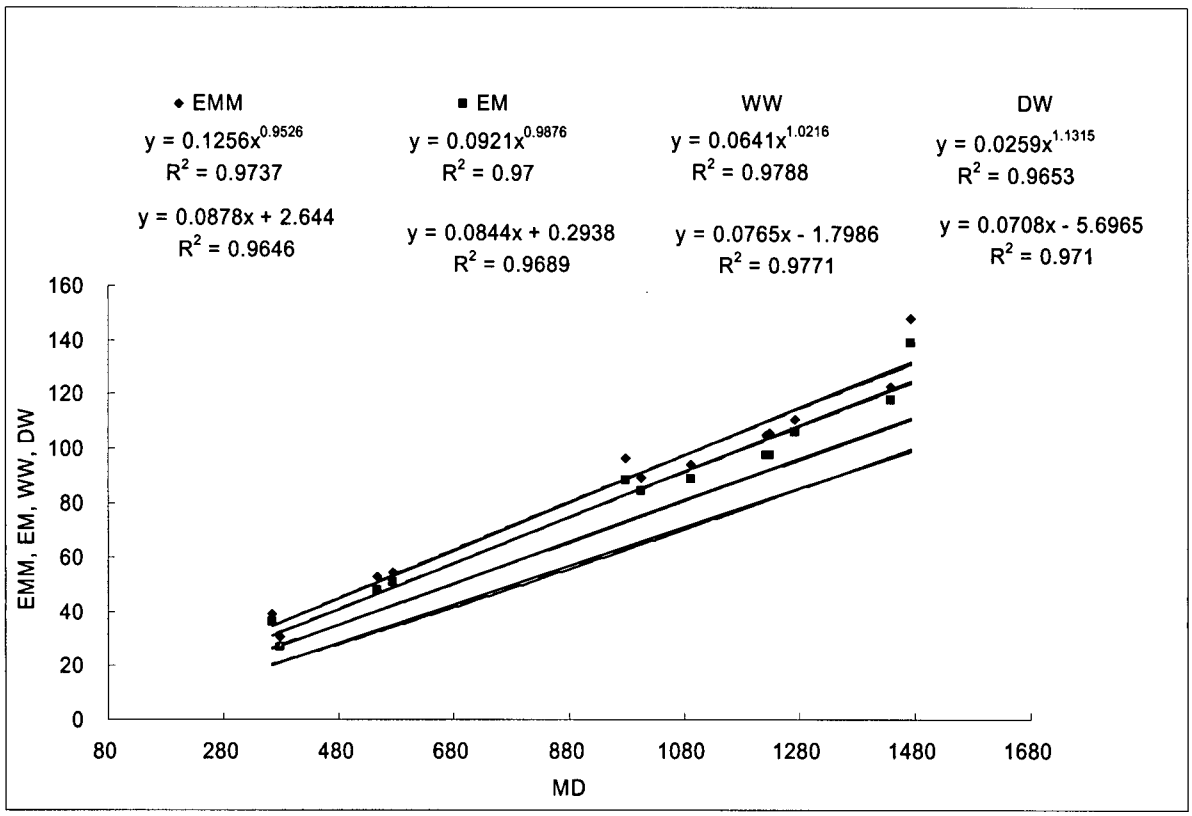

Figure 6.3 Estimated mass with marrow (EMM), estimated mass (EM), wet weight (WW), and dry weight (DW) plotted against the mass descriptor (MD). In each case, a power function, and a linear function have been fitted to the data.

respectively, see Figure 6.4, p160).

Table 6.4 (p160) includes coefficients of determination when the descriptors were used to predict EM, EMM, WW, DW, Ix, Iy, and Iz. In each case, TLD had the largest coefficient of determination.

6.4.6 Model sensitivity to mass properties

There was a marked difference in the magnitude of inter-incisal separation when the smaller mass properties representing the median of our adult dentate sample, and the larger properties reported by Koolstra and van Eijden (1995) were compared with the jaw resting in a vertical gravitational field (Figure 6.5, p161). Most of the motion from tooth contact to the rest position occurred within 250 msec, the heavier of the two jaws opening about 10 mm further than the lighter. In both cases, halving the respective moments of inertia (without changing the mass) had no effect on the incisor-point time-displacement curves. Movement of the mass centers anteriorly and posteriorly had a profound effect on the final resting positions (Figure 6.6, p162), whereas movement superiorly or inferiorly had no effect. In the heavier jaw, anterior movement of the mass center caused the descending jaw to overshoot its final resting position.

When driven by jaw-opening muscle "activation", both models reached 50 mm inter-incisal gape. Initially however, the heavier jaw opened wider than the lighter, sustaining an increased gape throughout the first 500 msec. The lighter jaw took almost 200 msec before opening significantly. In both cases, the final 10-15 mm was reached quickly (around 600 msec) at which time both active opening and passive closing "muscle" tensions were near-maximum (Figure 6.7, p163).

Table 6.4 Coefficients of determination (R^2) for power function curve fits between estimated mass (EM), estimated mass with marrow (EMM), wet and dry weights (WW, DW), moments of inertia (Ix, Iy, Iz), and all descriptors for dentate human mandibles. These include total length descriptor (TLD), length descriptor (LD), width descriptor (WD), height descriptor (HD), volume descriptor (VD), mass descriptor (MD), moments of inertia descriptors (IxD, IyD, IzD).

	TLD	WD	HD	LD	VD	MD	IxD	IyD	IzD
EM	0.98	0.81	0.91	0.94	0.94	0.97			
EMM	0.98	0.81	0.92	0.94	0.95	0.97			
WW	0.98	0.82	0.92	0.95	0.95	0.98			
DW	0.97	0.81	0.89	0.95	0.95	0.98			
Ix	0.99	0.83	0.94	0.96	0.97	0.99	0.99		
Iy	0.98	0.84	0.93	0.93	0.96	0.98		0.97	
Iz	0.99	0.85	0.95	0.96	0.98	0.99			0.98

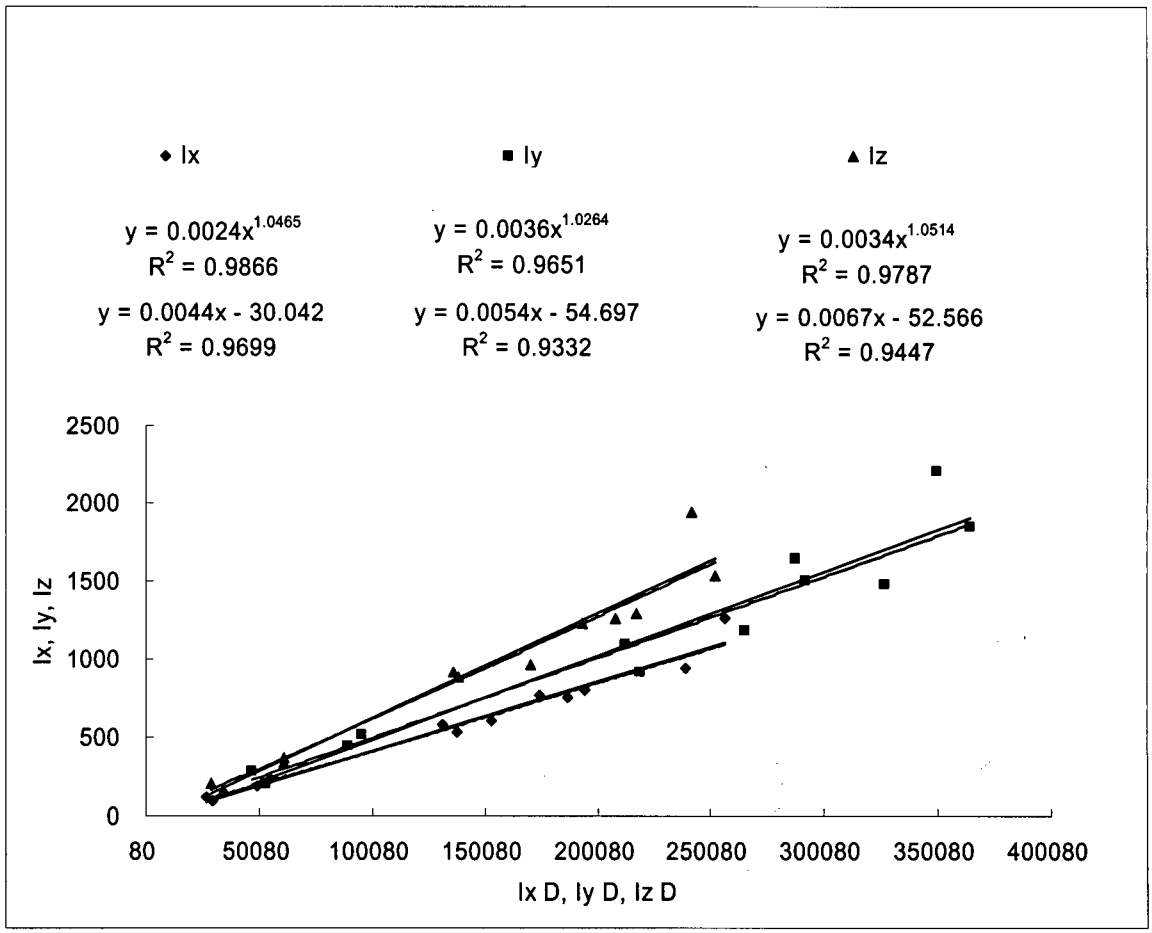

Figure 6.4 Moments of inertia (Ix, Iy, and Iz) plotted against the moment of inertia descriptors (IxD, IyD, and IzD). In each case, a power function and a linear function have been fitted to the data.

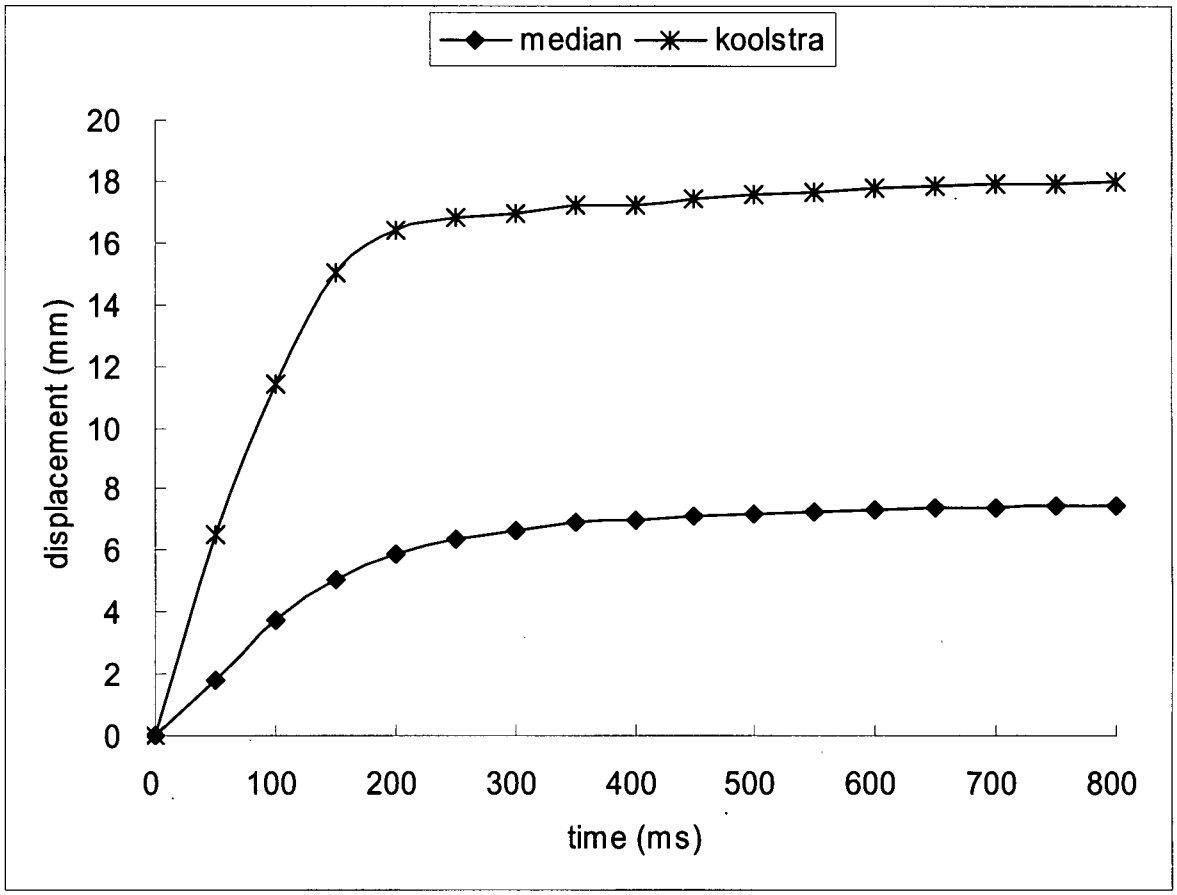

Figure 6.5 Incisor-point motion from tooth contact to the jaw's rest position, plotted against time. The curves represent mass properties used by Koolstra and van Eijden (1995) and median values from the present study. In both cases, halving the respective moments of inertia did not affect the curves.

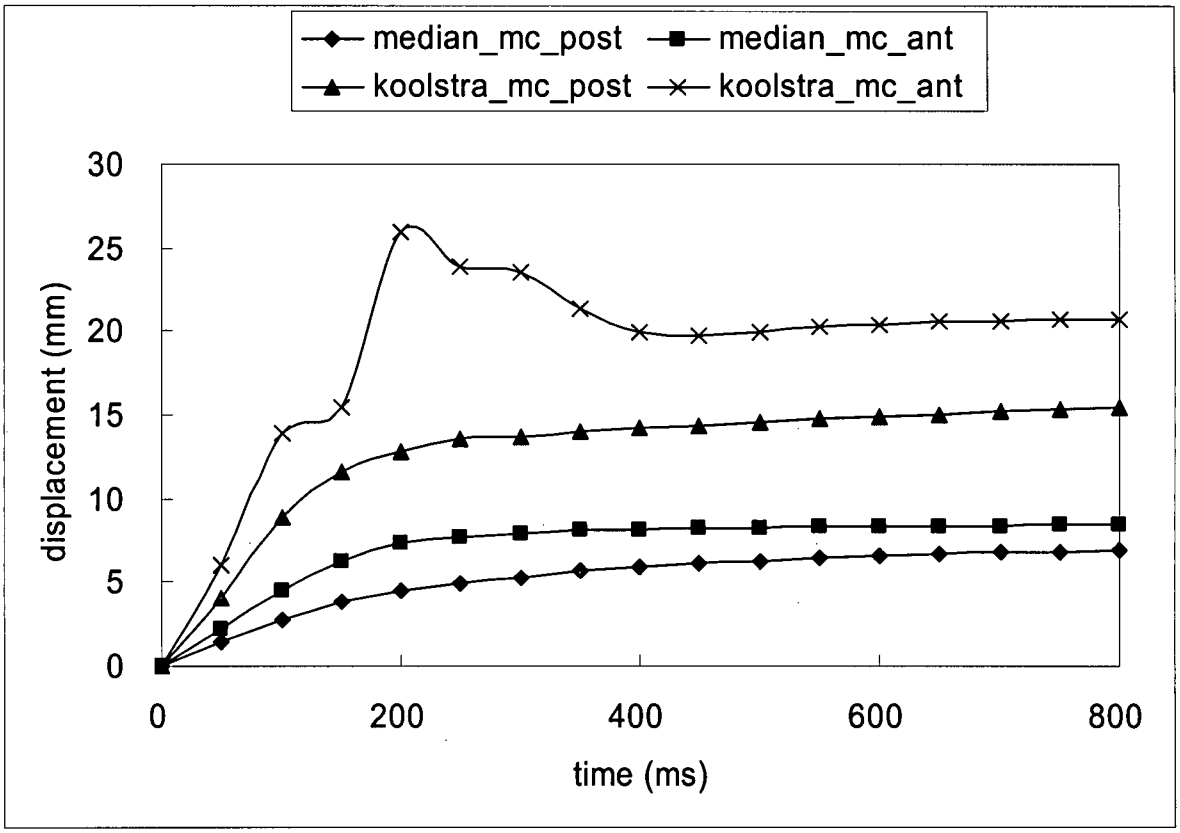

Figure 6.6 Incisor-point motion from tooth contact to the jaw's rest position, plotted against time. The curves represent mass center locations 10 mm anterior and 10 mm posterior to the original. Data are shown for mass properties used by Koolstra and van Eijden (1995) and median values from the present study. In both cases, moving mass centers superiorly and inferiorly had no effect.

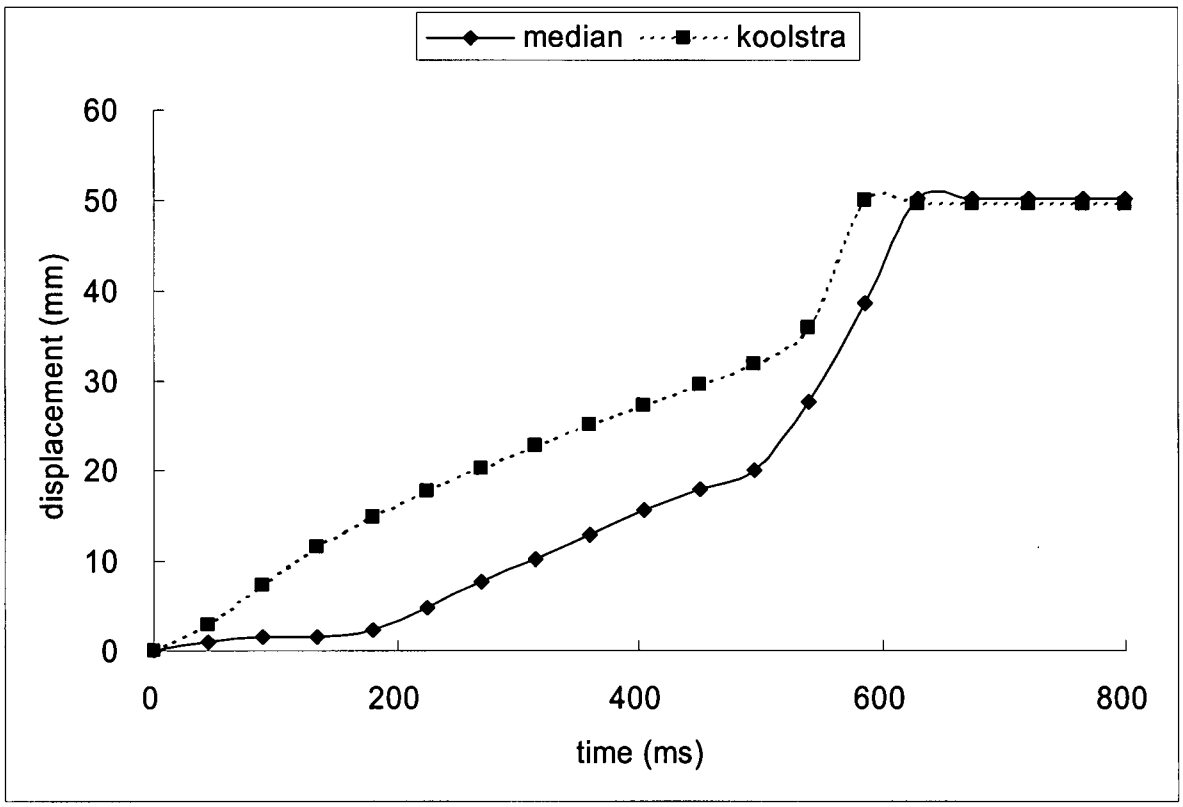

Figure 6.7 Incisor-point motion during maximum jaw opening, plotted against time. The curves represent mass properties used by Koolstra and van Eijden (1995) and median values from the present study.

6.5 DISCUSSION

Sources of error in the estimation of mass properties by CT scanning have been described elsewhere (Zhang *et al.*, 2001a, see Chapter III, p114), and all existed in the present study. They include limitations in the resolution of the CT scans, the threshold values employed, the medium filling the dry bone (water), tissue segmentation, the three-dimensional (3D) reconstruction process, and landmark identification. The lower kV value (100 kV) we used here generated much less heat than what we used in the previous study (120 kV, Zhang *et al.*, 2001a, see Chapter III, p114). It also produced a slightly different calibration curve than that obtained in the pig study. A low kV produces photons of low maximum energy (i.e., a "soft" x-ray beam); since more photon energy is absorbed (especially in tissues with high atomic density; see Morgan, 1983), the CT number increases, and a given pixel value will represent a lower density than that obtained with a higher kV.

Overestimation of bone mass by CT scanning with uniform calibrators has been reported previously. Cheng *et al.* (1995), using KH_2PO_4 as a bone-standard, reported a 15% overestimation of ash-apparent density for cow bone. In our pig study, we reported a 12% overestimation of jaw bone mass (Zhang *et al.*, 2001a, see Chapter III, p114). In the adult dentate mandibles here, the estimated mass was 13% greater than the wet weight, while in the pooled sample of dentate jaws, it was 14% greater, and in the entire sample, it was 15% greater. This is likely related to the porosity of the different jaws. While the EM/WW ratio was highly consistent for the adult dentate mandibles, its variation progressively increased with the addition of the mixed dentition, the deciduous dentition, and the edentulous jaw. The latter was the most

porous, and was overestimated by 23%. A second reason for overestimation may have been the lower kV. Although KH_2PO_4 solutions are often employed as calibration phantoms (Cheng *et al.*, 1995; Lampmann *et al.*, 1984; Zhang *et al.*, 2001a), their density ranges do not necessarily coincide with those in the imaged bone (solution densities typically range from 1.05 to 1.50 g/cm^3, whereas the mean bone density can approximate 1.7g/cm^3). High solution concentrations can reach their saturation points, and trigger heterogeneity. During imaging, lower-energy photons are preferentially absorbed by the harder tissues (e.g. bone) due to beam-hardening effects, and the resultant attenuation coefficients become non-linear (Morgan, 1983). The same photons, however, are hard enough to pass calibration solutions with linear attenuation. While our lower kV value may thus have produced a less-reliable calibration curve, we believe the error is small. In any event, the results are consistent with those reported by Cheng *et al.* (1995), and the previous study (Zhang *et al.*, 2001a, see Chapter III, p114).

In dynamic modeling, true specification of the mandible's mass and mass center is not a trivial undertaking. The effective mass constitutes the total instantaneous mass of all hard and soft tissue being moved, and could conceivably include the tongue (Langenbach and Hannam, 1999). Though neither the pig nor human jaw is regularly-shaped, it is possible to define the mass centers of irregular objects by direct experiment, e.g., by suspending the jaw in different orientations. In a different approach, Koolstra and van Eijden (1995) sectioned a cadaver jaw into elements, assumed the mass distribution was homogeneous, and used element locations to calculate the mass center. A drawback of all direct approaches, however, is their inapplicability to living subjects. The present imaging technique is essentially a modifed version of the general method used by Koolstra and van Eijden (1995, 1997b). The X-ray beam

and the small element size both permit a refined estimation of regional bone density.

The mean difference found between the mass and geometric centers was less than that we reported in the pig (Zhang *et al.*, 2001a, see Chapter III, p114), and the addition of simulated bone marrow made no difference statistically (Table 6.1, p153). We conclude that either the human mandible has relatively less bone-marrow space, and/or the marrow space is more evenly distributed in humans than in young pigs. Since the mass center in the adult dentate human mandible lies between the second and third molars (or at the last molar if there are no third molars) on the midsagittal plane, and is about one third of the distance from the occlusal surface of teeth to the lower border of the mandible, in most cases it could be approximated to within a few mm by linear measurement of conventional radiographic images.

Although moments of inertia can be estimated by suspending a body and measuring its oscillations, Koolstra and van Eijden (1995) used the equally-sized pieces from their sectioned jaw and integral calculus to calculate the moments of inertia from the elements' masses and their locations. In related studies, Hannam *et al.* (1997), Langenbach and Hannam (1999), and Peck *et al.* (2000) assigned mass properties predicted from a finite-element model of the human jaw developed by Korioth *et al.* (1992). The latter was derived from CT scanning, and included elements with properties specific to different jaw regions. These two approaches are somewhat similar to the one used here.

Smith *et al.* (1995) indicated a close approximation of mass properties can be made by assigning associated density to voxels comprising the structure; but it remains difficult to validate calculated moments of inertia,

and the use of inaccurate or imprecise physical methods does not make sense. Since, in the present context, the moment of inertia for each element is the product of its mass and the squared distance from the center of the element to the mass center, any moment of inertia estimated for each scanned element is theoretically valid provided the element's mass itself is valid. As the total moment of inertia equals the sum of the moments of inertia of all constituent elements, the validity of the total moment of inertia calculated ultimately depends on that of the total mass calculated. Thus, a 13% overestimation of the mass for the adult dentate human mandible would affect its moments of inertia similarly in all three axes.

The proportional magnitudes of the moments of inertia we have described are intuitively predictable. As in the pig, the largest moment of inertia occurred around the human jaw's superoinferior axis, due to the contribution of its largest anteroposterior, and second-largest transverse dimensions. The smallest moment occurred around its anteroposterior axis, due to the contribution of its smallest vertical and second-smallest transverse dimensions. In our sample, the mean jaw width was slightly greater than the mean length (data not reported), and the smallest moment of inertia would be expected to occur around the transverse axis.

Like others (Cheng *et al.*, 1995; Smith *et al.*, 1995), we assumed variations in the jaw's physical density would have a major effect on its mass properties. We found the mean bone density in the adult dentate human mandible to be quite consistent. In the pig, we reported linear relationships between jaw mass and a general mass descriptor (Zhang *et al.*, 2001a, see Chapter III, p114), and here we found the same (albeit with different constants). While there were strong correlations among the actual mass and all dimensional descriptors, TLD proved the best

predictor (Table 6.4, p159). Given the human jaw's relatively-homogenous density, it is perhaps unsurprising that a moment of inertia can be predicted with dimensional descriptors, because it is a function of the mass and the sum of the squares of two orthogonal dimensions. Since mass is proportional to an object's volume and density, it is a function of the dimensions cubed. Thus, the moment of inertia is a function of the object's density, and its dimensions raised to the fifth power, and moments of inertia might be expected to be predictable from three-dimensional scalar measurements of the jaw. The general similarity in the proportions among mass and moments of inertia when our data are compared to the more-direct estimations made by Koolstra and van Eijden (1995) also lends credence to the idea of total mass and jaw dimensional descriptors being primary determinants of mass properties. The Koolstra and van Eijden's (1995) jaw mass of 440g (which included all attached soft tissue) was about four times heavier than the median dentate jaw mass in our sample (about 105 g), yet the proportions among its mass properties are about the same as ours. It seems therefore, for modeling purposes, the density of human mandible can be considered homogeneous, and that a non-invasive imaging technique such as MR (which does not reveal bone density, but which can reveal bony contours) might be adequate for estimating jaw mass properties in living humans. If so, dynamic models of individual jaws would be practical in normal humans, and in cases like facial asymmetry, partially resected mandibles, etc. The segmentation technique we have described could be used with any 3D imaging method, allowing mass-property estimation for skeletal parts. As an example, in unreported experiments, we have sectioned the mandible into components, estimated their respective mass properties, and used these in dynamic models to measure the forces and torques transmitted through junctions between the reassembled parts.

The dependence of the resting posture of dynamic jaw models on at least some inertial properties is to be expected. A heavy mandible must reach a lower position than a light one, though it is less obvious how long it will take to reach it. Viscous damping by the muscles and other tissues surrounding the jaw can be expected to affect its speed in response to induced forces, including muscle contraction. Koolstra and van Eijden (1995) used a jaw-closing model driven by the medial pterygoid muscles, and damped it by applying friction at the center of gravity. Their findings on changing the mass center and moments of inertia, coupled with our observations here, confirm dynamic jaw models remain sensitive to the specification of both their masses and mass centers even when muscle tensions are present. Much depends upon what is considered the jaw's true mass, e.g. how much related soft tissue should be included, and whether or not this should include the tongue which weighs about 50-60g. Taken together, the studies suggest errors of several mm or more in any direction when mass centers are specified will affect jaw-opening and jaw-closing predictions to and from maximum gape. Errors in the anteroposterior direction will affect the jaw's resting posture, though deviations in vertical direction are unimportant here. Our demonstration that moments of inertia have little effect on jaw opening and resting posture complements similar findings during jaw closing (Koolstra and van Eijden, 1995). Both studies thus infer these in some latitude when specifying the jaw's moments of inertia, if its dynamics are modeled in the midline. Gravitational acceleration, viscous damping, and the generation of muscle tensions seem sufficient to ensure these relatively low moments do not play a significant role in shaping free jaw movements.

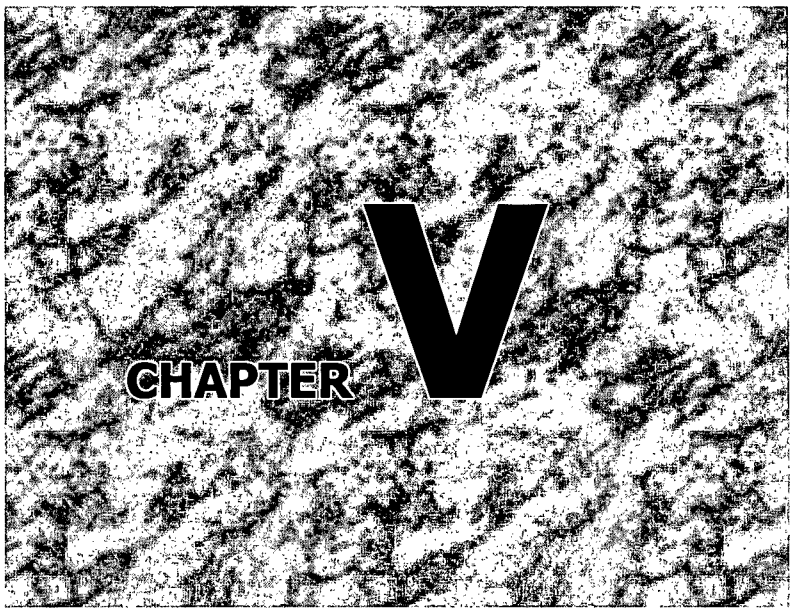
CHAPTER V

7 DYNAMIC MECHANICS IN THE PIG MANDIBULAR SYMPHYSIS

7.1 ABSTRACT

During function, various biomechanical events occur at the mammalian jaw symphysis. Previously, these have been studied in the static environment, or by direct recording of surface bone strains. So far however, it has not been possible to demonstrate directly the forces and torques passing through the symphysis in association with dynamically changing muscle tensions. Recently, dynamic models have been used to study jaw biomechanics in humans and pigs. Here, we modified a previously published dynamic pig jaw model to measure the forces and torques at the symphysis, and related these to simulated masticatory muscle tensions, bite, joint and food bolus forces. The model was based on an individual pig's musculoskeletal structure and included specific mass properties for each half of the mandible. An artificial rigid joint was created at the symphysis, allowing measurements of the tri-axial forces and torques passing through it. An artificial food bolus was placed at the right fourth deciduous premolars (DP4) during simulated right-sided chewing. The model successfully predicted three previously postulated loading patterns at the symphysis. Dorsoventral shear occurred when the lower teeth hit the artificial food bolus. It was associated with balancing-side jaw adductor forces, and reaction forces from the working-side food bolus. Medial transverse bending occurred during jaw opening, and was associated with bilateral tensions in the lateral pterygoid and digastric muscles. Lateral transverse bending occurred at the late stage of the power stroke, and was associated with the actions of the deep and

superficial masseters. The largest predicted force was dorsoventral shear force, and the largest torque was a "wishboning" torque about the superoinferior axis. We suggest dynamic modeling offers a new and powerful method for studying jaw biomechanics, especially when the parameters involved are difficult or impossible to measure *in vivo*.

7.2 INTRODUCTION

The biomechanics of the mammalian mandibular symphysis have been studied extensively *in vivo* by strain gauge measurements in non-human primates (Hylander, 1979a, 1984, 1985), electromyographic and cineradiographic recordings in non-human primates and mammals with unfused symphyses (Hylander *et al.*, 1998, 2000; Hylander and Johnson, 1994; Lieberman and Crompton, 2000) and by morphological analyses in a wide range of mammals (Daegling, 1993; Daegling and Jungers, 2000; Lieberman and Crompton, 2000; Ravosa, 1996, 1999; Ravosa and Simons, 1994). In addition, the relationship between symphyseal stress and strain has been estimated in a number of primate species (Vinyard and Ravosa, 1998), and in pigs and humans (Chapter II, p83).

In general, the unfused symphysis, by allowing independent inversion and eversion of the two halves of the mandible before and during the masticatory power stroke, enables the steep occluding surfaces of opposing teeth in some mammals to match during mastication (Hylander, 1979b; Kallen and Gans, 1972; Lieberman and Crompton, 2000; Oron and Crompton, 1985; Scapino, 1981). The fused symphysis strengthens and stiffens the jaw, reducing its risk of structural failure as a result of lateral transverse bending, and dorsoventral shear stresses occurring during unilateral mastication (Hylander, 1984; Hylander *et al.*, 2000; Ravosa, 1996; Ravosa and Hylander, 1993; Ravosa and Simons, 1994).

In mammals with fused symphyses, high stresses and strains can occur during function. Dorsoventral shear is created by the upward component of the balancing-side jaw-muscle force, and the downward component of the bite point reaction force during unilateral biting (Hylander, 1979a, 1984, 1985). Wishboning occurs at the very end of the power stroke, i.e. after the initial occurrence of maximum intercuspation, and is associated with the late peak activity of the balancing-side deep masseter coupled with the rapid decline in the activity of the balancing-side medial pterygoid and superficial masseter (Hylander and Johnson, 1994). While the lateral component of balancing-side deep masseter is considered the primary masticatory muscle force associated with symphyseal wishboning, the oppositely-directed lateral component of the working-side bite point reaction force and residual activity from the working-side superficial masseter may also contribute (Hylander, 1984, 1985; Hylander and Johnson, 1994). Previously (Chapter II, p83), we postulated that in addition to these contributions, the superior and medial parts of the working-side condylar fossa may play a role, especially as the working condyle is loaded at the end of the power stroke by residual elevator muscle activity (see Figure 4.4, p111). Wishboning produces compressive stress and strain on the facial aspect and high tensile stress and strain on the lingual aspect of the symphysis (Hylander, 1984, 1985).

A third loading pattern associated with the power stroke is medial transverse bending, which occurs during the opening phase and has been postulated to be caused mainly by the bilateral contraction of the lateral pterygoid muscles, producing a reversed wishboning effect (Hylander, 1984, 1985). This form of loading causes compression on the lingual aspect and tension on the facial aspect of the symphysis.

One limitation of previous morphological analyses and stress and

strain estimations is their consideration in static situations only. For example, Vinyard and Ravosa's (1998) approaches, and our own in Chapter II (p83) estimated maximum stress and strain occurring along the lingual surface of the symphysis as a consequence of tension inferred from the morphology of deep masseter only. Even previous *in vivo* studies, though measuring dynamic strains, have limitations. One cannot sample surface strains at more than a few sites in the primate mandible without compromising the structural and functional integrity of the masticatory system (Daegling and Hylander, 2000). Also, the interpretation of such strain data is not entirely unambiguous.

Recently, dynamic jaw models have been utilized to study jaw musculoskeletal mechanics in humans (Hannam *et al.*, 1997; Koolstra and van Eijden, 1995, 1996, 1997a, b; Langenbach and Hannam, 1999; Peck *et al.*, 2000), and in pigs (Langenbach *et al.*, 1999). These dynamic jaw models incorporate large amounts of structural and functional data including muscle active and passive tensions, joint reaction forces, occlusal forces and the jaw's mass properties, many of which change dynamically during function. A major advantage of the models is their ability to predict changing muscle tensions in real time, parameters which are presently impossible to record *in vivo*. Dynamic models thus have the unique potential to reveal internal forces and torques induced by multiple, changing muscle tensions.

Previously, we described a method, based on computed tomography (CT) for obtaining mass properties of the pig and human mandibles (Zhang *et al.*, 2001a, b). Specification of mass, mass center and other inertial properties is an essential step in dynamic modeling. In the current study, we used this method to estimate the mass properties for a pig mandible artificially divided into right and left halves, each with distinct

mass properties, and constructed a dynamic model in which the two halves were joined with a rigid link at the symphysis. This made it possible to measure the tri-axial dynamic forces, and torques passing through the link as a result of muscle activity during chewing; thus, we were able to estimate the resultant forces and torques likely to be transmitted across the symphysis during function, i.e. the forces and torques which presumably require a specific symphyseal morphology to withstand them.

7.3 MATERIALS AND METHODS

7.3.1 Model generation

The original model of the pig jaw has been reported previously (Langenbach *et al.*, 1999) and was based on a dynamic model of the human jaw (Langenbach and Hannam, 1999). It was designed with a commercial software package (ADAMS 10.0, Automatic Dynamic Analysis of Mechanical Systems; Mechanical Dynamics Inc., Ann Arbor, MI). Briefly, the model incorporated the muscular and skeletal morphology from an anaesthetized female miniature pig (*Sus scrofa*, 8 months). CT with a calibration phantom was performed to obtain its skeletal structure and mass properties (see Zhang *et al.*, 2001a, see Chapter III, p114). Muscle cross-sectional sizes and lines of actions were obtained through magnetic resonance imaging on a separate occasion. The criteria for designating muscle attachment sites were based on anatomical descriptions by Herring and Scapino (1973), the reconstructed muscle images, and bone surfaces with known muscle attachments. Three parts were assigned to the temporalis muscle (anterior temporalis; middle temporalis; and posterior temporalis), two parts to the masseter (superficial masseter, and deep masseter), one part to the medial pterygoid, one part to the

lateral pterygoid, and one part to the digastric muscle. Each muscle included fiber and tendon components. The fiber/tendon length ratios were defined according to Herring and Scapino (1973) and Anapol and Herring (1989).

The model was driven with muscle activity patterns based on electromyographic data. Muscle function was simulated as described previously by Langenbach and Hannam (1999). Briefly, motion of the mandible was produced by active muscle tensions generated by 'contracting' muscle fibers. Each active muscle tension was determined by the product of the muscle's cross-sectional area, a constant of 40 N/cm^2 (Weijs and Hillen, 1985) and a specified level of activation (0-1, where unity represents 100% activation). This value, expressed in Newtons (N), was scaled according to the muscle's instantaneous length and shortening velocity by means of length-tension and velocity-tension curves (see Langenbach and Hannam, 1999). Any passive muscle tension induced by damping or stretch was then added to this active tension. Passive stretch tensions were only present for lengths beyond the optimal muscle length, taken as the muscle length at an interincisal distance of 30 mm (for a detailed description of the damping forces and the muscle or tendon tensions, see Langenbach and Hannam, 1999).

Segmentation of the mandible from CT images has been described elsewhere (Zhang *et al.*, 2001a, see Chapter III, p114). Division of the mandible at the symphysis was accomplished midsagittally through the entire image set. Each half of the mandible was saved as a separate file for mass properties calculation with a customized program (Calimage - Calculate Image, Craniofacial Laboratory, The University of British Columbia; see http://condor.dentistry.ubc.ca or Appendix, p226).

The model thus consisted of two independent masses representing the split lower jaw, which were relinked with a rigid pin-joint placed at the center of the symphysis and oriented orthogonally to the dental occlusal plane (Figure 7.1, p178). The jaw's motions relative to the grounded cranium were shaped by various forces at different sites on the jaw, including gravity, reaction forces at the temporomandibular joints, dental occlusal reaction forces, food bolus resistance force, and active and passive muscle tensions. Condylar guidance was simulated with a horizontal plane. Under loading, the condylar center could indent this plane (the reaction force increased exponentially to reach 1000 N at 0.25 mm compression), but rotations and translations on the plane were frictionless. All muscle actuators linked the mandible to the cranium, except the digastric, which ran between the mandible and a grounded part equivalent to the hyoid bone.

The locations of three mandibular bite points (buccal cusp tip locations of the bilateral deciduous fourth premolar, DP4, and mid-incisor) in the dental arch were obtained from the 3D CT reconstruction of the mandible. Reaction forces at these bite points were assumed to be perpendicular to the occlusal plane, and were generated when the jaw reached the dental intercuspal position, where the interocclusal contact force at each bite point increased exponentially to reach 2000 N with 0.25 mm inter-occlusal compression. The model was designed to accommodate a food bolus on the working-side at the DP4 bite point. The bolus had a compressive resistance which depended on its thickness (equivalent to the distance separating the dental arches at that location). It was three mm thick, and "soft-edged", so that its resistance increased step-wise over the first 1.5 mm of compression, to reach a maximum of 60 N. Forces less than 60 N (or of insufficient duration) resulted in incomplete bolus compression.

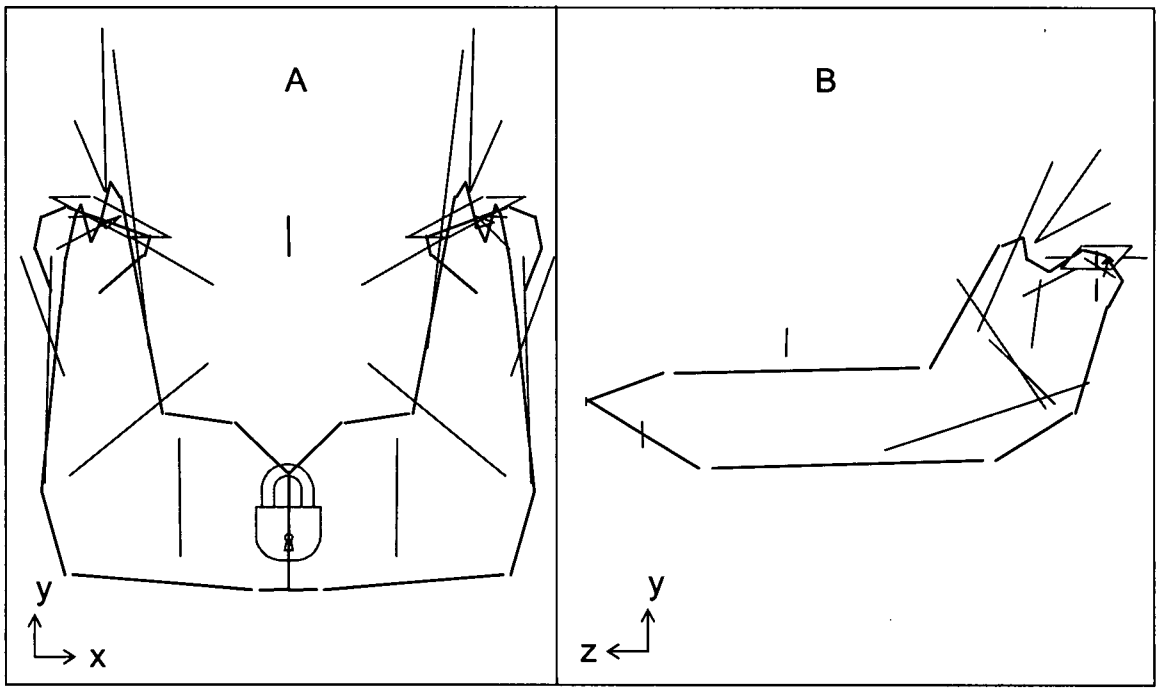

Figure 7.1 Frontal (A) and lateral (B) views of the ADAMS wireframe dynamic model. Muscle action lines are described elsewhere (Langenbach *et al.*, 1999). The rigid joint linking the two halves of the mandible is indicated by the lock icon located at the center of the symphysis.

7.3.2 Simulations

The plausibility of a pig dynamic model has been demonstrated previously (Langenbach *et al.*, 1999), i.e. the predicted jaw motion is an acceptable analogue of published average data for maximum opening, latero-deviation, and timing of the different parts of the pig chewing cycle (i.e. for opening, closing and power stroke). In the present study, we ran the simulation for one right-sided chewing cycle over 0.5 seconds. Output predictions included incisal point movement in vertical, horizontal, and anteroposterior dimensions, tensions of the 16 jaw muscles, reaction forces at the working-side bite points, reaction forces at the working-side temporomandibular joint and tri-axial forces and torques passing through the symphysis. All were time-related dynamic measurements. The conventions used to express symphyseal forces and torques are illustrated in Figure 7.2 (p180).

7.4 RESULTS

7.4.1 Incisor point motion

Figure 7.3 (p181) shows the shape of the simulated chewing cycle. The predicted jaw motion was reminiscent of that in previously published characteristics of pig chewing (cf. Herring, 1976).

Viewed frontally, jaw opening began in the midline. After the first 10 mm of gape, the jaw deviated from the midline towards the working-side. Maximum opening (33 mm) was followed by fast closure of the jaw combined with a further lateral deviation (7 mm) of the jaw. When the artificial food bolus was reached, the jaw moved back to the midline, and closed slowly. Vertical jaw motion stopped when the teeth came into

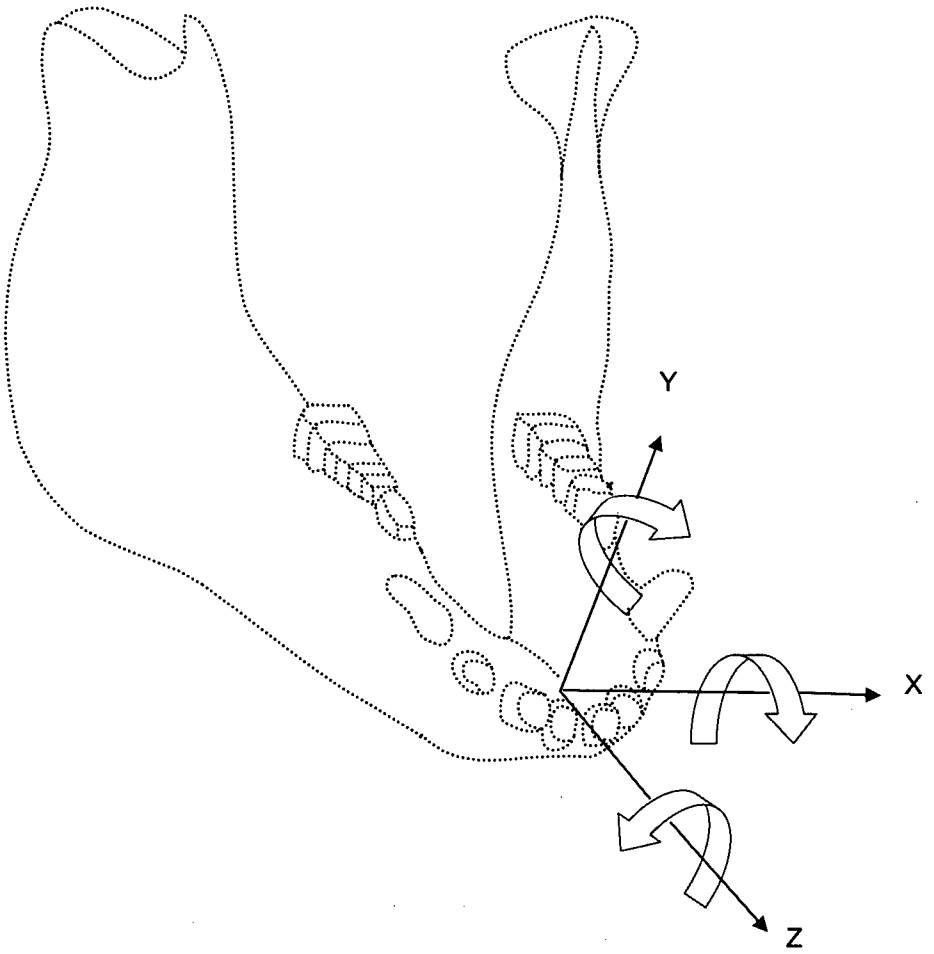

Figure 7.2 Conventions used to express symphyseal forces and torques. Forces exerted by the right corpus on the left are positive when they are in the same direction as the axes. Arrows around each axis indicate the directions of positive torques exerted by the right corpus on the left.

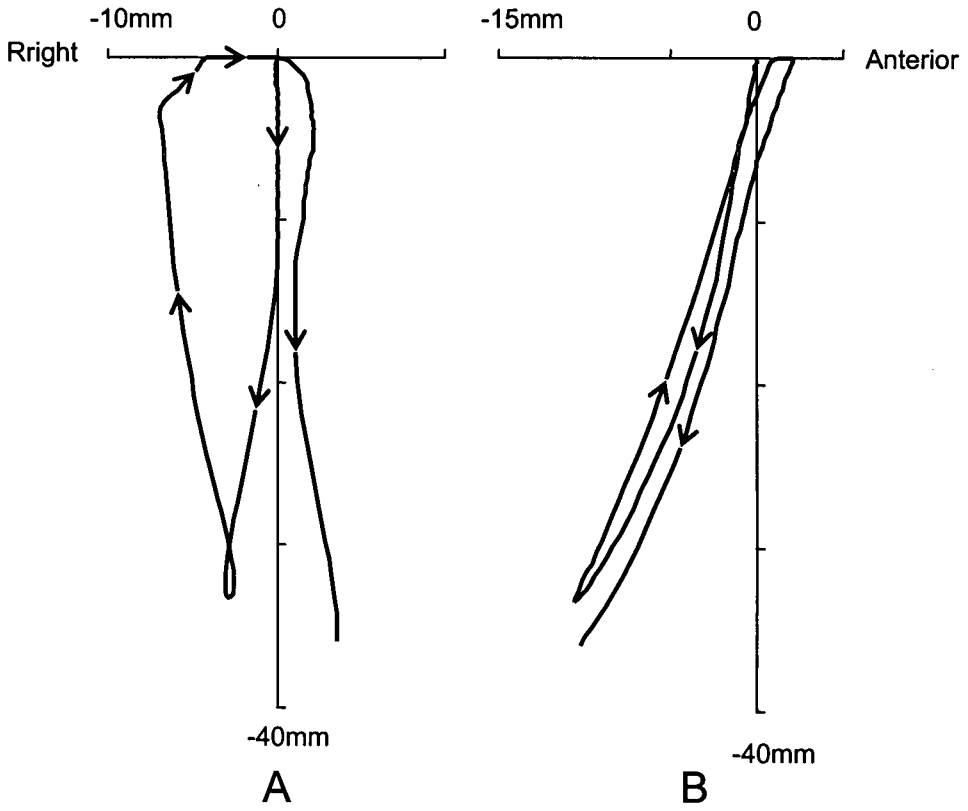

Figure 7.3 Incisor point motion during a simulated right-sided, 0.5 second chewing cycle. A: X-Y plot representing the frontal view of incisor point motion. B: Z-Y plot representing the lateral view of incisor point motion. All scales are in mm. Arrows indicate direction of motion, including the next stroke to the contralateral side. See text for full description.

contact, resulting in a horizontal slide through the midline towards the balancing-side. The right-sided cycle took 0.33 seconds before the next cycle began, which started on the balancing side of the midline (Figure 7.3, p181). The opening trajectory of this cycle was entirely on the balancing-side of the midline.

7.4.2 Muscle tension

Figure 7.4 (p183) shows the muscle tensions expressed in time for the simulated chewing stroke. The lateral pterygoid and digastric muscles on both sides initiated the cycle. The lateral pterygoid muscle on the working-side reached its peak tension earlier (about 0.02 seconds) than its balancing-side counterpart. The lateral pterygoid muscles reached maximum tension earlier than digastrics on both sides. This was the point where fast opening began (the first vertical line). When the jaw reached maximum gape (33 mm), the tension of lateral pterygoid muscles reduced to zero. The digastric muscle tensions disappeared when the closing phase began.

When jaw opening reached two thirds of its maximum gape, passive tensions were produced in the superficial and deep masseters. These passive tensions turned into active tensions at the beginning of the closing phase (the second vertical line). As soon as the teeth hit the artificial bolus (the third vertical line), all adductor muscles, as well as the lateral pterygoid, were active. On the working-side, while the deep masseter reached maximum tension immediately after the teeth began to crush the bolus, other adductors and lateral pterygoid muscle reached their maximum tensions later, i.e. when the bolus was almost completely crushed, and the lower teeth contacted the upper teeth (the fourth vertical line). On the balancing-side, the middle and posterior temporalis

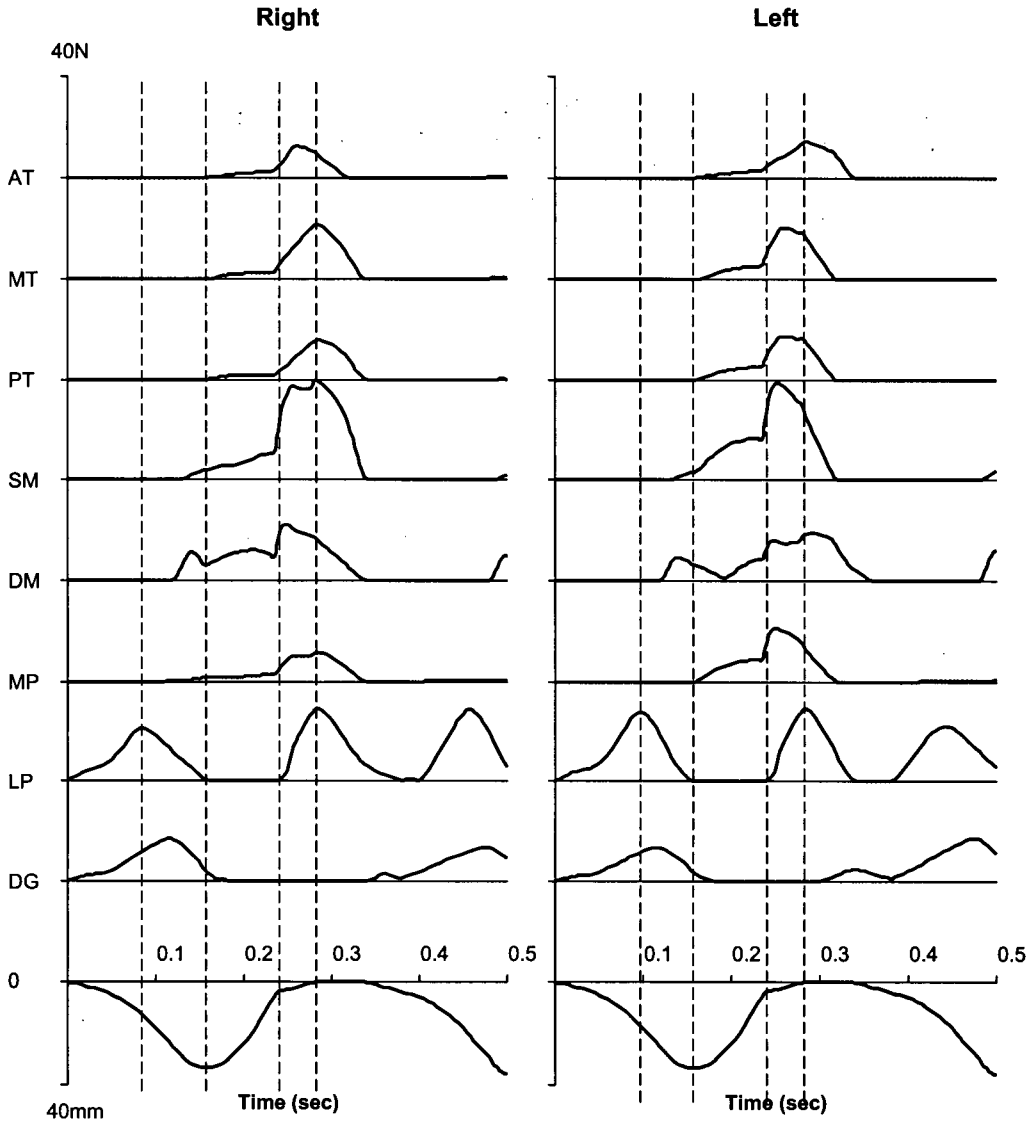

Figure 7.4 Muscle tensions expressed in time during simulated right-sided chewing. Data are shown for the right and left sided muscles. The lowest curves are the corresponding incisor point motions in the vertical dimension. The dotted lines in each figure (from left to right) represent fast jaw opening, maximum jaw opening, onset of bolus crush, and the onset of tooth-to-tooth contact in intercuspation. Abbreviations: AT, anterior temporalis; MT, middle temporalis; PT, posterior temporalis; SM, superficial masseter; DM: deep masseter; MP, medial pterygoid; LP, lateral pterygoid; DG, digastric.

muscles, superficial masseter, and medial pterygoid muscle all reached their maximum tensions earlier than the deep masseter and lateral pterygoid. The latter two muscles reached their maximum tensions late, i.e. during the intercuspal slide to the midline.

7.4.3 Forces at the artificial food bolus, tooth and joints

Figure 7.5 (p185) illustrates the forces expressed in time at the food bolus, working-side tooth point (DP4), working-side temporomandibular joint and balancing-side temporomandibular joint. Reaction forces at both joints commenced with opening, and reached small peaks just before maximum gape. These forces increased steeply when the tooth hit the artificial bolus. The balancing-side joint force reached maximum shortly after, and the working-side joint force reached maximum after initial tooth contact occurred. The reaction force at the food bolus began to increase when struck by the lower teeth, increased steeply in about 0.01 seconds, and after a slower phase of 0.02 seconds reached its maximum; this peak force continued for about 0.03 seconds, then decreased sharply when intercuspation occurred. Tooth force was produced and reached its maximum immediately after tooth contact was made. All these forces disappeared before the next cycle began.

7.4.4 Tri-axial symphyseal forces

Figure 7.6 (p186) demonstrates the tri-axial symphyseal forces expressed in time. During jaw opening, the artificial joint representing the symphysis underwent compression along its transverse X-axis (i.e. the left side corpus was compressed by the right side corpus in the occlusal plane; cf. Figure 7.2, p180). This compression coincided with peak tension in the lateral pterygoid and digastric muscles (cf. Figure 7.4,

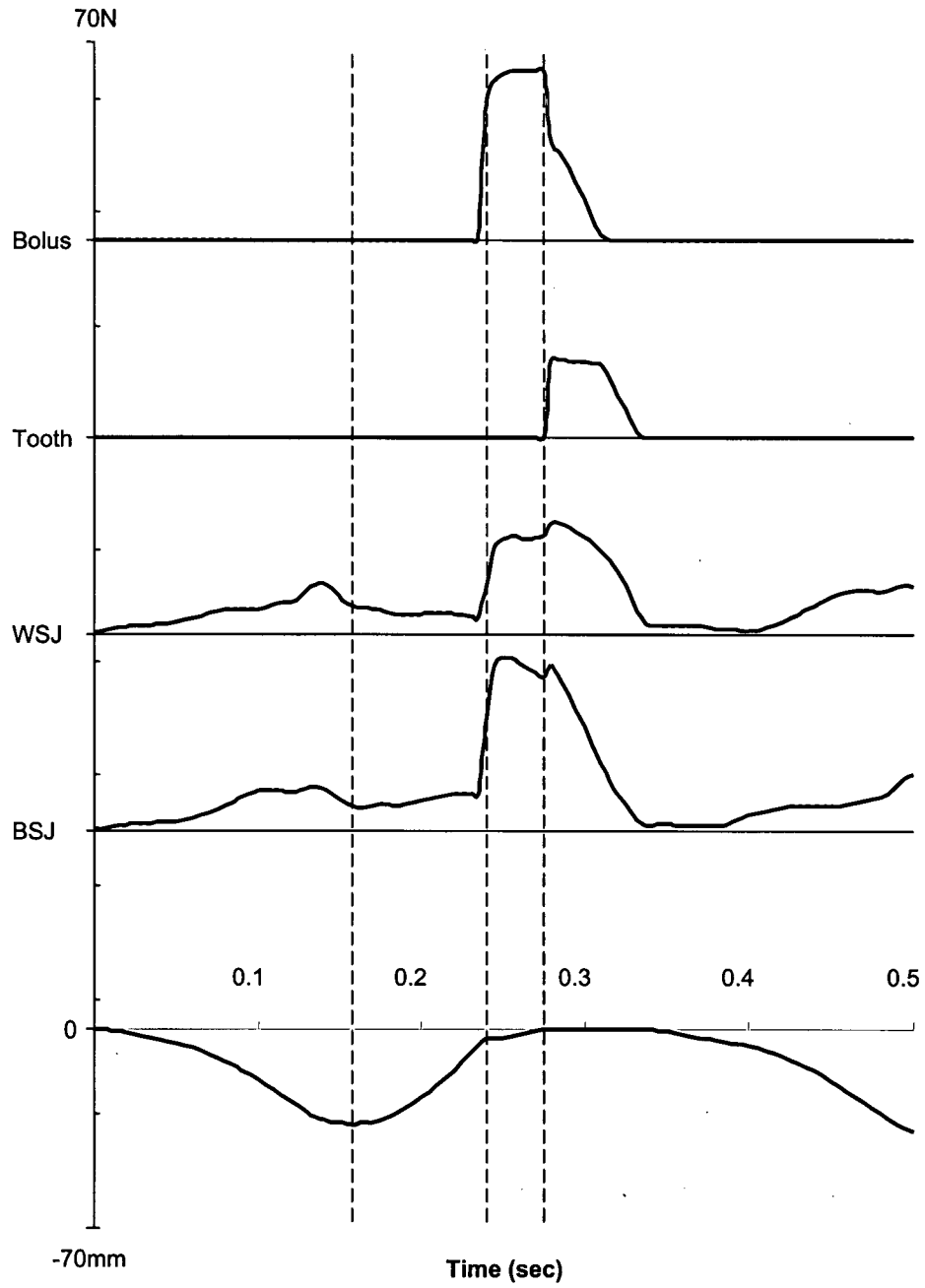

Figure 7.5 Predicted forces expressed in time. They include bolus, working-side bite point (DP4), working-side temporomandibular joint (WSJ) and balancing-side temporomandibular joint (BSJ) forces. The lowest curve is the corresponding incisor point motion in the vertical dimension. The dotted lines (from left to right) represent maximum jaw opening, onset of bolus crush, and the onset of tooth-to-tooth contact in intercuspation.

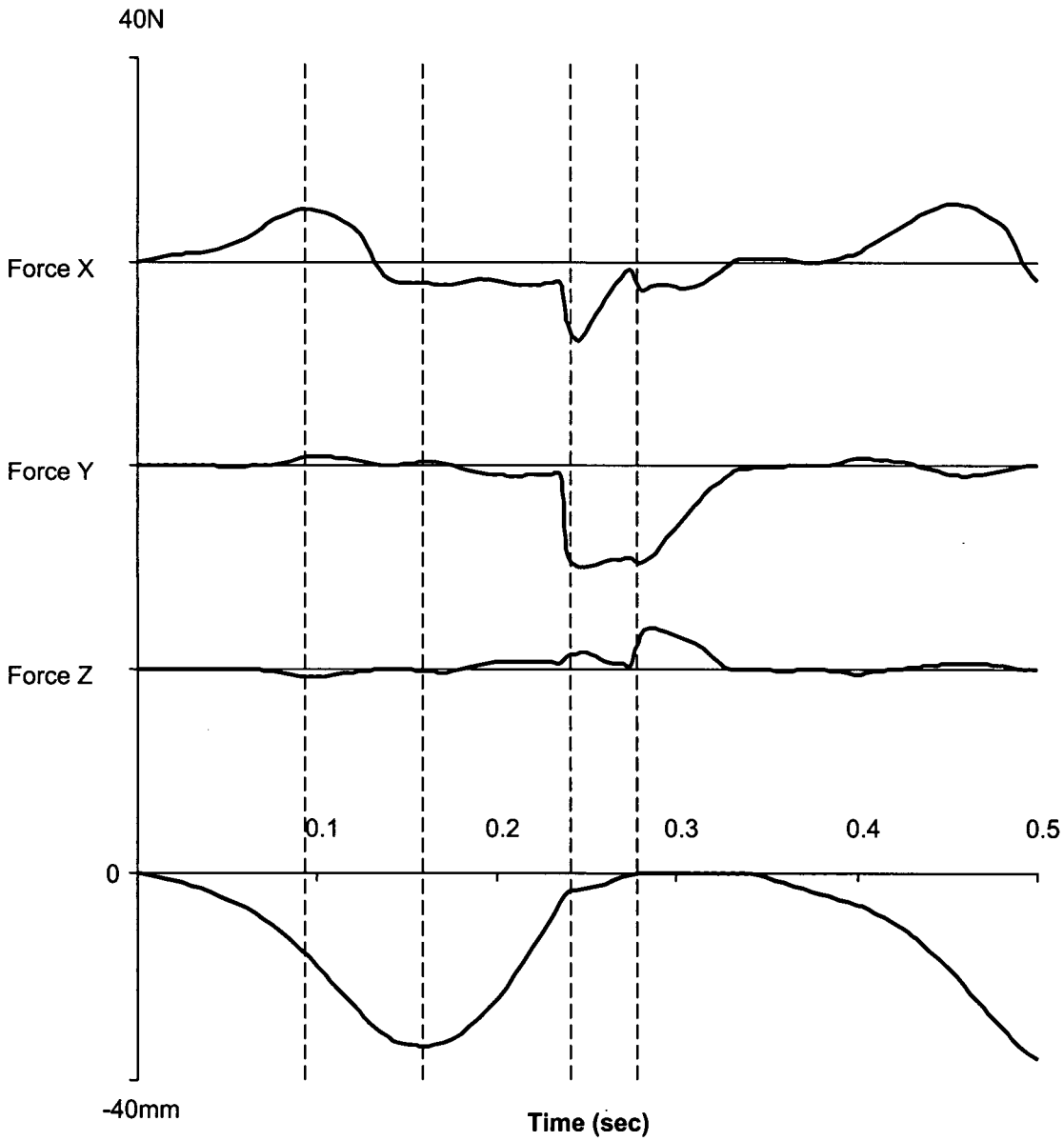

Figure 7.6 Tri-axial symphyseal forces expressed in time. The lowest curve is the corresponding incisor point motion in the vertical dimension. The dotted lines (from left to right) represent maximum jaw opening, onset of bolus crush, and the onset of tooth-to-tooth contact in intercuspation.

p183). When the jaw reached maximum opening, symphyseal tension was induced (i.e. the left side corpus was tensed by the right side corpus; cf. Figure 7.2, p180), and stayed almost constant until the lower teeth hit the artificial bolus. This tension reached maximum during the early stage of bolus crushing and then decreased. These effects were related to peak active tension in the closing muscles, most notably the superficial and deep masseters (cf. Figure 7.4, p183).

A negative shear force began along the superoinferior Y-axis when the food bolus was hit, and increased steeply. This shear was related to the reaction force applied on the working-side DP4, which tended to lower the working-side corpus, and jaw adductor forces on the balancing-side, which lifted the balancing-side corpus. The shear force continued until the bolus was completely crushed, and began to decrease when the lower teeth made contact with the upper teeth (cf. Figure 7.5, p185).

A small shear force along the anteroposterior Z-axis was caused by different timing in the temporalis, medial pterygoid, and masseter muscles, and as a result of muscle forces on the working-side exceeding those on the balancing-side after tooth contact commenced. The main contributor was the working-side superficial masseter due to its anteriorly directed force component (cf. Figure 7.4, p183).

7.4.5 Tri-axial symphyseal torques

Figure 7.7 (p188) shows the symphyseal torques around the three axes (see Figure 7.2, p180, for conventions). Two small positive torques (approximately 250 N·mm) occurred around the transverse X-axis. The first occurred at about 0.1 seconds. The balancing-side jaw tended to be twisted more than the working-side due to the balancing-side lateral

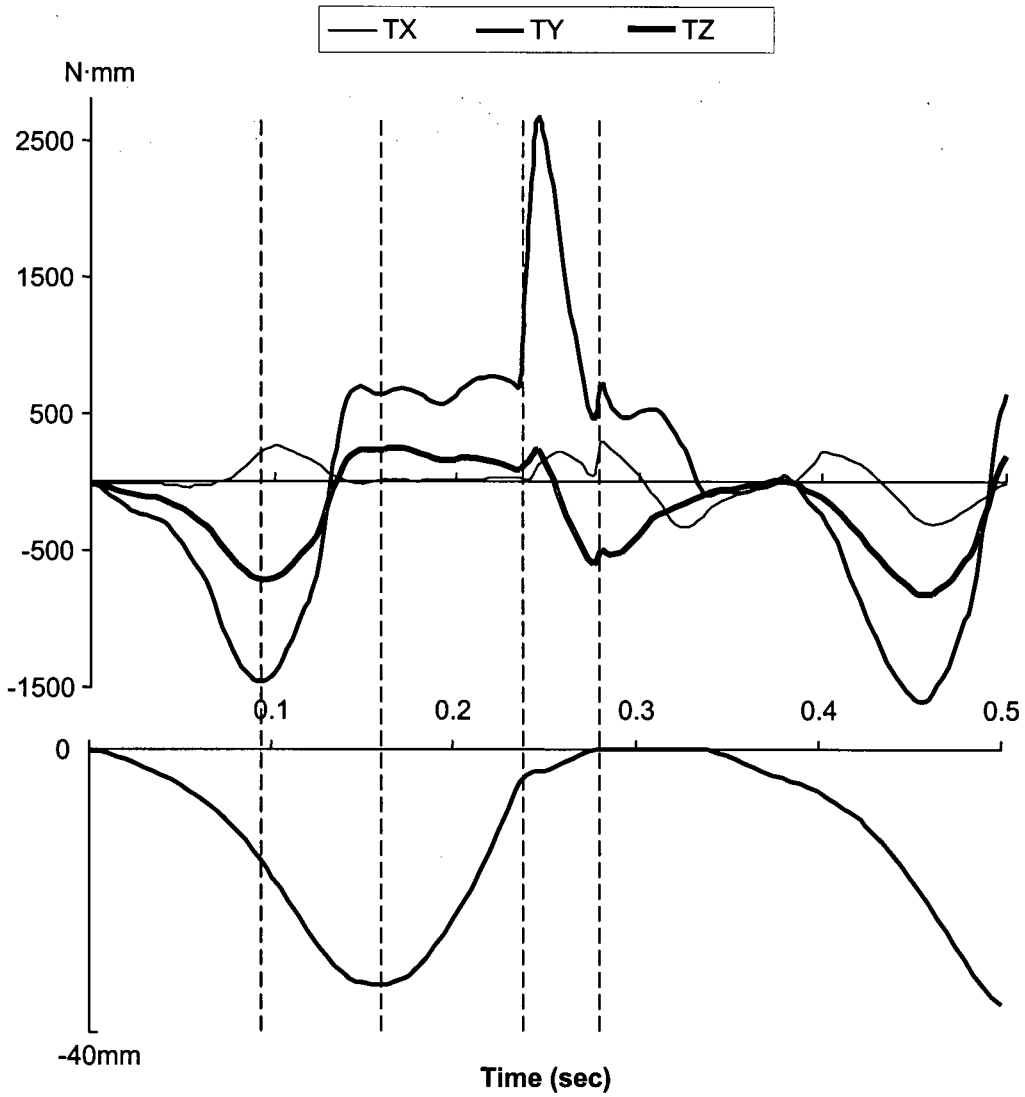

Figure 7.7 Tri-axial symphyseal torques expressed in time. The lowest curve is the corresponding incisor point motion in the vertical dimension. The dotted lines (from left to right) represent maximum jaw opening, onset of bolus crush, and the onset of tooth-to-tooth contact in intercuspation. TX, TY and TZ are torques about the X, Y, and Z axes, respectively.

pterygoid tension exceeding that of the working-side lateral pterygoid, so the twisting force exerted on the left side symphysis by the right side was in a clockwise direction (cf. Figure 7.2, p180). The second positive torque commenced with the onset of bolus crushing, reached peak after the bolus was completely crushed, and was due to the bolus reaction force coupling with the balancing-side jaw lifting forces (Figure 7.4, p183).

The torques around Y-axis were induced by twisting related to the transverse bending of the mandibular corpora. The initial negative torque was associated with the activity of the two jaw openers when the medial transverse bending occurred. The magnitude of this torque was about -1500 N·mm. This torque changed direction when passive tension of superficial and deep masseter (wishboning) began to increase and quickly reached about 750 N·mm the moment the jaw reached maximum opening. The torque stayed almost constant until the lower teeth began to crush the food bolus. It then rose steeply to a maximum of over 2500 N·mm during the first one third of the bolus crushing phase, followed by a sharp drop in magnitude. The peak torque coincided with the maximum tensions of the superficial and deep masseter muscles on both sides, and the peak bolus reaction force. The torque reduced to about 200 N·mm after tooth contact occurred, and started to decline before the next cycle (cf. Figure 7.4, p183).

The torques around Z-axis were the results of asymmetrical jaw opening and closing muscle forces, which tended to turn the mandible about its anteroposterior Z-axis. They coincided with the two transverse torques, and were the consequences of the same muscle contraction patterns.

7.5 DISCUSSION

7.5.1 The model

The dynamic model assumed the mandible was two rigid structures linked by a fixed joint placed centrally at the mandibular symphysis. Conceptually, it was equivalent to two rigid beams (independent of their cross-sectional forms) linked at a point through which all forces and torques were transmitted. While the model was incapable of predicting stress and strain within or between its components, it was able to reveal the environment in which the symphysis must work. The assumption was that the design of the corpora provides a high degree of rigidity in the intact animal; thus, any symphyseal link, whatever its form, would have to be designed to cope with the resultant total forces and torques demonstrated by the model.

The model simplified some of the pig's musculoskeletal properties. For example, the pig superficial masseter is large, and shows differential activities (Herring *et al.*, 1989), yet here we treated it as a single component because the detailed cross-sectional data for its components were unknown. Also, using a single pin-point joint to represent the symphysis was another simplification. It would be more ideal perhaps to use two or more of such joints, in which case facial and lingual side connections might separate compressive and tensile forces respectively, more like a real symphysis during wishboning. This would make the model more complex.

7.5.2 Predicted shear

The dynamic model suggested dorsoventral shear is the main dynamic loading pattern in the pig symphysis. This shear force starts to increase when reaction force on the lower teeth couples with balancing-side jaw

adductor forces (Figure 7.6, p186). The prediction accords with the hypothesis that like that in primates (Hylander, 1979a, 1984, 1985), the pig jaw symphysis undergoes dorsoventral shear during unilateral mastication. The magnitude of this shear force was the largest among all forces passing through the symphysis. To resist this large shearing force, a large symphyseal cross-sectional area would be necessary, as suggested by the findings in Chapter II (p83).

Our model also predicted a small amount of anteroposterior shear occurring at the very end of the power stroke, i.e. when the lower jaw moves back to the midline. It tends to shear the working-side jaw forward and the balancing-side jaw backward (Figure 7.6, p186). In a cinefluorographic analysis of jaw movements in galagos with unfused symphysis, Beecher (1977) noted that working-side jaw frequently moves anteriorly relative to the balancing-side jaw. He attributed this anteroposterior shear to the balancing-side posterior temporalis pulling the balancing-side mandible backwards, while the working-side corpus is simultaneously pulled forward by working-side masticatory force.

7.5.3 Predicted transverse bending

The dynamic model predicted medial transverse bending associated with jaw opening. The initial bending was expressed as compression, and started with the contraction of lateral pterygoid and digastric muscles on both sides, and reached a maximum when the lateral pterygoid muscles reached their peak tensions (Figure 7.4, p183 and Figure 7.6, p186). The effect is similar to one reported in primate studies (Hylander, 1984, 1985), coincident with the second largest torque (Figure 7.7, p188).

Lateral transverse bending (Hylander and Johnson, 1994) was also predicted by the current model. The predicted maximum torque (about the superoinferior axis) exceeded 2,500 N·mm, well beyond the largest torque during medial transverse bending (Figure 7.7, p188). In addition

to the masseter contribution, the model associated wishboning with bite and articular forces. As the artificial food bolus was crushed in a supero-medial direction by the lower tooth, the reaction force from the food bolus had a laterally directed component. Since the pig has a relatively flat articular fossa with a mediolateral cant, wishboning here would also have been influenced by joint reaction forces on both sides (cf. Figure 7.5, p185 and see Figure 7.8, p193).

To counter this wishboning torque effectively, not only the size, but also the shape and cortical bone distribution of the pig jaw symphysis are important (Hylander, 1984). A large cross-sectional moment of inertia with respect to the axis perpendicular to the bending plane is required (Hylander, 1985; van Eijden, 2000). This was accomplished by a horizontally oriented symphysis as seen in pigs. The results in this study offered further evidence for the hypothesis that the pig jaw symphyseal orientation is an adaptation to counter concentrated wishboning stresses during function (see Chapter II, p83).

7.6 SUMMARY

Dynamic models predict parameters which are difficult to measure *in vivo*. The validity of the current split-symphysis dynamic model was supported by its plausible jaw motion when driven with muscle activation patterns based on experimental data. Dynamic modeling offers alternative and powerful methods for studying mammalian jaw biomechanics. This study provides additional information regarding the forces and torques which the symphysis is called upon to resist during dynamic function. The size, shape, and orientation of the pig jaw symphysis appear ideal to accomplish this.

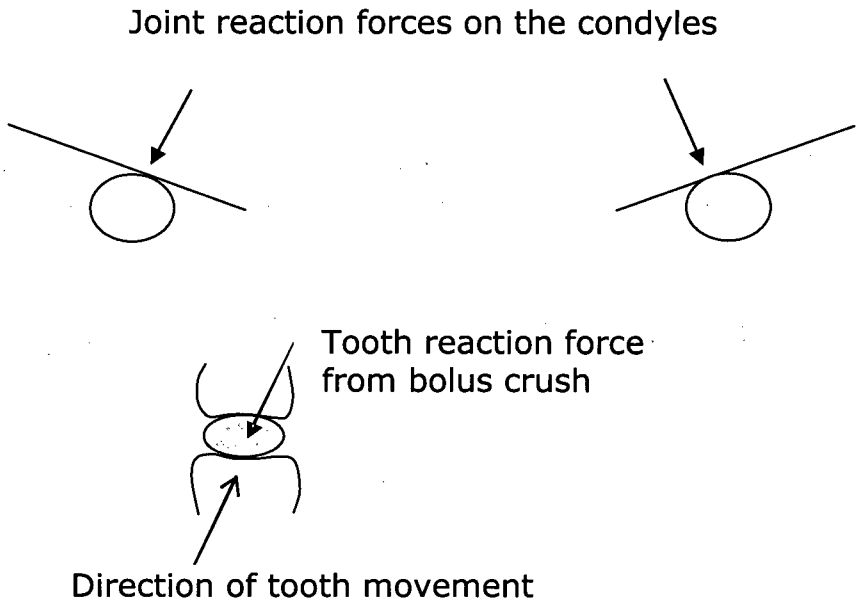

Figure 7.8 Joint reaction forces and bolus reaction force when the artificial food bolus is being crushed. Vectors show approximate direction only.

8 GENERAL DISCUSSION

The experiments reported in Chapters I through V support the hypotheses proposed in the statement of the problem.

In human mandibles, the densest bone occurred at the molar sections, which had the least cortical area. Despite the differences in areas, the cross-sectional masses were homogeneous. It seems the human mandible is uniform with respect to its ability to resist shearing stresses over the entire mandibular corpus and symphysis (see Chapter I, p47).

The fact that cortical bone density and thickness varied within each cross-section can be explained by local loading conditions, i.e. regional loading may be a determinant factor in human mandibular cross-sectional design. These regional variations should be taken into account when modeling the effect of jaw cross-sections on jaw biomechanics (see Chapter I, p47).

Despite their distinct jaw lengths, muscle forces, and symphyseal curvatures, the pig and human jaw symphyses apparently undergo similar stresses and strains. The results from Chapter II (p83) support the dynamic strain similarity hypothesis observed in a large range of different vertebrates. The pig jaw symphyseal shape and orientation seem to be an adaptation to resist concentrated wishboning stresses and strains; if the symphysis is oriented vertically, the estimated stresses and strains are high enough to cause possible symphyseal structure failure (see Chapter II, p83).

The mass properties in the pig and human mandibles can be estimated by CT. Since the mass and geometric centers coincided in the pig and

human mandibles, less-invasive methods than CT revealing 3D jaw shape alone might be used to estimate mass properties. Also, we found there were linear relationships between jaw mass and mass descriptor, and between moments of inertia and moments of inertia descriptors. These descriptors were obtained by simple jaw dimensional measurements. This indicates jaw mass and moments of inertia can be estimated with simple non-invasive, direct measurements. Since the jaw mass center was consistently located at the last molar region in both pig and human mandibles irrespective of age, mass estimation is a simple step in dynamic jaw modeling. Although moments of inertia are not very sensitive determinants of motion in dynamic modeling, the mass and mass center locations are significant (see Chapters III, p114 and IV, p144).

Dynamic models offer a powerful approach to study jaw internal forces and torques related to loading conditions. The three main symphyseal loading patterns were all successfully predicted by our dynamic pig model. Also, the model predicted conditions that are difficult or impossible to measure by *in vivo* experiments (see Chapter V, p171).

8.1 JAW CROSS-SECTIONAL MECHANICS

The beam theory of the jaw biomechanics requires definition of cross-sections. The entire mammalian jaw (including the dentary, i.e. mandibular corpora and symphysis, the condyles, and the rami, Iwasaki *et al.*, 1997; Nickel and McLachlan, 1994) undergoes various loads during function, and these loads demand a biomechanically optimized jaw system. Unfortunately, our understanding of the loads is limited, and the examination of jaw cross-sections cannot justify any optimization theory without their specification. Instead, such an analysis simply offers clues

to understanding, according to current knowledge and general assumptions. The study in Chapter I (p47) provided such hints.

8.1.1 Ideal cross-sectional models

Although apparently ovoidal, jaw cross-sections cannot be modeled as simple elliptical shapes. The results reported do not support either a solid elliptical model or a hollow elliptical model. However, a thin-walled tubular structure with different wall-thicknesses would seem an appropriate model under torsion. In such a model, the stress distribution does not follow the normal torsion formula (Equation 1.8, p13) in which the polar moment of inertia plays the important role.

The shape and regional difference in cortical thickness and density seem to be associated with local loading, especially bending. For example, the results showed the corpus was larger in its vertical dimension (the bending index was less than unity), a design suited to counter high sagittal bending. This bending incurs high compressive stress along the lower border of the corpus, and the results suggest this was the area with the densest and thickest cortical bone. The strong basal cortex seems also well designed for tooth loads. In the symphysis section, because wishboning causes the most stress on the lingual side cortex, this region has a high cortical rigidity index. In the canine section, the combination of bending and wishboning requires more cortical bone at the basal and lingual aspects. An interesting finding was provided by the edentulous mandible, where the bone distribution changed so that cortical bone was more evenly distributed around the entire section in the molar region (perhaps due to the reduction in heavy masticatory force), while in the canine and symphysis regions, the lingual cortex continued to be thick (perhaps because lateral transverse bending still occurred there). To

precisely model the jaw cross-sections, shape and regional cortical thickness both need to be taken into consideration.

8.1.2 Open vs. closed jaw models

The mandibular corpus section has been proposed to be "open" in that the teeth are separate structures from the bony section. However, the open model theory has been proved untenable theoretically and experimentally (Daegling *et al.*, 1992). Under torsional load, an open section only possesses a small fraction of the rigidity of a closed section, and the teeth, periodontal ligaments and alveoli apparently have a stiffening effect on the section. The present work does not provide direct support for this hypothesis. However, analysis of the edentulous mandible indirectly suggests the mandibular corpus acts more as a closed than a open section. The problem of utilizing simple open or closed models is related to the simplicity of these models, because neither takes into account factors such as regional bone density, cortical thickness, the health of the periodontium and trabeculation (Daegling *et al.*, 1992; Daegling and Grine, 1991). Therefore, the solution to the problem requires the development of more sophisticated modeling criteria. Finite element analysis is likely to provide the most productive future approach in this context.

8.1.3 Efficiency – how does bone structure meet mechanical and functional needs?

Based on the findings that denser bone occurs in region with less area (see Table 3.2, p63), it was suggested there was a compromise between biomechanical options and functional needs in the molar site, for here, a large space is required to accommodate molar roots, and the inferior

alveolar nerve and vessel complex. Also biomechanically, a minimal amount of bony material is necessary to resist shearing forces existing along the whole mandibular corpus. Though the problem could be solved by increasing the occupied space, i.e. increasing the cross-sectional area by extending its external dimension, this has other consequences, e.g. the increase in the lower jaw size may cause disparity between the lower and upper jaws. It has been suggested that the mandible is designed to use bone economically (Hylander, 1979b). It is postulated, for the same reason, that the jaw uses space economically.

8.1.4 Bone mechanical properties, density and CT numbers

The density revealed by CT numbers is close to the apparent density, for each voxel in the CT image matrix represents a small volume of bone. The CT number is taken from the mean attenuation of this bulk bone, which includes Haversian canals, marrow spaces, and other voids small enough to be contained within the volume. Therefore, it includes both porosity, and the degree of mineralization. Apparently, the CT number is mainly determined by bone mineralization. The relationship between bone mineralization and mechanical properties however is not highly consistent. Although it is generally agreed there is a positive correlation between them, large variations have been reported, especially for compact bone. Vose and Kubala (1959) suggested bone mechanical properties are functions of its mineral content, and have been supported by Ascenzi and Bonucci (1968) and Currey (1984a). Similarly, Carter and Hayes (1976) found that the compressive strength and stiffness of bone are power functions of its apparent density. In a more recent study, Stenström *et al.* (2000) found a significant correlation between bone mineral density (BMD) and all mechanical parameters and therefore suggested BMD is a consistent predictor of bone strength for cortical bone but not for

cancellous bone, where trabecular thickness is of more value. Other studies (Lang *et al.*, 1997; Martin and Ishida, 1989) however, have indicated bone mineralization and BMD alone are generally poor predictors of cortical bone strength, although they are better for trabecular bone. The best estimates of strength have been obtained with CT, which is capable of accounting for 90% of the strength variability in a simple *in vitro* test (see Martin, 1991).

Phantom studies support a linear relationship between phantom densities and CT numbers (Cheng *et al.*, 1995; Lampmann *et al.*, 1984; Zhang *et al.*, 2001a, see Chapter III, p114). A poor relationship has also been reported for CT numbers and cortical bone (Rho *et al.*, 1995). There are two possible explanations for this anomaly. One is that the phantoms used in these studies are usually potassium dihydrogen phosphate solutions. Even for the highest concentration used in these studies e.g. 0.50 g/cm^3 (Zhang *et al.*, 2001a, see Chapter III, p114), the density of solution is still not comparable to that of compact bone, i.e. linearity has been assumed to extend to include the density range of compact bone. Another explanation may be that because compact bone is so dense, some CT machines or filter algorithms simply treat it as the maximum CT number of uniform density (a good analogy is made when a bone filter is applied to enamel, and enamel is seen to be apparently of uniform density). This may explain why the same study found good relationships between CT numbers and cancellous bone densities (Rho *et al.*, 1995). Hence, the CT numbers may be a cortical bone density index only when the appropriate filter is applied. The raw CT number usually uses part of the signed 16-bit integer which covers from -32768 to 32767. This range should be large enough to represent the entire range from the lowest density (i.e. air) to the highest density (i.e. enamel) in living material. When converted to 8-bit integers (usually from 0 to 255) by an

inappropriate filter, the linearity alters, especially in the high density bone range. The program, we used in our studies (3Dviewnix, University of Pennsylvania Medical Center, Philadelphia, PA), while powerful in most aspects, does not accept negative numbers in the CT database. We previously used a command-line program to perform the conversion and found it was very difficult to set the low and high bounds accurately. The resultant CT image could indicate either not enough discrete numbers (when the selection range was too large) or the high density compact bone tissue became too uniform (when the selection range was too small). For this reason, we wrote a dedicated program (RIC - Raw Image Converter, Craniofacial Laboratory, The University of British Columbia, available online at http://condor.dentistry.ubc.ca) to perform the filter visually (for details of this program see RIC – Raw Image Converter, p222, in the Appendix).

The cortical bone rigidity index (CRI) we introduced earlier (see Chapter I, p47) may not be linearly related to cortical rigidity. This index, a combination of the cortical bone density and thickness, will arguably account for more of the cortical variability than any single variable. Lang *et al.* (1997) found while BMD alone accounts for only 48-77% of the variability in cortical bone strength, a combination of BMD and geometry variables can explain up to 93% of the variance. The variances among the three aspects we measured met our expectations. However, they did not provide insight into the mechanical contribution of the tooth, periodontal ligament, or alveolar process.

8.1.5 Bone mechanical properties, bone composition and organization

The mechanical properties of bone depend not only on the bone's

macroscopic structure, i.e. its shape and size, but also on the mechanical properties of the material within. The latter is assumed to depend on the composition (porosity and mineralization) and organization (trabecular or cortical bone architecture, and collagen fiber orientation) of the bone. The methods previously used (Daegling, 1989; Daegling *et al.*, 1992; Daegling and Grine, 1991; Daegling and Hylander, 1998) only provide information regarding macroscopic structure. The present work included some compositional elements, i.e. mineral density and porosity. A good example of the significance of bone material properties is the observation that the bone's elastic moduli differ directionally (Dechow *et al.*, 1993; Dechow and Hylander, 2000; van Eijden, 2000). Unfortunately, CT cannot reveal such information.

8.2 JAW MASS PROPERTIES

8.2.1 Significance of bone density, jaw dimensions, and jaw mass properties

It has been suggested that true distribution of bone mass should be taken into account when determining the moments of inertia in the human tibia (Cheng *et al.*, 1995) and in the human head (Smith *et al.*, 1995). For this purpose, CT has been proposed (Smith *et al.*, 1995). The present findings (Chapters III, p114 and IV, p144) indicate this is not necessary for either the pig or human mandible, since the centers defined by bone mass and volume are close, and this difference (around one mm) does not make a significant difference in dynamic modeling (see Chapter IV, p144). Therefore, regional bone density does not play an important role in determination of jaw mass properties in pigs and humans, and possibly in other mammals, too. In contrast, jaw dimensions are

important determinants of mass properties. Linear relationships between jaw mass and a mass descriptor and between moments of inertia and moments of inertia descriptors were demonstrated. These descriptors are determined by jaw dimensions. For example, our smallest pig mandible had a mass (dry weight) of 5.28 g and a mean bone density of 1.41 g/cm^3, while our largest pig jaw had a mass of 180.91 g and a mean bone density of 1.74 g/cm^3 (see Table 5.1, p126). Clearly, the mass difference is not mainly attributed to the density but to the size of the jaw.

The moment of inertia is a function of mass and two orthogonal dimensions. It is therefore also determined mainly by jaw dimensions. The relative magnitude of moments of inertia for the jaw can be estimated qualitatively by its dimensions. For example, since the pig jaw is longest anteroposteriorly, the moment of inertia with respect to this axis should be the smallest. Depending on the sizes in the other two dimensions, the moment of inertia is largest with respect to the smallest dimension.

8.2.2 Significance of mass properties in dynamic modeling

The significance of the mass properties in dynamic modeling were tested with a previously developed human jaw model. Jaw mass and anteroposterior mass center locations were important variables in simulated jaw opening, while the moments of inertia allowed larger variations in expression, complementing similar findings reported during jaw closing (Koolstra and van Eijden, 1995). Gravitational acceleration, viscous damping, and the generation of muscle tensions seem sufficient to ensure these relatively low moments do not play a major role in shaping free jaw movements.

8.2.3 Significance of the imaging method in dynamic modeling

The imaging method described here not only allows mass estimation for normal human mandibles; it is also applicable in cases such as facial asymmetry, and partially resected mandibles, where jaw mass centers may not coincide with volumetric centers.

The segmentation technique allows mass property estimation for virtually any skeletal part. The pig model (Chapter V, p171) is an example of this application. The method is also applicable to any CT-imaged physical materials with known densities, e.g. it has been used with good precision to estimate mass properties in an artificial denture model.

8.3 SYMPHYSEAL BIOMECHANICS

8.3.1 Stress and strain similarity

Fused ossified symphyses have to withstand bending, torsional and shearing stresses during various masticatory tasks (Hylander, 1984). Wishboning seems to be the most important load. Under wishboning, the lingual side of the symphysis can undergo tensile stress 2.5 times higher than the compressive stress on the facial side. Because bone is weaker in tension than compression, it seems reasonable that more bone is needed on this side. In Chapter I (p47), regional differences among the lingual, basal and facial cortices were measured. The results clearly showed that the lingual cortex was stiffer than its facial counterpart in the human mandibular symphysis. The orientation of the pig jaw symphysis should be taken into consideration when evaluating the bone distribution. In

Chapter II (p83), it was found more bone was deposited on the infero-lingual aspect of the pig symphysis when it was oriented functionally (i.e. normal). This was also attributed to the need for resistance to wishboning, because wishboning would tend to bend the pig mandible in its functional occlusal plane, rather than in a plane perpendicular to the long axis of the symphyseal section.

The stress and strain similarity between the pig and human symphyses may not be surprising because both the pig and human jaws use the same material. Despite variations in pig and human bone (Fung, 1981), their composition is similar, and their properties lie within the same range. It then follows that the functional stress and strain may be similar in mammals with fused ossified symphyses.

8.3.2 Symphyseal orientation

The distinct difference between the pig and human symphyses is their orientation. While the human jaw symphysis orients almost vertically relative to the functional occlusal plane, the pig jaw symphysis is angled more horizontally. There is a tendency that as pigs grow, this orientation becomes more horizontal (see Chapter II, p83). This pattern is very similar to that found in primates (Hylander, 1985; Vinyard and Ravosa, 1998). The present study supports the hypothesis that this orientation of the pig jaw symphysis functions to maintain the stress and strain caused by wishboning within an acceptable range. The results suggest an uprightly-oriented pig symphysis cannot withstand the high stress and strain caused by deep masseter tension. The reason that changing the symphyseal orientation alone increases its ability to resist lateral bending is due to the increase of the cross-sectional moments of inertia with respect to the axis perpendicular to the curvature of bending. The results

in Chapter V (p171) also confirmed this hypothesis in a dynamic pig chewing model, in that the torque related to wishboning was the largest among the three predicted tri-axial torques.

It may not be necessary for the human jaw symphysis to orient horizontally like the pig jaw because the human jaw has relatively small adductor muscles, short lever arms and low degrees of symphyseal curvature. The vertically-deeper human jaw symphysis seems related to sagittal bending, which can occur during incisor biting. Incision is very uncommon in pigs. However, they use their long snouts to root forcefully. This requires a horizontally-oriented symphysis. There seems to be a compromise between incisal functional needs and symphyseal strength in the long-jawed primates, in which superior tori and/or inferior simian shelves are developed (Daegling, 1993; Hylander, 1984; Hylander, 1985). These observations, as well as those of others, support the idea that wishboning is a major determinant of symphyseal form and function.

8.4 BONE GROWTH, MODELING, AND THE MECHANICAL ENVIRONMENT

While basic skeletal morphology is mainly determined genetically, its final mass and architecture are modulated by adaptive mechanisms sensitive to the mechanical environment. Relationships between the mechanical environment and the form of the skeleton have long been recognized (Forwood, 2001). The results of the mechanical environment can be expressed at organ, tissue, cellular and molecular levels (Carter *et al.*, 1998). Organ level mechanical signals can be characterized in terms of loading history, which includes the varying effects of such quantities as forces (i.e. muscle active and passive tensions, passive tensions from

various ligaments, reaction forces from joints and dental occlusion, and any accidental force not belonging to the aforementioned), movements, and deformations. Tissue level mechanics can be expressed in the material properties of bone tissue, such as elastic and shear moduli. The other two levels deal with such things as cell pressure, cell shape changes, oxygen tensions and cytoskeleton damage or disruptions (for review, see Carter *et al.*, 1998) .

Changes in skeletal form as a result of changes in muscle function have long been observed (see Miller, 1991). Hall and Herring (1990) demonstrated that paralysis of avian embryos reduces skeletal growth by reducing the loads imposed on the bones by muscle contraction, changes that represent alterations in the mechanical environment of the skeleton. Mechanical signals influence bone growth, modeling and remodeling activities. Applied mechanical loads can effect adaptations in both cortical and cancellous bone (Forwood, 2001). It is believed that tensile forces on the periostium are osteogenic, whereas compressive loads lead to resorption (Teng and Herring, 1998). The idea that the facial skeleton is optimized for countering or dissipating masticatory forces, invokes an "optimal strain environment" theory (Rubin *et al.*, 1994). According to this theory, during chewing and biting, there should be relatively high and near uniform amounts of bone strain throughout the facial skeleton. Counter-evidence however, has been collected by *in vivo* strain studies (Hylander *et al.*, 1991; Hylander and Johnson, 1997b) in that not all facial bones are especially designed so as to minimize bone tissue and maximize strength. The morphology of certain facial bones does not necessarily have any importance or special relationship to routine and habitual cyclical mechanical loads associated with chewing or biting, or in other words, bone formation here seems to be determined purely genetically.

8.5 SIGNIFICANCE OF DYNAMIC MODELS FOR STUDYING JAW BIOMECHANICS

Dynamic stress and strain patterns have been studied by *in vivo* approaches (Bouvier and Hylander, 1981a; Herring *et al.*, 1996; Herring and Mucci, 1991; Herring and Teng, 2000; Hylander, 1977, 1979a, 1984; Hylander *et al.*, 1998; Hylander and Bays, 1979; Hylander and Johnson, 1997a, 1997b; Liu and Herring, 2000; Rafferty and Herring, 1999; Teng and Herring, 1998). It is difficult though, to relate loading conditions inferred by this approach to muscle activities, bite and joint forces *in vivo*. The dynamic pig model (Chapter V, p171) however, demonstrated this possibility. For example, during the peak tension and torque in relation to wishboning, the model could correlate all muscle tensions, bite and joint forces, making possible to associate the activities of working-side deep and superficial masseters, bilateral joint reaction forces, balancing-side deep and superficial masseters, working-side reaction bite force, and wishboning (see Figure 4.4, p111 and Figure 7.8, p193). With this dynamic model, it was possible to detect a small degree of anteroposterior shear, which has only been possible previously to observe in mammals with unfused symphyses such as galagos (by cinefluorographic analysis; Beecher, 1977). Therefore, dynamic models can provide powerful tools for studying jaw dynamic mechanics.

8.6 PERSONAL COMMENT ON COMPUTING

I would not have been able to complete this thesis without a computer. The work required calculation of cross-sectional measurements and mass properties which would not have been so smooth if I had not been the programmer. In fact, the first step was difficult. I started to write this

program with Microsoft Visual Basic 4.0 (Microsoft Corp., Redmond, WA) because it was said to be the easiest language for non-professional programmers. Later I became interested in C++ and was immediately subdued by its power. I rewrote this program in Microsoft Visual C++ 5.0 (Zhang *et al.*, 2001a, see Chapter III, p114). The current version of this program (Calimage - Calculate Image, Craniofacial Laboratory, The University of British Columbia; available from http://condor.dentistry.ubc.ca) was written in Borland C++ Builder 5.0 (Imprise Corp., Scotts Valley, CA) because this is a package with both power and simplicity.

Originally, I used a command-line program to convert the raw CT images from signed 16-bit to unsigned 8-bit, which is suitable for work under 3DViewnix. It was very painful to select the appropriate filter by trial and error. I decided to write such a program with a user interface, and carry out the conversion under visual inspection. This program was finally named RIC (Raw Image Converter, Craniofacial Laboratory, The University of British Columbia, available online at http://condor.dentistry.ubc.ca).

The included CD-ROM (copyright © 2001 The University of British Columbia) contains my whole thesis (in portable document format, PDF, and HTML format). The CD-ROM complies with the Microsoft Windows ® AutoRun protocol. Both my programs, plus all source codes can be found there. I can customize these programs to fit special needs.

8.7 FUTURE DIRECTIONS

The study of mammalian jaw biomechanics includes many aspects, and the present work touched only a few.

Although my studies estimated the contribution of regional bone density and regional cortical thickness to cross-sectional mechanics, these, and previous ones (Daegling, 1989; Daegling *et al.*, 1992; Daegling and Grine, 1991; Daegling and Hylander, 1998) used small sample sizes. Thus the conclusions may be premature. Similar studies with larger samples might confirm the conclusion that denser bone occurs at cross-sections where the area is smaller, and that the human mandibular cross-sectional mass is homogeneous along the whole mandibular corpus and symphysis. My observation that a dense and thick basal cortex is related to normal tooth loading may seem interesting, but it needs larger samples of both dentate and edentulous mandibles for further defense of this proposition.

Although my stress and strain estimation involved more individual data than previously reported (Vinyard and Ravosa, 1998), I was unable to obtain individual muscle data for each of the specimens. As noted in the discussion (see p107), this may explain part of the large variation in the results. Understandably, repeating such a study in humans would not improve the results. It is certainly possible to perform a further study with living pigs using these imaging and estimation methods. Similar studies are also possible in other mammals such as monkeys, which are also good animal models (Herring, 1995). Future studies could focus on incorporating as much individual data as possible and hypotheses could be tested on more mammal species, especially those for which there is *in vivo* bone strain data in the symphysis, e.g., macaque mandibles. Also, an *in vivo* bone strain study would be useful to perform for the pig jaw symphysis, and would be a nice validation of my current stress and strain estimations. Validated estimations in pigs and other mammals would make human estimations more likely to be true, although these may never be possible to confirm.

Previously, dynamic models have been used to study muscle and joint biomechanics during jaw opening and closing movements (Koolstra and van Eijden, 1995, 1997a, b; Peck *et al.*, 2000), and during chewing (Langenbach and Hannam, 1999). Here, I performed the first study of the pig jaw symphysis. Although limited, this model successfully predicted the three main postulated symphyseal loading conditions, i.e. dorsoventral shear, medial transverse bending, and lateral transverse bending. A similar model might be expected in the human jaw for which dynamic models already exist, and where little is known about the loading conditions in the symphysis. It would also be appealing to build macaque dynamic jaw models to study their symphyseal loading conditions, for which more *in vivo* data are available. Similar models could be constructed to study loading conditions in other areas such as the molar and canine regions in pigs, humans and macaques.

Current dynamic models assume rigid-body conditions only, while current finite element (FE) models are limited to static simulations. Dynamic FE models are appealing but limited by the present computing power. As computers become faster, dynamic FE models will be the primary choice for such study of jaw biomechanics.

9 GENERAL SUMMARY AND CONCLUSIONS

In the current studies, a number of methods were used to investigate jaw biomechanics. These approaches required the use of basic physical and engineering principles. Although limited, application of these principles in mammalian jaw biomechanics seems promising. The jaw cross-sectional study supplemented existing studies on jaw cross-sections by including regions representing the entire mandibular corpus and symphysis, and by assessing contribution of bone distribution and density to jaw biomechanics. The stress and strain estimations of the jaw symphysis complemented previous *in vivo* bone strain studies, and provided more evidence in support of current hypotheses. The study also suggests a future for individual dynamic jaw models in living humans.

The jaw's cross-sectional shape, size and cortical bone distribution reflect its biomechanical design. In the cross-sectional study of the human mandible, the cross-sectional mass was uniform across the mandibular corpus and symphysis. This suggests the human jaw functions as a uniform curved beam resisting shearing stress. The differential cortical bone distribution among the molar, canine and symphysis cross-sections suggests stress and strain may be important factors regulating modeling and remodeling processes in mandibular bone. The stress and strain estimations in the pig and human symphyses support the conclusions that stress and strain similarity exists across mammalian orders, and that pig jaw symphyseal orientation is an important design factor for maintaining functional equivalence and dynamic strain. The finding that jaw mass properties can be estimated by direct measurements is especially useful if and when individual dynamic modeling in living humans becomes an issue. The successful application of a dynamic model in predicting jaw loading patterns suggests dynamic models may be powerful tools for studying jaw biomechanics.

10 BIBLIOGRAPHY

Anapol F and Herring SW. 1989. Length-tension relationships of masseter and digastric muscles of miniature swine during ontogeny. J Exp Biol 143:1-16.

Ascenzi A and Bonucci E. 1968. The compressive properties of single osteons. Anat Rec 161:377-391.

Baron P and Debussy T. 1979. A biomechanical functional analysis of the masticatory muscles in man. Arch Oral Biol 24:547-553.

Beecher RM. 1977. Function and fusion at the mandibular symphysis. Am J Phys Anthropol 47:325-335.

Beek M, Aarnts MP, Koolstra JH, Feilzer AJ, and van Eijden TM. 2001. Dynamic properties of the human temporomandibular joint disc. J Dent Res 80:876-880.

Beer FP and Johnston ER. 1981. Mechanics of materials. New York: McGraw-Hill Book Company.

Beer FP and Johnston ER. 1988. Vector mechanics for engineers: statics and dynamics. New York, NY: McGraw-Hill Company.

Bertram JE and Biewener AA. 1988. Bone curvature: sacrificing strength for load predictability? J Theor Biol 131:75-92.

Biewener AA. 1982. Bone strength in small mammals and bipedal birds: do safety factors change with body size? J Exp Biol 98:289-301.

Biewener AA, Swartz SM, and Bertram JE. 1986. Bone modeling during growth: dynamic strain equilibrium in the chick tibiotarsus. Calcif Tissue Int 39:390-395.

Biewener AA, Thomason J, Goodship A, and Lanyon LE. 1983. Bone stress in the horse forelimb during locomotion at different gaits: a comparison of two experimental methods. J Biomech 16:565-576.

Bouvier M and Hylander WL. 1981a. Effect of bone strain on cortical bone structure in macaques (Macaca mulatta). J Morphol 167:1-12.

Bouvier M and Hylander WL. 1981b. The relationship between split-line orientation and *in vivo* bone strain in galago (G crassicaudatus) and macaque (Macaca mulatta and M. fascicularis) mandibles. Am J Phys Anthropol 56:147-156.

Bouvier M and Hylander WL. 1984. The effect of dietary consistency on gross and histologic morphology in the craniofacial region of young rats. Am J Anat 170:117-126.

Braune W and Fischer O. 1988. Determination of the moments of inertia of the human body and its limbs. New York: McGraw-Hill Book Company.

Carter DR, Beaupre GS, Giori NJ, and Helms JA. 1998. Mechanobiology of skeletal regeneration. Clin Orthop S41-S55.

Carter DR and Hayes WC. 1976. Bone compressive strength: the influence of density and strain rate. Science 194:1174-1176.

Chen J, Akyuz U, Xu L, and Pidaparti RM. 1998. Stress analysis of the human temporomandibular joint. Med Eng Phys 20:565-572.

Chen J and Xu L. 1994. A finite element analysis of the human temporomandibular joint. J Biomech Eng 116:401-407.

Cheng S, Toivanen JA, Suominen H, Toivanen JT, and Timonen J. 1995. Estimation of structural and geometrical properties of cortical bone by computerized tomography in 78-year-old women. J Bone Miner Res 10:139-148.

Cook RD and Young WC. 1985. Advanced mechanics of materials. New York: Macmillan Publishing Company.

Crawley EO. 1990. *In vivo* tissue characterization using quantitative computed tomography: a review. J Med Eng Technol 14:233-242.

Currey JD. 1984a. Effects of differences in mineralization on the mechanical properties of bone. Philos Trans R Soc Lond B Biol Sci 304:509-518.

Currey JD. 1984b. The mechanical adaptations of bones. Princeton, NJ: Princeton University Press.

Curtis DA, Plesh O, Hannam AG, Sharma A, and Curtis TA. 1999. Modeling of jaw biomechanics in the reconstructed mandibulectomy patient. J Prosthet Dent 81:167-173.

Daegling DJ. 1989. Biomechanics of cross-sectional size and shape in the hominoid mandibular corpus. Am J Phys Anthropol 80:91-106.

Daegling DJ. 1993. Shape variation in the mandibular symphysis of apes: an application of a median axis method. Am J Phys Anthropol 91:505-516.

Daegling DJ and Grine FE. 1991. Compact bone distribution and biomechanics of early hominid mandibles. Am J Phys Anthropol 86:321-339.

Daegling DJ and Hylander WL. 1997. Occlusal forces and mandibular bone strain: is the primate jaw "overdesigned"? J Hum Evol 33:705-717.

Daegling DJ and Hylander WL. 1998. Biomechanics of torsion in the human mandible. Am J Phys Anthropol 105:73-87.

Daegling DJ and Hylander WL. 2000. Experimental observation, theoretical models, and biomechanical inference in the study of mandibular form. Am J Phys Anthropol 112:541-551.

Daegling DJ and Jungers WL. 2000. Elliptical fourier analysis of symphyseal shape in great ape mandibles. J Hum Evol 39:107-122.

Daegling DJ, Ravosa MJ, Johnson KR, and Hylander WL. 1992. Influence of teeth, alveoli, and periodontal ligaments on torsional rigidity in human mandibles. Am J Phys Anthropol 89:59-72.

Dechow PC and Carlson DS. 1997. Development of mandibular form: phylogeny, ontogeny, and

function. In: McNeill C, editor. Science and practice of occlusion. Chicago: Quintessence Publishing Co, Inc. p 3-22.

Dechow PC and Hylander WL. 2000. Elastic properties and masticatory bone stress in the macaque mandible. Am J Phys Anthropol 112:553-574.

Dechow PC, Nail GA, Schwartz-Dabney CL, and Ashman RB. 1993. Elastic properties of human supraorbital and mandibular bone. Am J Phys Anthropol 90:291-306.

Fisher LD and van Belle G. 1993. Biostatistics: a methodology for the health sciences. New York, NY: A Wiley-Interscience Publication.

Forwood MR. 2001. Mechanical effects on the skeleton: are there clinical implications? Osteoporos Int 12:77-83.

Fung YC. 1981. Biomechanics: material properties of living tissues. New York: Springer-Verlag.

Gere JM and Timoshenko SP. 1990. Mechanics of materials. Boston: PWS-KENT Publishing Company.

Greaves WS. 1978. The jaw lever system in ungulates: a new model. J Zool 184:271-285.

Grier SJ, Turner AS, and Alvis MR. 1996. The use of dual-energy x-ray absorptiometry in animals. Invest Radiol 31:50-62.

Hall BK and Herring SW. 1990. Paralysis and growth of the musculoskeletal system in the embryonic chick. J Morphol 206:45-56.

Hannam AG. 1994. Musculoskeletal biomechanics in the human jaw. In: Zarb GA, Carlsson GE, Sessle B.J., and Mohl ND, editors. Temporomandibular joint and masticatory muscle disorders. Copenhagen: Munksgaard. p 101-127.

Hannam AG. 1997. Jaw muscle structure and function. In: McNeill C, editor. Science and practice of occlusion. Chicago: Quintessence Publishing Co, Inc. p 41-49.

Hannam AG, Langenbach GE, and Peck CC. 1997. Computer simulation of jaw biomechanics. In: McNeill C, editor. Science and practice of occlusion. Chicago: Quintessence Publishing Co, Inc. p 187-194.

Hannam AG and Wood WW. 1981. Medial pterygoid muscle activity during the closing and compressive phases of human mastication. Am J Phys Anthropol 55:359-367.

Hannam AG and Wood WW. 1989. Relationships between the size and spatial morphology of human masseter and medial pterygoid muscles, the craniofacial skeleton, and jaw biomechanics. Am J Phys Anthropol 80:429-445.

Hearn EJ. 1997. Mechanics of materials 1. Oxford: Butterworth-Heinemann.

Herring SW. 1972. The facial musculature of the Suoidea. J Morphol 137:49-62.

Herring SW. 1976. The dynamics of mastication in pigs. Arch Oral Biol 21:473-480.

Herring SW. 1977. Mastication and maturity: a longitudinal study in pigs. J Dent Res 56:1377-1382.

Herring SW. 1995. Animal models of TMDs: How to choose. In: Sessle B.J., Bryant P.S., and Dionne R.A., editors. TMDs and related pain conditions. Seattle: IASP Press. p 323-328.

Herring SW and Mucci RJ. 1991. *In vivo* strain in cranial sutures: the zygomatic arch. J Morphol 207:225-239.

Herring SW, Muhl ZF, and Obrez A. 1993. Bone growth and periosteal migration control masseter muscle orientation in pigs (*Sus scrofa*). Anat Rec 235:215-222.

Herring SW and Scapino RP. 1973. Physiology of feeding in miniature pigs. J Morphol 141:427-460.

Herring SW and Teng S. 2000. Strain in the braincase and its sutures during function. Am J Phys Anthropol 112:575-593.

Herring SW, Teng S, Huang X, Mucci RJ, and Freeman J. 1996. Patterns of bone strain in the zygomatic arch. Anat Rec 246:446-457.

Herring SW, Wineski LE, and Anapol FC. 1989. Neural organization of the masseter muscle in the pig. J Comp Neurol 280:563-576.

Hobatho MC, Rho JY, and Ashman RB. 1997. Anatomical variation of human cancellous bone mechanical properties in vitro. Stud Health Technol Inform 40:157-173.

Houghton P. 1977. Rocker jaws. Am J Phys Anthropol 47:365-369.

Houghton P. 1978. Polynesian mandibles. J Anat 127:251-260.

Huang X, Zhang G, and Herring SW. 1993. Effects of oral sensory afferents on mastication in the miniature pig. J Dent Res 72:980-986.

Huang X, Zhang G, and Herring SW. 1994. Age changes in mastication in the pig. Comp Biochem Physiol Comp Physiol 107:647-654.

Hylander WL. 1975. The human mandible: lever or link? Am J Phys Anthropol 43:227-242.

Hylander WL. 1977. *In vivo* bone strain in the mandible of Galago crassicaudatus. Am J Phys Anthropol 46:309-326.

Hylander WL. 1979a. Mandibular function in Galago crassicaudatus and Macaca fascicularis: an *in vivo* approach to stress analysis of the mandible. J Morphol 159:253-296.

Hylander WL. 1979b. The functional significance of primate mandibular form. J Morphol 160:223-240.

Hylander WL. 1984. Stress and strain in the mandibular symphysis of primates: a test of competing hypotheses. Am J Phys Anthropol 64:1-46.

Hylander WL. 1985. Mandibular function and biomechanical stress and scaling. American J Zool 25:315-330.

Hylander WL. 1986. In-vivo bone strain as an indicator of masticatory bite force in Macaca fascicularis. Arch Oral Biol 31:149-157.

Hylander WL and Bays R. 1979. An *in vivo* strain-gauge analysis of the squamosal-dentary joint reaction force during mastication and incisal biting in Macaca mulatta and Macaca fascicularis. Arch Oral Biol 24:689-697.

Hylander WL and Crompton AW. 1986. Jaw movements and patterns of mandibular bone strain during mastication in the monkey Macaca fascicularis. Arch Oral Biol 31:841-848.

Hylander WL and Johnson KR. 1994. Jaw muscle function and wishboning of the mandible during mastication in macaques and baboons. Am J Phys Anthropol 94:523-547.

Hylander WL and Johnson KR. 1997a. *In vivo* bone strain patterns in the craniofacial region of primates. In: McNeill C, editor. Science and practice of occlusion. Chicago: Quintessence Publishing Co, Inc. p 165-178.

Hylander WL and Johnson KR. 1997b. *In vivo* bone strain patterns in the zygomatic arch of macaques and the significance of these patterns for functional interpretations of craniofacial form. Am J Phys Anthropol 102:203-232.

Hylander WL, Johnson KR, and Crompton AW. 1987. Loading patterns and jaw movements during mastication in Macaca fascicularis: a bone-strain, electromyographic, and cineradiographic analysis. Am J Phys Anthropol 72:287-314.

Hylander WL, Picq PG, and Johnson KR. 1991. Masticatory-stress hypotheses and the supraorbital region of primates. Am J Phys Anthropol 86:1-36.

Hylander WL, Ravosa MJ, Ross CF, and Johnson KR. 1998. Mandibular corpus strain in primates: further evidence for a functional link between symphyseal fusion and jaw-adductor muscle force. Am J Phys Anthropol 107:257-271.

Hylander WL, Ravosa MJ, Ross CF, Wall CE, and Johnson KR. 2000. Symphyseal fusion and jaw-adductor muscle force: an EMG study. Am J Phys Anthropol 112:469-492.

Iwasaki LR, Nickel JC, and McLachlan KR. 1997. Relationship between growth, function, and stress in the temporomandibular joint. In: McNeill C, editor. Science and practice of occlusion. Chicago: Quintessence Publishing Co, Inc. p 125-136.

Jergas MD, Majumdar S, Keyak JH, Lee IY, Newitt DC, Grampp S, Skinner HB, and Genant HK. 1995. Relationships between young modulus of elasticity, ash density, and MRI derived effective transverse relaxation T2* in tibial specimens. J Comput Assist Tomogr 19:472-479.

Kallen FC and Gans C. 1972. Mastication in the little brown bat, Myotis lucifugus. J Morphol 136:385-420.

Kingsmill VJ and Boyde A. 1998. Variation in the apparent density of human mandibular bone with age and dental status. J Anat 192 (Pt 2):233-244.

Koo WW, Massom LR, and Walters J. 1995. Validation of accuracy and precision of dual energy X-ray absorptiometry for infants. J Bone Miner Res 10:1111-1115.

Koolstra JH and van Eijden TM. 1995. Biomechanical analysis of jaw-closing movements. J Dent Res 74:1564-1570.

Koolstra JH and van Eijden TM. 1996. Influence of the dynamical properties of the human masticatory muscles on jaw closing movements. Eur J Morphol 34:11-18.

Koolstra JH and van Eijden TM. 1997a. Dynamics of the human masticatory muscles during a jaw open-close movement. J Biomech 30:883-889.

Koolstra JH and van Eijden TM. 1997b. The jaw open-close movements predicted by biomechanical modelling. J Biomech 30:943-950.

Koolstra JH, van Eijden TM, Weijs WA, and Naeije M. 1988. A three-dimensional mathematical model of the human masticatory system predicting maximum possible bite forces. J Biomech 21:563-576.

Korioth TW. 1997. Simulated physics of the human mandible. In: McNeill C, editor. Science and practice of occlusion. Chicago: Quintessence Publishing Co, Inc. p 179-186.

Korioth TW and Hannam AG. 1994a. Deformation of the human mandible during simulated tooth clenching. J Dent Res 73:56-66.

Korioth TW and Hannam AG. 1994b. Mandibular forces during simulated tooth clenching. J Orofac Pain 8:178-189.

Korioth TW, Romilly DP, and Hannam AG. 1992. Three-dimensional finite element stress analysis of the dentate human mandible. Am J Phys Anthropol 88:69-96.

Korioth TW and Versluis A. 1997. Modeling the mechanical behavior of the jaws and their related structures by finite element (FE) analysis. Crit Rev Oral Biol Med 8:90-104.

Lampmann LEH, Duursma SA, and Ruys JHJ. 1984. CT Densitometry in Osteoporosis. Hingham: Maritinus Nijhoff Publishers.

Lang TF, Keyak JH, Heitz MW, Augat P, Lu Y, Mathur A, and Genant HK. 1997. Volumetric quantitative computed tomography of the proximal femur: precision and relation to bone strength. Bone 21:101-108.

Langenbach GE, Brugman P, and Weijs WA. 1992. Preweaning feeding mechanisms in the rabbit. J Dev Physiol 18:253-261.

Langenbach GE and Hannam AG. 1999. The role of passive muscle tensions in a three-dimensional dynamic model of the human jaw. Arch Oral Biol 44:557-573.

Langenbach GE, Hannam AG, Liu ZJ, and Herring SW. Prediction of masticatory biomechanics in the pig temporomandibular joint. J Dent Res 78 [Special issue], 125. 1999. Abstract

Langenbach GE and Weijs WA. 1990. Growth patterns of the rabbit masticatory muscles. J Dent Res 69:20-25.

Lanyon LE. 1974. Experimental support for the trajectorial theory of bone structure. Journal of Bone Jt Surg - Br Vol 56:160-166.

Lanyon LE and Rubin CT. 1984. Static vs dynamic loads as an influence on bone remodelling. J Biomech 17:897-905.

Lieberman DE and Crompton AW. 2000. Why fuse the mandibular symphysis? A comparative analysis. Am J Phys Anthropol 112:517-540.

Lindh C, Nilsson M, Klinge B, and Petersson A. 1996. Quantitative computed tomography of trabecular bone in the mandible. Dentomaxillofac Radiol 25:146-150.

Liu ZJ and Herring SW. 2000. Bone surface strains and internal bony pressures at the jaw joint of the miniature pig during masticatory muscle contraction. Arch Oral Biol 45:95-112.

Martin RB. 1991. Determinants of the mechanical properties of bones. J Biomech 24 Suppl 1:79-88.

Martin RB and Ishida J. 1989. The relative effects of collagen fiber orientation, porosity, density, and mineralization on bone strength. J Biomech 22:419-426.

Mazess RB, Barden HS, Bisek JP, and Hanson J. 1990. Dual-energy x-ray absorptiometry for total-body and regional bone- mineral and soft-tissue composition. Am J Clin Nutr 51:1106-1112.

Mikic B and Carter DR. 1995. Bone strain gauge data and theoretical models of functional adaptation. J Biomech 28:465-469.

Miller AJ. 1991. Craniomandibular muscle function and morphology. In: Craniomandibular muslces: their role in function and form. Boston: CRC Press. p 207-269.

Morgan CL. 1983. Basic principles of computed tomography. Baltimore: University Park Press.

Mott RL. 1996. Applied strength of materials. Englewood Cliffs, NJ: Prentice Hall.

Ng F. Modeling, analysis and dynamics of the human jaw system. 1994. The University of British Columbia. Thesis

Nickel JC and McLachlan KR. 1994. An analysis of surface congruity in the growing human temporomandibular joint. Arch Oral Biol 39:315-321.

Oron U and Crompton AW. 1985. A cineradiographic and electromyographic study of mastication in Tenrec ecaudatus. J Morphol 185:155-182.

Otten E. 1987. A myocybernetic model of the jaw system of the rat. J Neurosci Methods 21:287-302.

Peck CC. Dynamic musculoskeletal biomechanics in the human jaw. 1999. The University of British Columbia. Thesis

Peck CC, Langenbach GE, and Hannam AG. 2000. Dynamic simulation of muscle and articular properties during human wide jaw opening. Arch Oral Biol 45:963-982.

Powell K, Atkinson PJ, and Woodhead C. 1973. Cortical bone structure of the pig mandible. Arch Oral Biol 18:171-180.

Rafferty KL and Herring SW. 1999. Craniofacial sutures: morphology, growth, and *in vivo* masticatory strains. J Morphol 242:167-179.

Ravosa MJ. 1996. Mandibular form and function in North American and European Adapidae and Omomyidae. J Morphol 229:171-190.

Ravosa MJ. 1999. Anthropoid origins and the modern symphysis. Folia Primatol 70:65-78.

Ravosa MJ and Hylander WL. 1993. Functional significance of an ossified mandibular symphysis: a reply. Am J Phys Anthropol 90:509-512.

Ravosa MJ, Johnson KR, and Hylander WL. 2000. Strain in the galago facial skull. J Morphol 245:51-66.

Ravosa MJ and Simons EL. 1994. Mandibular growth and function in Archaeolemur. Am J Phys Anthropol 95:63-76.

Rho JY, Hobatho MC, and Ashman RB. 1995. Relations of mechanical properties to density and CT numbers in human bone. Med Eng Phys 17:347-355.

Richtsmeier JT, Paik CH, Elfert PC, Cole TM, and Dahlman HR. 1995. Precision, repeatability, and validation of the localization of cranial landmarks using computed tomography scans. Cleft Palate Craniofac J 32:217-227.

Roark RJ and Young WC. 1975. Formulas for stress and strain. New York: McGraw-Hill Book Company.

Robertson DM and Smith DC. 1978. Compressive strength of mandibular bone as a function of microstructure and strain rate. J Biomech 11:455-471.

Rubin CT, Gross TS, Donahue Hj, Guilak F, and McLeod KJ. 1994. Physical and environmental influences on bone formation. In: Brighton C, Friedlander G, and Lane J, editors. Bone formation and repaire. Rosemont, IL: American Academy of Orthopaedic Surgeons. p 61-78.

Rubin CT and Lanyon LE. 1984. Dynamic strain similarity in vertebrates; an alternative to allometric limb bone scaling. J Theor Biol 107:321-327.

Sadowsky PL. 1995. The geometry of cephalometry. In: Jacobson A., editor. Radiographic cephalometry from basics to vieoimaging. Chicago: Quintessence Publishing Co, Inc. p 127-136.

Sasaki K, Hannam AG, and Wood WW. 1989. Relationships between the size, position, and angulation of human jaw muscles and unilateral first molar bite force. J Dent Res 68:499-503.

Scapino R. 1981. Morphological investigation into functions of the jaw symphysis in carnivorans. J Morphol 167:339-375.

Smith KE, Bhatia G, and Vannier MW. 1995. Assessment of mass properties of human head using various three- dimensional imaging modalities. Med Biol Eng Comput 33:278-284.

Smith RJ. 1983. The mandibular corpus of female primates: taxonomic, dietary, and allometric correlates of interspecific variations in size and shape. Am J Phys Anthropol 61:315-330.

Snyder SM and Schneider E. 1991. Estimation of mechanical properties of cortical bone by computed tomography. J Orthop Res 9:422-431.

Stenström M, Olander B, Lehto-Axtelius D, Madsen JE, Nordsletten L, and Carlsson GA. 2000. Bone mineral density and bone structure parameters as predictors of bone strength: an analysis using computerized microtomography and gastrectomy-induced osteopenia in the rat. J Biomech 33:289-297.

Straney DO. 1990. Median axis methods in morphometrics. In: Rohlf FJ and Bookstein FL, editors. Processdings of the Michigan morphometrics workshop. Ann Arbor: The University of Michigan Museum of Zoology. p 179-200.

Ström D, Holm S, Clemensson E, Haraldson T, and Carlsson GE. 1986. Gross anatomy of the mandibular joint and masticatory muscles in the domestic pig (*Sus scrofa*). Arch Oral Biol 31:763-768.

Teng S and Herring SW. 1998. Compressive loading on bone surfaces from muscular contraction: an *in vivo* study in the miniature pig, *Sus scrofa*. J Morphol 238:71-80.

Turner CH. 1989. Yield behavior of bovine cancellous bone. J Biomech Eng 111:256-260.

Ugural AC and Fenster SK. 1987. Advanced strength and applied elasticity. New York: Elsevier Science Publishing Co., Inc.

van den Bogert AJ and Nigg BM. 1999. Simulation. In: Nigg BM and Herzog W, editors. Biomechanics of the musculoskeletal system. Chester: Wiley. p 594-616.

van Eijden TM. 2000. Biomechanics of the mandible. Crit Rev Oral Biol Med 11:123-136.

van Eijden TM, Klok EM, Weijs WA, and Koolstra JH. 1988. Mechanical capabilities of the human jaw muscles studied with a mathematical model. Arch Oral Biol 33:819-826.

van Eijden TM, Koolstra JH, and Brugman P. 1995. Architecture of the human pterygoid muscles. J Dent Res 74:1489-1495.

van Eijden TM, Koolstra JH, and Brugman P. 1996. Three-dimensional structure of the human temporalis muscle. Anat Rec 246:565-572.

van Eijden TM, Korfage JA, and Brugman P. 1997. Architecture of the human jaw-closing and jaw-opening muscles. Anat Rec 248:464-474.

van Eijden TM and Raadsheer MC. 1992. Heterogeneity of fiber and sarcomere length in the human masseter muscle. Anat Rec 232:78-84.

Vinyard CJ and Ravosa MJ. 1998. Ontogeny, function, and scaling of the mandibular symphysis in papionin primates. J Morphol 235:157-175.

Vose GP and Kubala AL. 1959. Bone strength and its relationship to X-ray determined ash content. Hum Biol 31:261-270.

Weijs WA. 1973. Morphology of the muscles of mastication in the albino rat, Rattus norvegicus (Berkenhout, 1769). Acta Morphol Neerl Scand 11:321-340.

Weijs WA. 1975. Mandibular movements of the albino rat during feeding. J Morphol 145:107-124.

Weijs WA. 1989. The functional significance of morphological variation of the human mandible and masticatory muscles. Acta Morphol Neerl Scand 27:149-162.

Weijs WA and Dantuma R. 1975. Electromyography and mechanics of mastication in the albino rat. J Morphol 146:1-33.

Weijs WA and Hillen B. 1985. Cross-sectional areas and estimated intrinsic strength of the human jaw muscles. Acta Morphol Neerl Scand 23:267-274.

Williams G, Bydder GM, and Kreel L. 1980. The validity and use of computed tomography attenuation values. Br Med Bull 36:279-287.

Zajac FE. 1989. Muscle and tendon: properties, models, scaling, and application to biomechanics and motor control. Crit Rev Biomed Eng 17:359-411.

Zhang F, Langenbach GE, and Hannam AG. 2001a. Mass properties of the pig mandible. J Dent Res 80:325-337.

Zhang F, Peck CC, and Hannam AG. Mass properties of the human mandible. J Dent Res 80[Special issue], 270. 2001b. Abstract

11 APPENDIX

11.1 RIC – RAW IMAGE CONVERTER

11.1.1 Purpose of this program

RIC (short for Raw Image Converter) was designed to convert grayscale 16-bit raw image files into 8-bit raw image files or bitmap files. The process is carried out under direct visual control.

Commonly, the input data are computed tomographic (CT) or magnetic resonance (MR) images in single or multi-slice formats.

RIC supports big endian and little endian input data formats, either signed or unsigned. Multiple single-slice files, and single multi-slice files can be taken into the program.

Output files can be generated as either 8-bit raw image files, or bitmap files. There are two options when saving raw and bitmap files. One can save the current slice, or a selected sub-set of slices. An alternative option allows one to save the whole set of stacked slices. These options are provided by a menu and shortcut tool button system.

11.1.2 Main interface

Here is the main interface of this program. For complete use of the program, see its help manual on the accompanied CD-ROM.

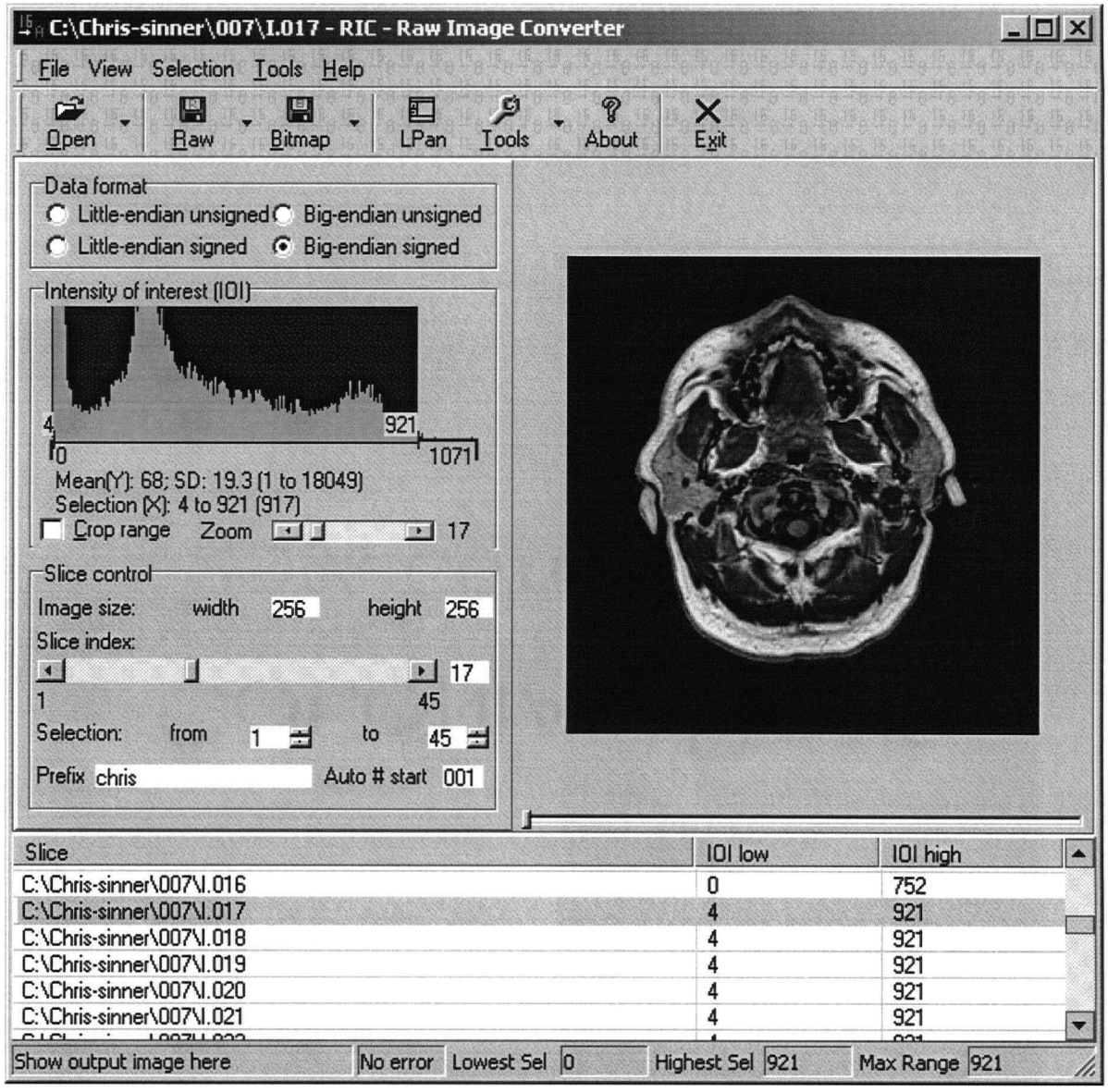

11.1.3 Core algorithm

The core algorithm of the program is the conversion from 16-bit pixels to 8-bit pixels. This was done by a component called TRawImage, which will take a 16-bit raw image buffer and convert it into an 8-bit raw image buffer and display the 8-bit image as bitmap on the screen.

The following code is the C++ routine for this conversion only. Full source codes for this program are over 500 thousand lines, and are

available on the CD-ROM.


```
int len=Width*Height; //width and height of the image
if (!Data8)
      Data8=new Byte[len]; //create 8bit buffer
ZeroMemory(Data8, len); //initialize the buffer
int range=UBound-LBound+1;    //user selected lower and upper bounds
if (FDataFormat==dfLEU){
      //unsigned little endian format
      for (int i=0; i<len; ++){
            unsigned short* u=(unsigned short*)Data16+i;
            if (*u<LBound)
                  continue;
            if (*u>UBound && !FCropRange)
                  Data8[i]=255;
            else
                  Data8[i]=((*u)-LBound)*255/range;   //actual conversion
      }
}
else if (FDataFormat==dfLES){
      //signed little endian format
      for (int i=0; i<len; ++){
            short* s=(short*)Data16+i;
            unsigned short u=(*s)+32768;
            if (*s<LBound)
                  continue;
            if (*s>UBound && !FCropRange)
                  Data8[i]=255;
            else
                  Data8[i]=(*s-LBound)*255/range;     //actual conversion
      }
}
else if (FDataFormat==dfBEU){
      //unsigned big-endian format
      for (int i=0; i<len; ++){
            unsigned short* u=(unsigned short*)Data16+i;
            unsigned short v=Convert(u);  //Convert is a routine to swap
                  //the two bytes that represent the 16-bit integer.
            if (v<LBound)
                  continue;
            if (v>UBound && !FCropRange)
                  Data8[i]=255;
            else
                  Data8[i]=((v)-LBound)*255/range;    //actual conversion
      }
}
else if (FDataFormat==dfBES){
```

```
        //signed little endian format
        for (int i=0; i<len; ++){
              short* s=(short*)Data16+i;
              short t=Convert(s);
              unsigned short u=t+32768;
              if (t<LBound)
                    continue;
              if (t>UBound && !FCropRange)
                    Data8[i]=255;
              else
                    Data8[i]=(t-LBound)*255/range;      //actual conversion
        }
}
```

11.2 CALIMAGE – CALCULATE IMAGE

11.2.1 Purpose of this program

This program was designed to calculate mass properties form 3D CT images, and also to perform cross-sectional measurements from single slice images.

For mass properties calculation, the program takes a number of multi-slice 3D CT image files (they must be raw image files or 3DViewnix IM0 image files) and separate landmark files (with the same names but ".lmk" as extension) as input files, and it calculates the mass, mass center, geometric center and moments of inertia with respect to the landmark defined coordinate system. If no landmark file counterparts are found in the image source directory, the program will calculate the mass, mass and geometric centers the same way, but it will calculate the moments of inertia with respect to the image matrix coordinate system.

For cross-sectional measurements, the program takes multiple single-slice images (can be either raw image files or bitmap image files or 3DViewnix IM0 files each containing a single image slice) as input source and calculate their cross-sectional areas, masses, centroids of area, centroids of mass, second moments of inertia with respect to their image matrix coordinate systems.

In both cases, the user is allowed to specify a calibration curve by which Calimage converts pixel values into real densities.

The output is comma delimited text which can be easily imported into Microsoft Excel for further processing.

11.2.2 Main interface

Here is the main interface of this program. For complete use of the program, see its help manual on the accompanied CD-ROM.

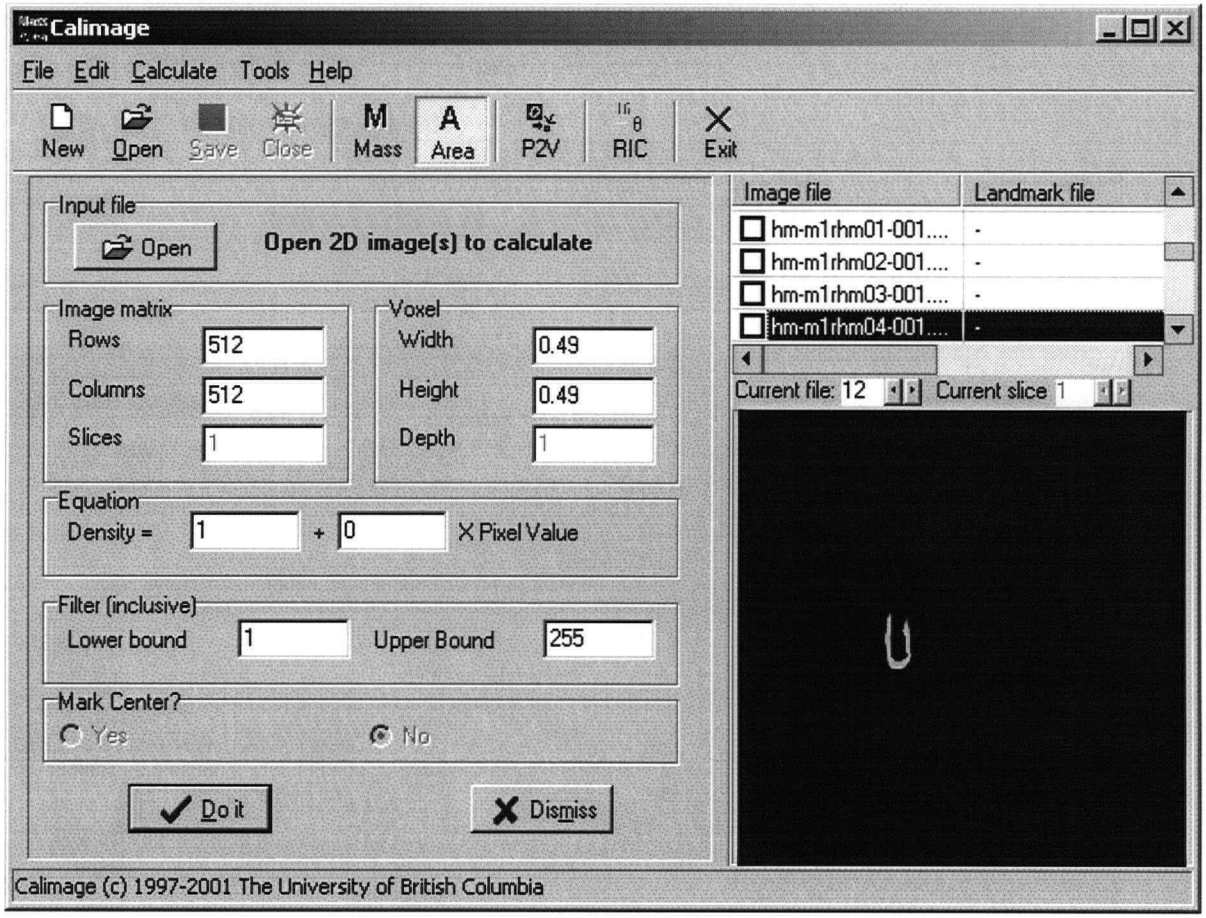

11.2.3 Core algorithms

The core algorithms are the calculation of mass properties and cross-sectional measurements. Full source codes for this program are millions of lines, and are available on the CD-ROM. Here, only the codes for actual calculation are given. The calculation is based on formulae presented in the Introduction (p1) and Chapter III (p114).

11.2.3.1 C++ code for mass properties calculation


```
//Funciton: CalcMassProperties
//Parameter: image file name
//Return value: none
void __fastcall TCalimage::CalcMassProperties(AnsiString fn)
{
      TFileStream* fs;//define a file stream
      try{
            fs=new TFileStream(fn,fmOpenRead);//try to open the file
      }
      catch (...){
            GlobalWarning("Can not open "+fn);
            return; //if fails, return
      }
      //if file is opened successfully
      //first calculate the header size
      int header=fs->Size-ipData.rows*ipData.columns*ipData.slices;
      fs->Seek(header,soFromBeginning);//go to the first pixel position

      int r, c, s; //loop integers
      double totalX=0, totalY=0, totalZ=0; //mass weighted total x, y, z
      double totalGX=0, totalGY=0, totalGZ=0; //for geometric center
      int vn=0; //calculated number of voxels
      double totalMass=0; //calculated total mass
      double Ixx=0, Iyy=0, Izz=0; //moments of inertia
      double Ixy=0, Ixz=0, Iyz=0; //product of inertia

      //create the read buffer of size r;
      unsigned char* rb=new unsigned char[ipData.rows];

      //precalculate these variables to improve performance
      double x2, y2, z2;//square current x, y, z coordinates of the voxel
      double xp, yp, zp;//current x, y, z position of the voxel center
      double vv=ipData.width*ipData.height*ipData.depth/1000;//volume of
            //each voxel in cm3

      //loop and calculate
      for (s=0; s<ipData.slices; s++)//loop each slice
      {
            zp=(s+0.5)*ipData.depth;
            z2=zp*zp;//square the current position on Z-axis
            for (c=0; c<ipData.columns;c++)
            {
                  yp=(c+0.5)*ipData.height;
                  y2=yp*yp; //sqare the current position on Y-axis
                  fs->Read(rb,ipData.rows); //read a row
```

```
                for (r=0;r<ipData.rows;r++)
                {
                      if (rb[r]==0)
                      continue; //ignore pixels of value 0 to
                            //improve performance


                      if (rb[r]<ipData.lowerbound ||
                      rb[r]>ipData.upperbound)
                            continue; //out of range, ignore

                      vn++; //increase the calculated number of voxels
                      xp=(r+0.5)*ipData.width;
                      x2=xp*xp; //square the current position on X-axis
                      double m=(rb[r]*ipData.slope+ipData.intercept)*vv;
                      //g
                      totalMass+=m; //calculated mass

                      //mass weighted total x, y, z
                      totalGX+=r+0.5;
                      totalGY+=c+0.5;
                      totalGZ+=s+0.5;
                      totalX+=(r+0.5)*m;
                      totalY+=(c+0.5)*m;
                      totalZ+=(s+0.5)*m;

                      //Moments of inertia with respect to image matrix
                      origin
                      Ixx+=m*(y2+z2); //g.mm2
                      Iyy+=m*(x2+z2);
                      Izz+=m*(x2+y2);

                      //product of inertia
                      Ixy+=xp*yp*m; //g.mm2
                      Ixz+=xp*zp*m;
                      Iyz+=yp*zp*m;
                }
          }
}
delete fs;
delete []rb;//delete buffer

//Calculate center of mass
double cx, cy, cz;
cx=ipData.width*totalX/totalMass;
cy=ipData.height*totalY/totalMass;
cz=ipData.depth*totalZ/totalMass;
double gx,gy,gz;
gx=ipData.width*totalGX/vn;
gy=ipData.height*totalGY/vn;
gz=ipData.depth*totalGZ/vn;

double cdx, cdy, cdz, cd;
cdx=cx-gx;
cdy=cy-gy;
cdz=cz-gz;
cd=sqrt(cdx*cdx+cdy*cdy+cdz*cdz);
```

```
//translating mass center to image matrix origin,
//and moments of inertia are
//converted to MIs with respect to the mass center
//the original unit of MI is g.mm2, convert it to g.cm2
Ixx=(Ixx-totalMass*(cy*cy+cz*cz))/100;
Iyy=(Iyy-totalMass*(cx*cx+cz*cz))/100;
Izz=(Izz-totalMass*(cx*cx+cy*cy))/100;

double Ix=0, Iy=0, Iz=0;
//if no landmark data, ignore the following
if (mpData.p!=0)
{
      Ixy=(Ixy-totalMass*(cx*cy))/100;
      Ixz=(Ixz-totalMass*(cx*cz))/100;
      Iyz=(Iyz-totalMass*(cy*cz))/100;

      //Reorient moments of inertia
      //Points in landmark database are
      //1. Id-infradentale
      //2. Left premolar
      //3. Left molar
      //4. right molar
      //5. right premolar
      //6. right condylar pole
      //7. left condylar pole
      //8. mass center
      //First, LM-LPM(P3-P2) x LM-RM(P3-P4), get the y-axis
      //Second, y-axis x MidCondylar-ID, obtain x-axis
      //Third, x-axis x y-axis to achieve z axis
      //Forth, rotate the moments of inertia
      Vector3D Ox, Oy, Oz;
      Oy=Normalize(CrossProd(mpData.p[2]-mpData.p[3],mpData.p[4]-
      mpData.p[3]));
      Ox=Normalize(CrossProd(mpData.p[1]-
      (mpData.p[6]+mpData.p[7]),Oy));
      Oz=Normalize(CrossProd(Ox, Oy));
      //finnal moments of inertia
      Ix=Ixx*Ox.x*Ox.x+Iyy*Ox.y*Ox.y+Izz*Ox.z*Ox.z-2*Ixy*Ox.x*Ox.y-
      2*Iyz*Ox.y*Ox.z-2*Ixz*Ox.x*Ox.z;
      Iy=Ixx*Oy.x*Oy.x+Iyy*Oy.y*Oy.y+Izz*Oy.z*Oy.z-2*Ixy*Oy.x*Oy.y-
      2*Iyz*Oy.y*Oy.z-2*Ixz*Oy.x*Oy.z;
      Iz=Ixx*Oz.x*Oz.x+Iyy*Oz.y*Oz.y+Izz*Oz.z*Oz.z-2*Ixy*Oz.x*Oz.y-
      2*Iyz*Oz.y*Oz.z-2*Ixz*Oz.x*Oz.z;
}

//Fill mpData
mpData.duration=elapsed;
mpData.vn=vn; //calculated voxels
mpData.volume=FormatFloat("0.00", vn*vv); //total volumecm3
mpData.mass=FormatFloat("0.00",totalMass);//mass
mpData.mbd=FormatFloat("0.00",totalMass/(vn*vv)); //mean bone
      //density g/cm3
mpData.mcx=FormatFloat("0.00", cx); //mass center
mpData.mcy=FormatFloat("0.00", cy);
mpData.mcz=FormatFloat("0.00", cz);
mpData.gcx=FormatFloat("0.00", gx); //geometric center
```

```
        mpData.gcy=FormatFloat("0.00", gy);
        mpData.gcz=FormatFloat("0.00", gz);
        mpData.cd=FormatFloat("0.00", cd);//two center difference
        mpData.ixx=FormatFloat("0.00", Ixx);//moments of inertia
        mpData.iyy=FormatFloat("0.00", Iyy);
        mpData.izz=FormatFloat("0.00", Izz);
        mpData.Ix=FormatFloat("0.00", Ix);//moments of inertia
        mpData.Iy=FormatFloat("0.00", Iy);
        mpData.Iz=FormatFloat("0.00", Iz);

        //mark center
        if (!ipData.markcenter)
              return;
        int vx, vy, vz;
        vz=cz/ipData.depth+0.5;
        vx=cx/ipData.width+0.5;
        vy=cy/ipData.height+0.5;

        try{
              fs=new TFileStream(fn,fmOpenWrite);
        }
        catch (...){
              GlobalWarning("Can not open "+fn);
              return; //if fails, return
        }

        fs->Seek(header+(vz-1)*ipData.rows*ipData.columns+(vy-
        1)*ipData.rows+vx,soFromBeginning);
        char wr[1]={2};
        fs->Write(wr,1);
        delete fs;

        //output results
        mpData.Output(REdit->Lines, 1); //data
}
```

11.2.3.2 C++ code for cross-sectional measurements


```
//Funciton: CalcAreaProperties
//Parameter: image file name
//Return value: none
void __fastcall TCalimage::CalcAreaProperties(AnsiString fn)
{
      //read bitmap or raw
      int rows=ipData.rows, columns=ipData.columns;
      int size=rows*columns;
```

```
Byte* buff; //define a buffer to hold data
if (LowerCase(ExtractFileExt(fn))==".bmp")
      buff=ReadBitmap(fn, size);
else
      buff=ReadRaw(fn, size);

if (size!=rows*columns)
{
      GlobalWarning("The specified size is different from the bitmap
      image");
      return;
}

int r, c; //loop integer
double totalX=0, totalY=0; //mass weighted total x, y
double totalGX=0, totalGY=0; //for geometric center
int pn=0; //calculated number of pixels
double totalMass=0; //calculated total areal mass
double Ixm=0, Iym=0; //mass moments of inertia
double Ix=0, Iy=0;//area moments of inertia

//precalculate these variables to improve performance
double x2, y2;//square current x, ycoordinates of the pixel
double xp, yp;//current x, yposition of the pixel center
double ps=ipData.width*ipData.height;//pixel size in mm2
double Xmin=10000, Ymin=10000, Xmax=0, Ymax=0;

int cb;

//loop and calculate
for (c=0; c<columns;c++)
{
      yp=(c+0.5)*ipData.height; //mm
      y2=yp*yp; //sqare the current position on Y-axis mm2
      for (r=0;r<rows;r++)
      {
            cb=c*columns+r;
            if (buff[cb]==0)
                  continue; //ignore pixels of value 0
                        //to improve performance

            if (buff[cb]<ipData.lowerbound ||
                  buff[cb]>ipData.upperbound)
                  continue; //out of range, ignore

            pn++; //increase the calculated number of voxels
            xp=(r+0.5)*ipData.width;
            if (Ymin>yp)
                  Ymin=yp;
            if (Ymax<yp)
                  Ymax=yp;
            if (Xmin>xp)
                  Xmin=xp;
            if (Xmax<xp)
                  Xmax=xp;
            x2=xp*xp; //square the current position on X-axis
            double m=(buff[cb]*ipData.slope+ipData.intercept)*ps;
```

```
                //areal mass mg
                totalMass+=m; //calculated mass

                //mass weighted total x, y
                totalGX+=r+0.5;
                totalGY+=c+0.5;
                totalX+=(r+0.5)*m;
                totalY+=(c+0.5)*m;

                //Moments of inertia with respect to image matrix origin
                Ixm+=m*y2; //mass moments of inertia, mm4
                Iym+=m*x2;
                Ix+=ps*y2;//area moments of inertia, mm4
                Iy+=ps*x2;
        }
}

delete []buff;//delete buffer

//Calculate center of mass
double cx, cy;
cx=ipData.width*totalX/totalMass;
cy=ipData.height*totalY/totalMass;
double gx,gy;
gx=ipData.width*totalGX/pn;
gy=ipData.height*totalGY/pn;

double cdx, cdy, cd;
cdx=cx-gx;
cdy=cy-gy;
cd=sqrt(cdx*cdx+cdy*cdy);

double major=Ymax-Ymin;
double minor=Xmax-Xmin;

//translating mass center to image matrix origin,
//and moments of inertia are
//converted to MIs with respect to the mass center
//convert to cm4 or g.cm2
Ixm=(Ixm-totalMass*cy*cy);
Iym=(Iym-totalMass*cx*cx);
Ix=(Ix-ps*pn*gy*gy);
Iy=(Iy-ps*pn*gx*gx);

//Fill apData
apData.pn=pn; //calculated pixels
apData.area=FormatFloat("0.00",ps*pn/100);//total area in cm2
apData.major=FormatFloat("0.00",major); //major axis
apData.minor=FormatFloat("0.00",minor); //minor axis
apData.mass=FormatFloat("0.00",totalMass/100);//mass in cm2
apData.mbd=FormatFloat("0.00",totalMass/(pn*ps)); //mean
      //grayscale value
apData.mcx=FormatFloat("0.00", cx); //mass center
apData.mcy=FormatFloat("0.00", cy);
apData.gcx=FormatFloat("0.00", gx); //geometric center
apData.gcy=FormatFloat("0.00", gy);
```

```
        apData.cd=FormatFloat("0.00", cd);//two center difference
        apData.ix=FormatFloat("0.00",Ix/10000);    //mi in cm4
        apData.iy=FormatFloat("0.00",Iy/10000);
        apData.jo=FormatFloat("0.00", (Ix+Iy)/10000);
        apData.ixm=FormatFloat("0.00",Ixm/10000);
        apData.iym=FormatFloat("0.00",Iym/10000);
        apData.jom=FormatFloat("0.00", (Ixm+Iym)/10000);
        apData.Xmin=FormatFloat("0.00", Xmin);
        apData.Ymin=FormatFloat("0.00", Ymin);
        apData.Xmax=FormatFloat("0.00", Xmax);
        apData.Ymax=FormatFloat("0.00", Ymax);
        apData.cx=FormatFloat("0.00", cx-Xmin);
        apData.cy=FormatFloat("0.00", cy-Ymin);


        //output results
        apData.Output(REdit->Lines, 1);
}
```

12 PUBLICATIONS

12.1 RECENT PUBLICATIONS

Zhang F, Langenbach GEJ, Hannam AG, Herring SW. 1999. Estimation of bone mass properties by CT in pig mandibles. Journal of Dental Research, 78 (special issue): 440.

Zhang F, Langenbach GEJ, Hannam AG, Herring SW. 2001. Mass properties of the pig mandible. Journal of Dental Research 80(1): 327-335.

Zhang F, Peck CC, Hannam AG. 2001. Mass properties of the human mandible. Journal of Dental Research 80 (special issue): 270.

12.2 PROSPECTIVE PUBLICATIONS

Zhang F, Peck CC, Hannam AG. 2001. Mass properties of the human mandible. Journal of Biomechanics. (Currently in review)

Zhang F, Hannam AG. 2001. Cross-sectional biomechanics of the human mandible. (Submitted to American Journal of Physical Anthropology)

Zhang F, Herring SW, Hannam AG. 2001. Symphyseal mechanics in pig and human mandibles. (Submitted to American Journal of Physical Anthropology)

Zhang F, Langenbach GEJ, Herring SW, Hannam AG. 2001. Dynamic mechanics in the pig mandibular symphysis. (To be submitted to Archives

of Oral Biology)

Langenbach GEJ, Zhang F, Herring SW, Hannam AG. 2001. Reconstruction of the pig's jaw system and the prediction of its masticatory biomechanics. (In preparation)

Hannam AG and Zhang F. 2001. Jaw structure and function in the virtual environment. (In preparation)

Zhang F and Hannam AG. 2001. Three-dimensional surface reconstruction, morphometric measurement, and mesh construction of pig and human jaws. (In preparation)